



**NTNU – Trondheim**  
Norwegian University of  
Science and Technology

# Heat Capacity Measurements of Porous Materials at Cryogenic Temperatures

**Thea Ragna Storesund Mohn**

Master of Energy and Environmental Engineering

Submission date: June 2012

Supervisor: Erling Næss, EPT

Norwegian University of Science and Technology  
Department of Energy and Process Engineering



EPT-M-2012-64

**MASTER THESIS**

for

student Thea Ragna Mohn

Spring 2012

**Heat capacity measurements of porous materials at cryogenic temperatures***Varmekapasitetsmålinger av porøse materialer ved kryogene temperaturer***Background and objective**

Hydrogen can be an energy carrier for the future. The main challenges of the investigation in hydrogen technology are the potential disadvantages in handling. The present project work efforts are focused on hydrogen material properties for hydrogen storage technologies.

The most promising hydrogen storage methods are: gas compression, liquefaction, chemical storage via metal hydrides and gas adsorption via physisorption. Adsorption type storage systems are inexpensive alternatives that also have the potential to reach the goals for handling hydrogen in on-board storage systems. Sorption type materials, like e.g. metal organic frameworks (MOF) have been identified as a viable option. These are characterized by high porosity and specific surface areas.

However, the transient processes during charging and discharging of a storage system play an important role in the utilization of the hydrogen adsorption storage systems, and the heat distribution in the sorption material plays a major role during charging and discharging of a storage system.

The main objective of this work is to measure specific heat capacity of porous materials at the working temperature range of the storage. This work is a continuation of the project work.

**The following tasks are to be considered:**

1. Perform a literature survey on theoretical models and published results for gas adsorption in porous materials. The findings shall be presented and discussed.
2. The thermodynamics of the test sample (e.g. adsorption, pressure) during a measurement cycle shall be described in detail.
3. Perform setup calibration and measurements to determine the specific heat capacity of selected materials in the temperature region of interest. Experimental results shall be compared with the theoretical models where possible, as well as published data on reference materials. The results shall be presented and discussed.

4. An uncertainty analysis on the experimental results shall be performed and presented.
5. Suggestions for further work shall be presented and discussed.

Within 14 days of receiving the written text on the master thesis, the candidate shall submit a research plan for his project to the department.

When the thesis is evaluated, emphasis is put on processing of the results, and that they are presented in tabular and/or graphic form in a clear manner, and that they are analyzed carefully.

The thesis should be formulated as a research report with summary both in English and Norwegian, conclusion, literature references, table of contents etc. During the preparation of the text, the candidate should make an effort to produce a well-structured and easily readable report. In order to ease the evaluation of the thesis, it is important that the cross-references are correct. In the making of the report, strong emphasis should be placed on both a thorough discussion of the results and an orderly presentation.

The candidate is requested to initiate and keep close contact with his/her academic supervisor(s) throughout the working period. The candidate must follow the rules and regulations of NTNU as well as passive directions given by the Department of Energy and Process Engineering.

Risk assessment of the candidate's work shall be carried out according to the department's procedures. The risk assessment must be documented and included as part of the final report. Events related to the candidate's work adversely affecting the health, safety or security, must be documented and included as part of the final report.

Pursuant to "Regulations concerning the supplementary provisions to the technology study program/Master of Science" at NTNU §20, the Department reserves the permission to utilize all the results and data for teaching and research purposes as well as in future publications.

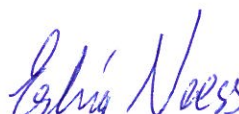
The final report is to be submitted digitally in DAIM. An executive summary of the thesis including title, student's name, supervisor's name, year, department name, and NTNU's logo and name, shall be submitted to the department as a separate pdf file. Based on an agreement with the supervisor, the final report and other material and documents may be given to the supervisor in digital format.

Department of Energy and Process Engineering, 16. January 2012



---

Olav Bolland  
Department Head



---

Erling Næss  
Academic Supervisor

Research Advisor:

Ph.d-candidate Christian Schlemminger, EPT

## Preface

This paper, *Heat capacity measurements of porous materials at cryogenic temperatures*, is written as a master thesis at the Norwegian University of Science and Technology. This master thesis comprises 30 credits in the 10<sup>th</sup> semester for the 5-year Master of Science Degree in the field of Energy and Process Engineering.

I would like to express my gratitude to my supervisor, Erling Næss and our weekly meetings this spring. It has been really helpful for the progression of my work and the guidance has at times been crucial for my own motivation. I would also like to thank my co-supervisor Christian Schlemminger for his constant help and guidance throughout this semester. He has always been available for me and shown interest and enthusiasm all the way. I especially value his efficiency in the lab, which has been very important for the measurement progression.

In addition I would like to thank all of my fantastic fellow students in office B430. They have kept my motivation up and filled my year with humor, laughter and great coffee runs. Especially have I appreciated the amount of chocolate and cakes brought to the office this semester.

At last I would like to thank my fellow flat mates, which have always been there after a long day at the office, supporting and positive.

  
Thea Ragna Storesund Mohn

Trondheim, June 05 2012





## Abstract

In the search for new technology, new materials are prerequisite for major breakthrough. One of these classes of functional materials is the metal-organic framework (MOF). The MOFs offer higher surface areas because of its porous structure and a potential for improved adsorption activity than other currently used materials. This makes it attractive for physical adsorption, which is a hydrogen storage technique. Adsorption type storage systems are alternatives that have the potential to reach the goals for handling hydrogen in on-board storage systems. However, the transient processes during charging and discharging of a storage system play an important role in the utilization of the hydrogen adsorption storage systems, and the heat distribution in the sorption material plays a major role during charging and discharging of a storage system.

The specific heat capacity for activated carbon, Norit R0.8 (1), and three microporous MOFs, Cu-btc (2), Fe-btc (3), and MIL-100(Fe) (4), have been measured, both for inactivated and activated material. The compounds were measured using an MDSC method on a Q2000 differential scanning calorimeter with an appurtenant liquefied nitrogen cooler system (LNCS). The heat capacities were measured from  $-180^{\circ}\text{C}$  to  $150^{\circ}\text{C}$ .

The uncertainties for the different measurements were determined; it varied from 5% to 7%, depending on the assumed water content adsorbed. Further the measurement accuracy was found to depend very little on the inert gases present in the sample.

In addition to measuring the porous material's specific heat capacity, is it performed and presented a literature survey on theoretical models and published data for both gas adsorption and heat capacities in porous materials. The experimental results are compared with published data on reference materials where possible, and a complete uncertainty analysis on the experimental results presented.

The inactivated sample curves showed a general trend, where the heat capacities for inactivated material normally were higher than the heat capacities for the respective activated material, which most probably was due to higher water content in the inactivated material.

A considerable number of measurements on each material were performed, without obtaining the expected results for the activated samples. The principal reason was that an unexplainable transition around  $-150^{\circ}\text{C}$  was present on almost half of the obtained data.

The exact reason behind this anomaly was not found. However, the most likely error was the activation of the samples, based on analysis and investigation of the results. This presumption was stated mainly because the heat capacities for the inactivated samples increased in a smooth and continuous manner with increasing temperature, without this sudden heat capacity change around  $-150^{\circ}\text{C}$ . The conclusion is due to the time perspective of this work an assumption based on observations and personal experience. Further investigation on the matter is recommended, especially to find out if there was a problem in the actual activation procedure or a chemical change in the investigated materials.





## Sammendrag

I jakten på ny teknologi er nye materialer en forutsetning for store gjennombrudd. En av disse klassene av funksjonelle materialer er den metall-organiske gitterstrukturen (MOF). MOF tilbyr større overflater på grunn av sin porøse struktur og et økt brukspotensial i forhold til andre materialer som brukes i dag. Dette gjør materialet attraktivt for fysisk adsorpsjon, som er en hydrogenlagrings teknikk. Adsorpsjonslagring er et lagringssystem som har potensiale å nå de målene for håndtering av hydrogen i innebygde lagringssystemer. Forbigående prosesser under ladning og utladning av et lagringssystem spiller en viktig rolle i utnyttelsen av hydrogenadsorpsjon i lagringssystemene, og varmfordeling i adsorpsjonsmaterialet spiller en viktig rolle under ladningen og utladningen i et lagringssystem.

Den spesifikke varmekapasitet for aktivt kull, R0.8 Norit (1), og tre mikroporøse MOF, Cu-btc (2), Fe-btc (3), og MIL-100(Fe) (4), har blitt målt, både for inaktivert og aktivert materiale. Prøvene ble målt ved hjelp av en MDSC metode på en Q2000 differensial skanning kalorimeter med et tilhørende flytende nitrogen kjøler system (LNCS). Varmekapasiteten ble målt fra  $-180\text{ }^{\circ}\text{C}$  til  $150\text{ }^{\circ}\text{C}$ .

Usikkerheten for de ulike målingene ble bestemt, den varierte fra 5 % til 7 %, avhengig av antatt vannopptak. Videre målenøyaktigheten ble funnet å avhenge svært lite på de inerte gassene som finnes i materialet.

I tillegg til å måle det porøse materialets spesifikke varmekapasitet, er det utført og presentert et litteraturstudium over teoretiske modeller, og publisert data for både gass adsorpsjon og varmekapasitet i porøse materialer. De eksperimentelle resultatene er sammenlignet med publisert data for referansematerialer om mulig, og en komplett usikkerhetsanalyse over de eksperimentelle resultatene presenteres.

De inaktiverte prøvene viste en generell trend, der varmekapasitetene for inaktivert materiale normalt var høyere enn varmekapasitetene for de respektive aktiverte materialene. Dette skyldtes mest sannsynlig høyere vanninnhold i inaktivert materialet.

Et betydelig antall målinger på hvert materiale ble utført, uten å få de forventede resultatene for de aktiverte prøvene. Hovedårsaken var en uforklarlig varmekapasitets forandring rundt  $-150\text{ }^{\circ}\text{C}$  som var til stede på nesten halvparten av de innhentede dataene.

Den eksakte årsaken bak denne anomalien ble ikke funnet. Imidlertid var den mest sannsynlige feilen aktivering av prøvene, denne antagelsen var basert på nøye analyse og studering av resultatene. Denne antakelsen er gitt i hovedsak fordi varmekapasiteten for de inaktiverte prøvene økte jevnt og kontinuerlig med økende temperatur, uten denne plutselige endringen rundt  $-150\text{ }^{\circ}\text{C}$ . Konklusjonen er på grunn av tidsperspektivet for arbeidet basert på observasjoner og personlig erfaring. Ytterligere arbeid er anbefalt, særlig for å finne ut om det var et problem i selve aktiveringsprosedyren eller faktisk en kjemisk forandring i de undersøkte materialene.



## Table of Contents

<b>1</b>	<b>INTRODUCTION</b>	<b>- 1 -</b>
<b>1.1</b>	<b>BACKGROUND</b>	<b>- 1 -</b>
<b>1.2</b>	<b>SCOPE OF THESIS</b>	<b>- 2 -</b>
<b>2</b>	<b>THEORY</b>	<b>- 3 -</b>
<b>2.1</b>	<b>THEORY OF SPECIFIC HEAT OF SOLIDS</b>	<b>- 3 -</b>
2.1.1	EINSTEIN'S SPECIFIC HEAT THEORY	- 6 -
2.1.2	DERBY'S SPECIFIC HEAT THEORY	- 8 -
<b>2.2</b>	<b>DSC Q2000</b>	<b>- 11 -</b>
2.2.1	CONVENTIONAL DSC	- 11 -
2.2.2	MDSC	- 13 -
<b>2.3</b>	<b>GAS ADSORPTION IN POROUS MATERIALS</b>	<b>- 15 -</b>
2.3.1	ADSORPTION MODELS	- 16 -
2.3.1.1	Langmuir Method	- 16 -
2.3.1.2	BET Method	- 17 -
2.3.2	POROUS MATERIALS	- 18 -
2.3.2.1	Activated Carbon Norit R0.8	- 18 -
2.3.2.2	Metal-organic Frameworks (MOFs)	- 19 -
2.3.2.2.1	Cu-btc	- 20 -
2.3.2.2.2	Fe-btc	- 22 -
2.3.2.2.3	MIL-100 (Fe)	- 22 -
<b>2.4</b>	<b>THERMODYNAMICS OF THE TEST SAMPLE</b>	<b>- 24 -</b>
2.4.1	CASE 1	- 24 -
2.4.2	CASE 2	- 26 -
2.4.3	CASE 3	- 26 -
2.4.4	CASE 4	- 27 -
<b>2.5</b>	<b>THEORETICAL SUMMARY</b>	<b>- 28 -</b>
<b>3</b>	<b>EXPERIMENTAL</b>	<b>- 29 -</b>
<b>3.1</b>	<b>EQUIPMENT</b>	<b>- 29 -</b>
<b>3.2</b>	<b>PROCEDURES</b>	<b>- 30 -</b>
3.2.1	SAMPLE PREPARATION	- 30 -
3.2.2	ACTIVATION	- 30 -
3.2.3	METHOD FOR MEASUREMENT AND CALIBRATION	- 31 -
<b>3.3</b>	<b>MATERIALS INVESTIGATED</b>	<b>- 32 -</b>
<b>4</b>	<b>RESULTS AND DISCUSSION</b>	<b>- 33 -</b>
<b>4.1</b>	<b>CALIBRATION WITH SAPPHIRE (A-AL<sub>2</sub>O<sub>3</sub>)</b>	<b>- 33 -</b>
<b>4.2</b>	<b>ACTIVATED CARBON NORIT R0.8</b>	<b>- 34 -</b>
<b>4.3</b>	<b>CU-BTC</b>	<b>- 39 -</b>

4.4	FE-BTC	- 46 -
4.5	MIL-100(Fe)	- 50 -
4.6	HEAT CAPACITY MEASUREMENTS FOR ALL POROUS MATERIALS	- 54 -
4.7	POTENTIAL ERROR SOURCES BASED ON EXPERIENCE	- 55 -
<b>5</b>	<b>UNCERTAINTY ANALYSIS</b>	<b>- 59 -</b>
5.1	HEAT CAPACITY UNCERTAINTY ANALYTICAL CALCULATION	- 59 -
5.2	SAMPLE BASIS	- 59 -
5.3	DIFFERENT CASES OVER THE INERT GASES PRESENT IN THE SAMPLE	- 60 -
5.4	VARIATIONS OF THE DIFFERENT PARAMETERS	- 60 -
5.4.1	ESTIMATION OF $\Delta M_{MAT}$	- 60 -
5.4.2	ESTIMATION OF $\Delta M_{GAS}$	- 61 -
5.4.3	DETERMINATION OF $\Delta C_{P MAT}$	- 62 -
5.4.4	ESTIMATION OF $\Delta C_{P GAS}$	- 62 -
5.5	TOTAL UNCERTAINTY FOR THE MEASURED RESULTS	- 64 -
5.5.1	CASE 1 - AIR	- 64 -
5.5.2	CASE 2 - N <sub>2</sub>	- 64 -
5.5.3	CASE 3 - HE	- 64 -
5.5.4	CASE 4 - AIR + H <sub>2</sub> O(G) ADSORBED	- 64 -
<b>6</b>	<b>CONCLUSIONS</b>	<b>- 65 -</b>
<b>7</b>	<b>FURTHER WORK</b>	<b>- 67 -</b>
<b>8</b>	<b>REFERENCES</b>	<b>- 69 -</b>

## **APPENDICES** **I**

Appendix I – Using the DSC	i
Appendix II – Sample List	xi
Appendix III – Selected Data Activated Carbon Norit R0.8	xiii
Appendix IV – Selected Data Cu-btc	xiv
Appendix V – Selected Data Fe-btc	xv
Appendix VI – Selected Data MIL-100(Fe)	xvi
Appendix VII – Heat Capacity Measurement Values Activated Carbon Norit R8.0	xvii
Appendix VIII – Heat Capacity Measurement Values Cu-btc	xix
Appendix IX – Heat Capacity Measurement Values Fe-btc	xxiii
Appendix X – Heat Capacity Measurement Values MIL-100(Fe)	xxv
Appendix XI – Risk Assessment Report	xxix

## List of Figures

FIGURE 2-1: THE HEAT CAPACITY OF SEVERAL SOLID METALS AS A FUNCTION OF THE EINSTEIN TEMPERATURE $\theta_E$ [27].	- 7 -
FIGURE 2-2: THE ACCURACY OF THE EINSTEIN TEMPERATURE AT LOW TEMPERATURES. THE CLASSICAL MODEL IS EFFECTIVE AT TEMPERATURES ABOVE 10 EINSTEIN TEMPERATURES [27].	- 7 -
FIGURE 2-3: EINSTEIN VS. DEBYE. PREDICTED HEAT CAPACITY OF A SOLID, AS A FUNCTION OF TEMPERATURE DIVIDED BY THE DEBYE TEMPERATURE. THE REGION OF THE $T^3$ LAW IS BELOW $0.1\theta$ , AND THE RED LINE CORRESPONDS TO THE CLASSICAL LIMIT OF THE DULONG-PETIT LAW.	- 9 -
FIGURE 2-4: THEORETICAL HEAT CAPACITY DATA CALCULATED BY EINSTEIN'S AND DEBYE'S MODELS AND COMPARED WITH THE EXPERIMENTAL VALUES OF AL (WHITE) AND CU (BLACK) METALS [29].	- 9 -
FIGURE 2-5: GAS ADSORPTION/DESORPTION ISOTHERMS OF A CU MOF ( CU(FMA)(4,4'-BPE) <sub>0.5</sub> ) AT 77 K (N <sub>2</sub> , BLUE; AR, RED; CO, YELLOW) [42].	- 15 -
FIGURE 2-6: (LEFT) NORIT R0.8 PELLETS. (RIGHT) SCANNING ELECTRON MICROGRAPHS OF ACTIVATED CARBON NORIT R0.8 WITH A MAGNIFICATION OF $\times 500$ [52].	- 18 -
FIGURE 2-7: SPECIFIC HEAT CAPACITY OF CARBON (GRAPHITE) [56].	- 19 -
FIGURE 2-8: (LEFT) SEM IMAGES OF CU-BTC [64]. (RIGHT) CU-BTC PELLETS.	- 20 -
FIGURE 2-9: (LEFT) THE METAL COMPLEX (ORANGE) CONSISTS OF TWO COPPER ATOMS COORDINATED BY TEN OXYGEN ATOMS (RED). MIDDLE: THE METAL COMPLEXES ARE INTERCONNECTED BY BTC LIGANDS (C: DARK GRAY). (RIGHT) STRUCTURE OF CU-BTC WITH ORE DIAMETERS OF 5 Å (DARK YELLOW SPHERE) AND 9 Å (LIGHT YELLOW SPHERE) [64].	- 20 -
FIGURE 2-10: (CU <sub>2</sub> (OH)(2,2'-BPY) <sub>2</sub> (BTC) · 2H <sub>2</sub> O) <sub>N</sub> , CU-BTC MOF HEAT CAPACITY EXPERIMENTAL DATA [16].	- 21 -
FIGURE 2-11: (LEFT) SEM IMAGES OF FE-BTC [66]. (RIGHT) FE-BTC GEL.	- 22 -
FIGURE 2-12: (LEFT) SEM IMAGES OF MIL-100(Fe) [66]. (RIGHT) MIL-100(Fe) MATERIAL POWDER.	- 22 -
FIGURE 2-13: STRUCTURE OF MIL-100(Fe). (A) A TRIMER OF IRON OCTAHEDRA AND TRIMESIC ACID. (B) SCHEMATIC VIEW OF ONE UNIT CELL OF MIL-100(Fe). (C) THE TWO TYPES OF CAGES IN POLYHEDRAL MODE. (D) PENTAGONAL AND HEXAGONAL WINDOWS IN BALLS AND STICKS (Fe: GREY; O: RED; C: BLACK).	- 23 -
FIGURE 2-14: TOTAL AND PARTIAL PRESSURE FOR THE AIR AND THE DIFFERENT COMPOUNDS IN THE SAMPLE, RESPECTIVELY.	- 25 -
FIGURE 2-15: THE ENTHALPY BEHAVIOR FOR THE HUMID AIR PRESENT IN THE SAMPLE [70].	- 25 -
FIGURE 2-16: THE ENTHALPY BEHAVIOR FOR THE DIFFERENT GASES THAT CAN BE PRESENT IN THE SAMPLE [70].	- 26 -
FIGURE 3-1: A DIFFERENTIAL SCANNER CALORIMETER (DSC) Q2000 TA INSTRUMENTS INC.	- 29 -
FIGURE 3-2: (LEFT) THE TZERO™ PRESS WITH ITS CORRESPONDING ENCAPSULATION PARTS. (RIGHT) AN ENCAPSULATED SAMPLE WITH TZERO™ PAN AND HERMETIC LID.	- 29 -
FIGURE 3-3: THE ACTIVATION SET-UP. (LEFT) AN ACTIVATION IN PROCESS WITH HEATING BAND, ISOLATION AND CONNECTED TO THE VACUUM PUMP. (RIGHT) SHOW THE PIPE SET-UP WITH ITS CORRESPONDING FOUR METAL END CAPS.	- 31 -

---

FIGURE 4-1: HEAT CAPACITIES OF STANDARD SAPPHIRE ( $A\text{-Al}_2\text{O}_3$ ). EXPERIMENTAL VALUES FOR CALIBRATION (RUN 1-4), TABULATED VALUES (BLUE) [2], AND A TEST RUN AFTER ENDED USE OF THE DSC (ORANGE).....	33 -
FIGURE 4-2: HEAT CAPACITIES OF AC NORIT R0.8 ACTIVATED SAMPLES (1. ACTIVATION – BLACK; 2. ACTIVATION – BLUE).....	34 -
FIGURE 4-3: HEAT CAPACITIES OF AC NORIT R0.8 INACTIVATED SAMPLES (1. SET – GREEN; 2. SET – RED); ACTIVATED SAMPLES (BLACK). ....	35 -
FIGURE 4-4: HEAT CAPACITIES OF AC NORIT R0.8 SELECTED ACTIVATED SAMPLES (1. ACTIVATION – BLACK; 2. ACTIVATION – BLUE).....	36 -
FIGURE 4-5: (LEFT) DEBYE TEMPERATURE FOR CARBON (GRAPHITE AND DIAMOND) VARYING WITH TEMPERATURE [72]. (RIGHT) MOLAR HEAT CAPACITIES FOR SOLIDS ACCORDING TO THE DEBYE FUNCTION [26]. ....	37 -
FIGURE 4-6: ACTIVATED CARBON NORIT R0.8 HEAT CAPACITIES FROM DIFFERENT REFERENCES; MEASUREMENTS FROM THIS REPORT (RED), CARBON (GRAPHITE) VALUES [56] (BLUE), MEASUREMENTS MADE IN EARLIER STUDY [5] (GREEN), AND HEAT CAPACITIES ACCORDING TO THE DEBYE FUNCTION[26, 72] (PURPLE). ....	38 -
FIGURE 4-7: HEAT CAPACITIES OF CU-BTC ACTIVATED SAMPLES (1. ACTIVATION – ORANGE; 2. ACTIVATION (1. AND 2. RUN) – GREEN; 3. ACTIVATION – RED).....	39 -
FIGURE 4-8: HEAT CAPACITIES OF CU-BTC INACTIVATED SAMPLES (1. SET – RED; 2. SET – BLUE; TEST SET – YELLOW/GREEN); ACTIVATED SAMPLES (BLACK).....	40 -
FIGURE 4-9: CU-BTC ACTIVATED SAMPLES; THE THREE FROM THE LEFT ARE SET 1, THE NEXT THREE ARE SET 2, ALL IN CHRONOLOGICAL ORDER ACCORDING TO THE EXPERIMENTAL SEQUENCE, AND THE LAST ONE IS AN INACTIVATED SAMPLE. ....	42 -
FIGURE 4-10: CU-BTC ACTIVATED SAMPLES; THE FIRST ONE FROM THE LEFT ARE A CORRECTLY ACTIVATED SAMPLE, THE NEXT THREE ARE SET 1, THEN THE FOLLOWING THREE ARE SET 2, ALL IN CHRONOLOGICAL ORDER ACCORDING TO THE EXPERIMENTAL SEQUENCE, AND THE LAST ONE AN INACTIVATED SAMPLE. ....	43 -
FIGURE 4-11: HEAT CAPACITIES OF CU-BTC SELECTED ACTIVATED SAMPLES (1. ACTIVATION – ORANGE; 2. ACTIVATION – GREEN).....	43 -
FIGURE 4-12: THE CU-BTC EXPERIMENTAL RESULTS (RED) COMPARED TO OTHER PUBLISHED VALUES FOR BOTH THE SAME CU-BTC MATERIAL (GREEN) AND ANOTHER CUMOF [16] (BLUE), AND COMPARED TO THEORETICAL CU VALUES (PURPLE AND TURQUOISE). ....	44 -
FIGURE 4-13: HEAT CAPACITIES OF FE-BTC ACTIVATED SAMPLES (1. ACTIVATION – BLACK; 2. ACTIVATION – GREEN).....	46 -
FIGURE 4-14: HEAT CAPACITIES OF FE-BTC INACTIVATED SAMPLES (1. SET – PURPLE; 2. SET – ORANGE); ACTIVATED SAMPLES (BLACK). ....	47 -
FIGURE 4-15: FE-BTC ACTIVATED SAMPLES; THE THREE FROM THE LEFT ARE SET 1, AND THE LAST FOUR SET 2, ALL IN CHRONOLOGICAL ORDER ACCORDING TO THE EXPERIMENTAL SEQUENCE. ....	48 -
FIGURE 4-16: FE-BTC ACTIVATED SAMPLES; THE DIFFERENCE BETWEEN THE 1. SET (UP) AND THE 2. SET (DOWN). (RIGHT) THE FE-BTC INACTIVATED GEL. ....	48 -
FIGURE 4-17: HEAT CAPACITIES OF FE-BTC SELECTED ACTIVATED SAMPLES (1. ACTIVATION – BLACK). ....	49 -
FIGURE 4-18: HEAT CAPACITIES OF MIL-100(FE) ACTIVATED SAMPLES (1. ACTIVATION – BLACK; 2. ACTIVATION – BLUE; 3. ACTIVATION – ORANGE/YELLOW). ....	50 -
FIGURE 4-19: HEAT CAPACITIES OF MIL-100(FE) INACTIVATED SAMPLES (1. SET – GREEN; 2. SET – RED); ACTIVATED SAMPLES (BLACK).....	51 -
FIGURE 4-20: MIL-100(FE) ACTIVATED SAMPLES; THE THREE FIRST ONES FROM THE LEFT ARE SET 1, THE NEXT FOUR SAMPLES ARE SET 2, ALL IN CHRONOLOGICAL ORDER ACCORDING TO THE EXPERIMENTAL SEQUENCE, AND THE LAST ONE IS AN INACTIVATED SAMPLE. -	52 -
FIGURE 4-21: MIL-100(FE) ACTIVATED SAMPLES; THE FOUR FIRST ONES FROM THE LEFT ARE SET 1, THE NEXT THREE SAMPLES ARE SET 2, ALL IN CHRONOLOGICAL ORDER ACCORDING	

TO THE EXPERIMENTAL SEQUENCE, AND THE LAST ONE IS AN INACTIVATED SAMPLE. - 52 -

-

FIGURE 4-22: MIL-100(Fe) ACTIVATED SAMPLES SET 3, ALL IN CHRONOLOGICAL ORDER  
ACCORDING TO THE EXPERIMENTAL SEQUENCE. ....- 52 -

FIGURE 4-23: HEAT CAPACITIES OF MIL-100(Fe) SELECTED ACTIVATED SAMPLES (1. ACTIVATION  
– BLACK; 3. ACTIVATION – ORANGE/YELLOW). ....- 53 -

FIGURE 4-24: THE AVERAGE HEAT CAPACITIES FROM THE SELECTED MEASUREMENT CURVES  
FOR EACH MATERIAL MEASURED. ....- 54 -

FIGURE 4-25: EFFECTS FROM AN UNEVEN PAN BOTTOM AFTER A POOR SAMPLE PREPARATION  
[73]. ....- 55 -

FIGURE 4-26: EFFECTS FROM SAMPLE PREPARATION, AND HOW IT AFFECTS THE HEAT FLOW  
[73]. ....- 56 -

FIGURE 6-1: THE AVERAGE HEAT CAPACITIES FROM THE SELECTED MEASUREMENT CURVES  
FOR EACH MATERIAL MEASURED. ....- 66 -

FIGURE 7-1: THE ACTIVATED SAMPLE VALUES FROM MIL-100(Fe), Fe-BTC AND Cu-BTC,  
RESPECTIVELY FROM ABOVE. ....- 67 -





## Nomenclature

### Abbreviations

AC Norit R0.8 – Activated carbon type Norit R0.8

Cu-btc - Copper(II) benzene-1,3,5-tricarboxylate

Fe-btc - Ferric benzene-1,3,5-tricarboxylate

MIL – Materials of Institute Lavoisier

MIL-100(Fe) – iron(III) benzene-1,3,5-tricarboxylate

MOF – Metal-organic framework

DSC – Differential scanning calorimeter

MDSC – Modulated differential scanning calorimeter

LNCS – Liquefied nitrogen cooling system

NTNU – Norwegian University of Science and Technology

BET – Brunauer, Emmet, and Teller

MTN – Framework symmetry

Atm – Atmospheric pressure – 1.01325 (bar)

Sx – Sample number x

Set x – Sample set number x

### Symbols

$C_{\text{mol}}$  – Molar heat capacity ( $\frac{J}{\text{mol}\cdot\text{K}}$ )

$c$  – Specific heat capacity ( $\frac{J}{\text{kg}\cdot\text{K}}$ )

$C_V$  – Heat capacity at constant volume ( $\frac{J}{\text{K}}$ )

$C_p$  – Heat capacity at constant pressure ( $\frac{J}{\text{K}}$ )

$Q$  – Heat flow, energy (J)

T – Temperature (K)

H – Enthalpy ( $\frac{kJ}{kg}$ )

P – Pressure (bar)

U – Thermal energy (J)

W – Work (J)

V – Volume (m<sup>3</sup>)

$\alpha$  – Coefficient of thermal expansion

$\beta_T$  – Isothermal compressibility

S – Entropy ( $\frac{J}{kg \cdot K}$ )

T<sub>f</sub> – Final temperature (K)

R – The universal gas constant - 8.314 (J/mol K)

$\omega_E$  – Einstein frequency (1/s)

N<sub>A</sub> – Avogadro constant - 6.022·10<sup>23</sup> (1/mol)

$\theta_E$  – Einstein temperature (K)

h – Planck constant - 6.626·10<sup>-34</sup> (J·s)

k<sub>B</sub> – Boltzmann constant – 1.3806·10<sup>-23</sup> (J/K)

C<sub>v,E</sub> – Specific heat capacity at constant volume according to Einstein's theory (J/g K)

n – Integer

$\epsilon$  – Energy of an oscillator at a certain temperature (J)

E – Vibrational energy (J)

$\omega_D$  – Debye frequency (1/s)

$\theta_D$  – Debye temperature (K)

C<sub>v,D</sub> – Specific heat capacity at constant volume according to Debye's theory (J/g K)

q<sub>s</sub> – Sample heat flow (J)

R<sub>t</sub> – Resistance of the thermoelectric disc (J/K)

T<sub>s</sub> – Measured sample temperature (K)

$T_r$  – Measured reference temperature (K)

$\Delta T_{rs}$  – Measured sample temperature minus measured reference temperature (K)

$\Delta T_0$  – Measured base temperature of sensor minus measured sample temperature (K)

$R_r$  – Reference sensor thermal resistance (J/K)

$R_s$  – Sample sensor thermal resistance (J/K)

$C_r$  – Reference sensor heat capacity (J/K)

$C_s$  – Sample sensor heat capacity (J/K)

$\text{\AA}$  – Angstrom  $1 \cdot 10^{-10}$  (m)

$P_i$  – Partial pressure (bar)

RH% - Relative humidity (%)

$M_i$  – Molar mass (g/mol)

$Q_{ads}$  – Adsorbed mass (g)

$\phi$  - Relative humidity (%)

$C_p$  – Specific heat capacity (J/g K)

$C_{p\ mat}$  – Specific heat capacity for material (J/g K)

$C_{p\ gas}$  – Specific heat capacity for inert gases (J/g K)

$C_{p\ N_2}$  – Specific heat capacity for nitrogen (J/g K)

$C_{p\ He}$  – Specific heat capacity for helium (J/g K)

$C_{p\ air}$  – Specific heat capacity for air (J/g K)

$C_{p\ H_2O(g)}$  – Specific heat capacity for water vapor (J/g K)

$m_{mat}$  – Mass of material (g)

$m_{total}$  – Mass of sample pan & lid + material (g)

$m_{pan\&lid}$  – Mass of sample pan & lid (g)

$m_{gas}$  – Mass of inert gases (g)

$m_{air}$  – Mass of air (g)

$m_{N_2}$  – Mass of nitrogen (g)

$m_{He}$  – Mass of helium (g)

$m_{\text{H}_2\text{O}(\text{g})}$  – Mass of water vapor (g)

$C_{\text{p mat lower}}$  – Specific heat capacity for material at lower temperature limit (J/g K)

$C_{\text{p mat higher}}$  – Specific heat capacity for material at higher temperature limit (J/g K)

$t$  – Time (s)

$\rho_{\text{air}}$  – Density air ( $\text{kg}/\text{m}^3$ )

## 1 Introduction

### 1.1 Background

The transport sector stands for about 30% of total commercial energy consumption in the world and is said to be the sector with the greatest energy demand growth in the future [1]. Every day passing, new solutions are presented by scientists in literature to lessen our dependence on fossil fuels, and recent years have seen a recognition of the future need for a hydrogen based economy. Hydrogen can be an energy carrier for the future. As a fuel it is both strategic and environmental arising from decreasing oil and gas availability, and a major reduction in air pollution. During the last years there have been great developments in the research of hydrogen use as fuel gas in combination with fuel cells.

Hydrogen storage is one of the main challenges to be conquered for the successful implementation of fuel cell technology and it represents a major materials science challenge. The method of storage currently under consideration includes high pressure gas, liquid hydrogen, adsorption on porous materials, complex hydrides, and hydrogen intercalation in metals.

In the search for new technology, new materials are prerequisite for major breakthrough. One of these classes of functional materials is the metal-organic framework (MOF). The MOFs offer higher surface areas because of its porous structure and a potential for improved adsorption activity than other currently used materials. This makes it attractive for a variety of applications, including: catalysis, gas purification, gas separation, sensing, and gas storage [2-8]. Physical adsorption of hydrogen is favorable for a hydrogen storage technique, and one of the main methods being considered for vehicle applications [6]. Adsorption type storage systems are alternatives that have the potential to reach the goals for handling hydrogen in on-board storage systems. Sorption type materials have been identified as a viable option.

This increased interest revolving these materials comes from their great amount of hydrogen adsorption. Improvements have been reported in both volumetric and gravimetric storage capacity the last decade and currently, maximum excess of hydrogen uptake reported is 7.5 wt.% on metal-organic frameworks (MOF-177) at 77 K and saturation pressure [9].

However, the transient processes during charging and discharging of a storage system play an important role in the utilization of the hydrogen adsorption storage systems, and the heat distribution in the sorption material plays a major role during charging and discharging of a storage system. Finding the heat capacity for new materials, such as MOFs, has attracted many researchers' attentions [10-16].

Norwegian University of Science and Technology (NTNU) participates in a development project of so-called Metal-Organic Framework (MOF) together with Max Planck Institut für Metallforschung and Technische Universität Dresden, both located in Germany. Research has shown that the thermal effects during filling and discharging have a great influence on the utilization of the storage system. The thermal properties of the porous materials such as activated carbons and MOFs need to be characterized for further investigation.

## 1.2 Scope of Thesis

The main objective of this work is to measure specific heat capacity of porous materials at cryogenic temperatures, the working temperature range of the hydrogen adsorption storage system. The heat distribution in the sorption materials used in adsorption processes plays a significant role during charging and discharging of the storage system, it is therefore necessary to measure the heat capacity at these temperatures. In addition there are very little published data for the materials under investigation in this work.

The porous materials that will be measured are activated carbon Norit R0.8, and the MOFs; Cu-btc, Fe-btc and MIL-100(Fe) from -180°C to 150°C, both in an activated and inactivated state. TA Instruments has provided NTNU with a Differential scanner calorimeter (DSC) Q2000 with an appurtenant liquefied nitrogen cooler system (LNCS). This instrument provides a modulated temperature method (MDSC), which gives quite accurate heat capacity results. The inaccuracy is exlaimed to be 5% [17].

The measurements will be performed using this MDSC method and the accuracy of MDSC will be established by comparing the measured heat capacities of standard sapphire ( $\alpha\text{-Al}_2\text{O}_3$ ) with previously reported values [18].

In addition to measuring the porous material's specific heat capacity, is it going to be performed and presented a literature survey on theoretical models and published data for both gas adsorption and heat capacities in porous materials. The experimental results will be compared with published data on reference materials where possible, and an uncertainty analysis on the experimental results presented.

In addition, a detailed measurement method description, all experimental data for the measurements, and a risk assessment report regarding precautions handling with the DSC and different MOFs are attached in appendices.



## 2 Theory

### 2.1 Theory of Specific Heat of Solids

The molar heat capacity is a basic data in chemistry and engineering. It derives to several other important thermodynamic properties, like enthalpy and entropy to mention a few. Advances in science and technology have led to a general realization that limitations in many technical developments are a direct result of inadequate knowledge of the thermophysical properties of materials [19]. This is one of the reasons why it over the years has been very attracting for researchers finding the heat capacity for new materials [12-15].

Heat capacity is known as the internal energy of a system, or the systems microscopic kinetic and potential energy. Heat capacity or thermal capacity  $C$ , is a measurable physical quantity of a substance that characterizes the amount of heat needed to change the temperature of the substance to a given degree, in other words the ratio between the amount of heat transferred to the sample  $\partial Q$ , and the resulting increase in temperature  $dT$ , by the absorbed heat.

$$C = \frac{\partial Q}{dT} \quad (2.1)$$

The property can be specified in different terms, *molar heat capacity*, which is per mole of a pure substance, and the *specific heat capacity*, which is per unit mass of a material.

$C_{\text{mol}}$  – Molar heat capacity ( $\frac{J}{\text{mol}\cdot K}$ )

$c$  – Specific heat capacity ( $\frac{J}{Kg\cdot K}$ )

The quantity of the heat absorbed  $\partial Q$ , depends on the predominant conditions as the temperature increases. It will for instance take a different amount of heat  $\partial Q$ , if the process is at constant pressure than when the process is at constant volume. The two processes most commonly used in thermodynamics are those at constant volume and constant pressure. These are defined by the First Law of Thermodynamics,

$$dU = dQ - dW \quad (2.2)$$

Work as a result of compression or expansion of a closed systems volume can be expressed by its pressure  $P$ , and its differential volume  $dV$ . With a process at constant volume, you get the definition of *heat capacity at constant volume* by dividing every term in (2.2) with the differential temperature,  $dT$ .

$$C_V = \left(\frac{\partial U}{\partial T}\right)_V = \left(\frac{\partial Q}{\partial T}\right)_V \quad (2.3)$$

The definition of *heat capacity at constant pressure* is derived from the First Law of Thermodynamics and the enthalpy of the system,

$$dH = dU + d(PV) \quad (2.4)$$

Combining (2.2) and (2.4), at constant pressure and dividing every term with the differential temperature  $\partial T$ , gives  $C_P$ .

$$\left(\frac{\partial H}{\partial T}\right)_P = \left(\frac{\partial Q}{\partial T}\right)_P = C_P \quad (2.5)$$

The heat capacity is usually referred to in literature as the volumetric heat capacity  $C_V$ , because it is more fundamental than the heat capacity at constant pressure  $C_P$ . However, measuring heat capacity at constant volume can for liquids and solids be very difficult because of the change in volume with increasing or decreasing temperature. Maintaining a constant volume requires very high pressures, it is therefore easier to measure heat capacity at constant pressure and solve the  $C_V$  using mathematical relationships derived from the basic thermodynamic laws. [20]

$$C_P - C_V = VT \frac{\alpha^2}{\beta_T} \quad (2.6)$$

Heat capacity of a sample is directly proportional to the amount of substance it contains. However, when divided by its own quantity, the resulting specific heat capacity is a function of its own substance structure. More precisely, it depends on how many degrees of freedom available in the substance particles. A degree of freedom is any form of energy in which heat transferred into an object can be stored. The heat transferred to the material can be absorbed in several ways. For instance an increase in the kinetic energy of the molecules is one form of absorbing energy, and for “monoatomic” molecules, it is the only way to absorb energy from the surroundings. Other forms of absorption can be an increase in energy that leads to an increase in translational motion, vibrational motion and rotational motion. This implies that the number of bonds in a molecule is proportional to the number of ways energy can be stored, since each bond can absorb some energy for vibrational motion and for rotational motion. However, this is only valid at high temperatures, but it gives some understanding on how molecular heat capacity depends on molecular structure.

Kinetic energy is the only of the degrees of freedom which manifests in a temperature change in the substance. This gives every degree of freedom available in the samples particles, except for the kinetic energy, an increase in the specific heat capacity for the substance. In other words the substance heat capacity is a measure of how it stores additional energy at the molecular level as it is heated. If the material is a crystal for example, and can only vibrate, it has a low heat capacity, but if the structure gives room for rotation and translation as well, then the heat capacity is higher. One can say that the heat capacity indicates changes in structure. This means that in any case except for monoatomic molecules is the heat capacity depending on the temperature, and it increases with temperature. One way of explaining it could be considering statistical thermodynamic concepts, whereas the temperature increases implies that the molecules can exist in a larger number of states and access several levels of rotation and vibration. This is the opposite of a molecule at low temperatures which do not have all energy levels accessible. This means that from having a solid at a finite low temperature with its rotational and vibrational degrees of freedom not fully available, an increase in temperature increase the ability of the solids molecules to absorb energy, thus  $C_V$  and  $C_P$  normally increases with temperature.

For gases, the volumetric heat capacity never reaches a minimum lower than  $3/2 R$  per mole, where  $R$  is the ideal gas constant. This is because the kinetic energy of gas molecules always is able to store this much heat energy. Solids, on the other hand, will for cryogenic temperatures have a heat capacity that falls towards zero as temperature approaches absolute zero [21] [22].

In order to prove that the heat capacity must be zero at zero temperature one need to begin with the definition of entropy.

$$TdS = \delta Q \quad (2.7)$$

Then the absolute entropy can be calculated by integrating from zero Kelvin to the final temperature,  $T_f$ .

$$S(T_f) = \int_{T=0}^{T_f} \frac{\delta Q}{T} = \int_0^{T_f} \frac{\delta Q}{dT} \frac{dT}{T} = \int_0^{T_f} C(T) \frac{dT}{T} \quad (2.8)$$

This shows that to avoid that the integral yield infinite absolute entropy at zero temperature, and the violation of the third law of thermodynamics, heat capacity needs to approach zero as well.

Pierre Louis Dulong and Alexis Thèrèse Petit published in 1918 the results of their measurements on the specific heat capacity at constant pressure of thirteen solid elements at room temperature [23]. The observations made from these measurements showed that all solids had a heat capacity of approximately  $2.49 \times 10^4 \text{ J/kmol K}$  at around 298 K [19]. The explanation considered every atom inside the solid as a three-dimensional oscillator with six degrees of freedom, where each atom has an internal energy of  $1/2 k_B T$  at thermal equilibrium contributed by the degree of freedom. The heat capacity at constant volume for a gram-atom of an element which has  $N_A$  atoms is obtained by differentiating the internal energy with respect to temperature at constant volume.

$$\left(\frac{\partial E}{\partial T}\right) = C_V = 3N_A k_B = 3R \quad (2.9)$$

This explanation, which was according to Petit and Dulong the foundation for the heat capacity for solids, was not sufficient when Weber in 1875 [24] showed that the atomic specific heat capacity of silicon, boron, and diamond were found to be lower than the values predicted. The heat capacity decreased as temperature approached absolute zero, while the degrees of freedom do not slow down or cease to move. An additional model was therefore needed to explain this deviance.

Two main theories were developed to explain the deviation in Dulong and Petits heat capacity experiments. The first was constructed by Einstein and the second was authored by Debye.

### 2.1.1 Einstein's Specific Heat Theory

In 1907 published Einstein [25] a simple model for specific heat capacity. The model accounted for the decrease in specific heat at low temperatures below the values already obtained at elevated temperatures to be  $3R$ . When investigating the theory, three assumptions were made. Firstly he assumed that every solid was composed of lattice structure that consisted of  $N_A$  atoms. Each atom moved independently in three dimensions within the lattice, or in other words each atom had three degrees of freedom. This assumption was supported by his experimental data.

However, secondly he assumed that each of the atoms inside the lattice did not interact with each other, which cannot be true for several reasons. If the atoms could not interact within the solid, that would mean that neither sound could propagate through it nor heat transfer through it. When energy is added to the system, the oscillators in a solid interact much in the same way as the molecules in a solid interact to transfer heat, and it is the extent of these interactions that lead to the physically observed heat capacity.

Thirdly he assumed that all the atoms inside the solid would vibrate with the same frequency  $\omega_E$ . This third assumption is actually the point that highlights the main difference between Einstein's and Debye's heat capacity models.

The energy of the oscillators Einstein quantized in accordance with the results obtained by Planck, which stated that a harmonic oscillator does not have a continuous energy spectrum, but can accept energy values equal to an integer  $n$ , times Planck constant  $h$ , and the frequency  $\omega_E$ .

$$\epsilon = n h \omega_E \quad (2.10)$$

The average energy of an oscillator at temperature  $T$ , according to the Planck distribution function [26], is

$$\bar{\epsilon} = \frac{h \omega_E}{e^{h \omega_E / k_B T} - 1} \quad (2.11)$$

Every atom has in Einstein's model three degrees of freedom, which makes the vibrational energy ( $E$ ) of a solid element containing  $N_A$  atoms equivalent to  $3N_A$  harmonic oscillators, each vibrating independently at frequency  $\omega_E$ . However, the average energy of an oscillator is according to results obtained in quantum mechanics [19] showed to be

$$\bar{\epsilon} = \frac{h \omega_E}{2} + \frac{h \omega_E}{e^{h \omega_E / k_B T} - 1} \quad (2.12)$$

The specific heat capacity for one atom of an element is obtained by differentiating the average energy of  $N_A$  atoms, and the result is the same whether differentiating the average energy equation according to Planck (2.11) or quantum mechanics (2.12),  $\left(\frac{\partial E}{\partial T}\right)_V$ . In any case the specific heat capacity at constant volume is therefore

$$C_{V,E} = 3N_A k_B (x)^2 \frac{e^x}{(e^x - 1)^2}, \quad x = \frac{h \cdot \omega_E}{k_B \cdot T} = \frac{\theta_E}{T} \quad (2.13)$$

The Einstein characteristic temperature is defined as

$$\theta_E = \frac{h\omega_E}{k_B} \tag{2.14}$$

This temperature is different for every solid and reflects the rigidity of the lattice.

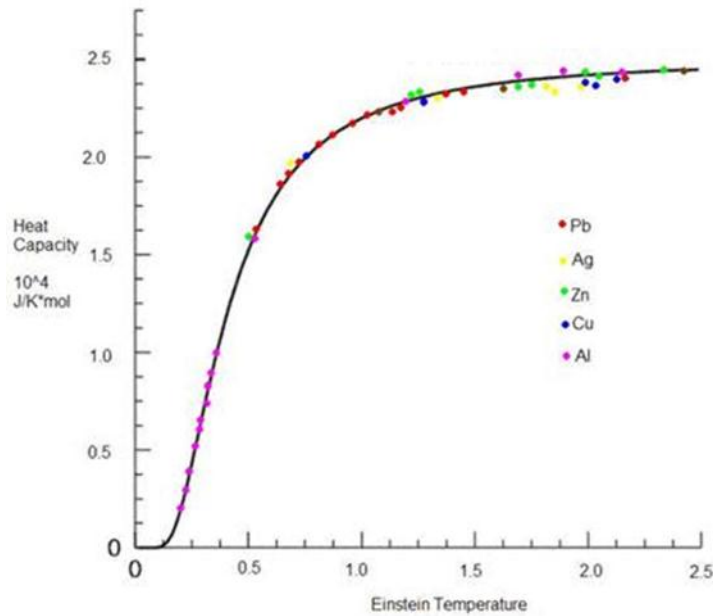


Figure 2-1: The heat capacity of several solid metals as a function of the Einstein temperature  $\theta_E$  [27].

At the high temperature limit, when  $T \gg \theta_E$  (and  $x \ll 1$ ) [19], the Einstein heat capacity reduces to  $C_V = 3R$ , and Einstein’s theory yields the classical Dulong and Petit value.

At the low temperature limit, when  $T \ll \theta_E$  (and  $x \gg 1$ ),  $C_V \rightarrow 0$  as  $T \rightarrow 0$ . This corresponds to what is required by the third law of thermodynamics. While the heat capacity according to (2.13) should approach zero exponentially indicates experimental evidence that  $C_V$  approaches zero more slowly than this [19]. This discrepancy from Einstein’s predicted values may be explained on the basis of his assumption that each atom in a solid vibrates independently of the others, but with the exact same frequency.

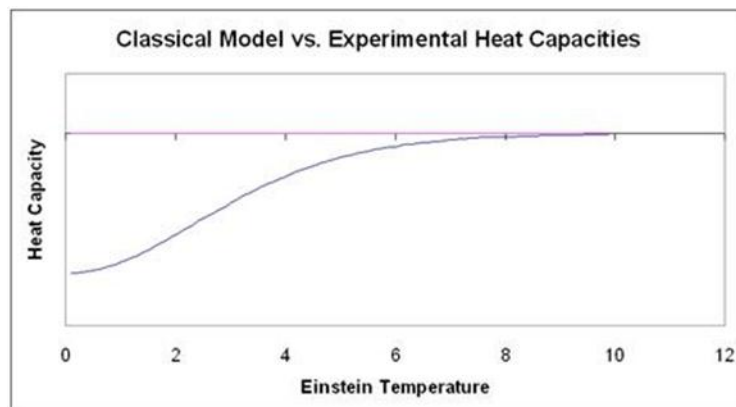


Figure 2-2: The accuracy of the Einstein temperature at low temperatures. The classical model is effective at temperatures above 10 Einstein temperatures [27].

### 2.1.2 Derby's Specific Heat Theory

In 1912 published Peter Debye Debye's theory of specific heat [28]. Debye's model treats the vibrations of the atomic lattice as phonons in a box, each with its own frequency. The Einstein model on the other hand, treats the solid as many individual, non-interacting harmonic oscillators, each with the exact same frequency. Debye assumes the continuum model for all possible vibrational modes of the solid, where the wavelength is large compared with the interatomic distances, and a solid may appear like a continuous elastic medium. He has also given a limit to the total number of vibrational modes equal to  $3N_A$ , and the frequency spectrum is cut off in order to comply with a total of  $3N_A$  modes. This procedure should provide a maximum frequency  $\omega_D$  (Debye frequency), which is common to both longitudinal and transverse modes.

Debye improved Einstein's theory by treating the coupled vibrations of the solid in terms of  $3N_A$  normal modes of vibration of the whole system, each with its own frequency. He associated therefore each vibrational mode with an independent harmonic oscillator of the same frequency and obtained an expression for the vibrational energy [19, 26, 29, 30].

$$\bar{E} = 9N_A k_B T \left(\frac{T}{\theta_D}\right)^3 \int_0^{x_D} dx \frac{x^3}{e^x - 1} \quad (2.15)$$

$$x_D = \frac{h\omega_D}{k_B T} = \frac{\theta_D}{T} \quad x = \frac{h\omega}{k_B T} \quad (2.16)$$

The lattice heat capacity at constant volume is calculated by differentiating (2.15) with respect to the temperature  $\left(\frac{\partial \bar{E}}{\partial T}\right)_V$ .

$$C_{V,D} = 9N_A k_B \left(\frac{T}{\theta_D}\right)^3 \int_0^{x_D} dx \frac{x^4 e^x}{(e^x - 1)^2} \quad (2.17)$$

The Debye heat capacity depends only on the Debye temperature  $\theta_D$ .

At high temperatures, when  $T \gg \theta_D$  (and  $x_D \ll 1$ ), the Debye heat capacity reduces to

$$C_{V,D} = 3N_A k_B = 3R \quad (2.18)$$

At very low temperatures, when  $T \ll \theta_D$  (and  $x_D \gg 1$ ), the upper limit of integration in the equation for vibrational energy (2.15) may be replaced by infinity since  $\frac{h\omega}{k_B T} \rightarrow \infty$  as  $T \rightarrow 0$ .

$$\int_0^\infty dx \frac{x^3}{e^x - 1} = \int_0^\infty dx x^3 \sum_{s=1}^\infty e^{-sx} = 6 \sum_{s=1}^\infty \frac{1}{s^4} = \frac{\pi^4}{15} \quad (2.19)$$

This gives

$$C_{V,D} = \left(\frac{\partial \bar{E}}{\partial T}\right)_V \cong \frac{12\pi^4}{5} N_A k_B \left(\frac{T}{\theta_D}\right)^3 \quad (2.20)$$

The heat capacity will in low temperatures be proportional to  $T^3$ , the Debye  $T^3$  approximation, and in high temperatures it also recovers the Dulong-Petit law, but due to simplifying assumptions the accuracy at intermediate temperatures will suffer [26].

This approximation has now been restricted to  $T < \frac{\theta_D}{50}$  as a result of more recent theoretical work on specific heat studies [26, 31].

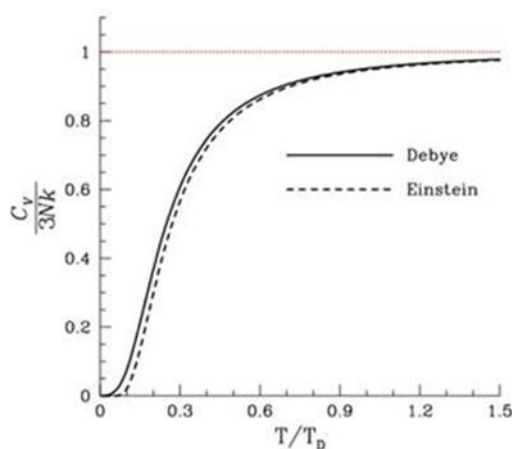


Figure 2-3: Einstein vs. Debye. Predicted heat capacity of a solid, as a function of temperature divided by the Debye temperature. The region of the  $T^3$  law is below 0.10, and the red line corresponds to the classical limit of the Dulong-Petit law [32].

This is a marked improvement on Einstein’s theory.

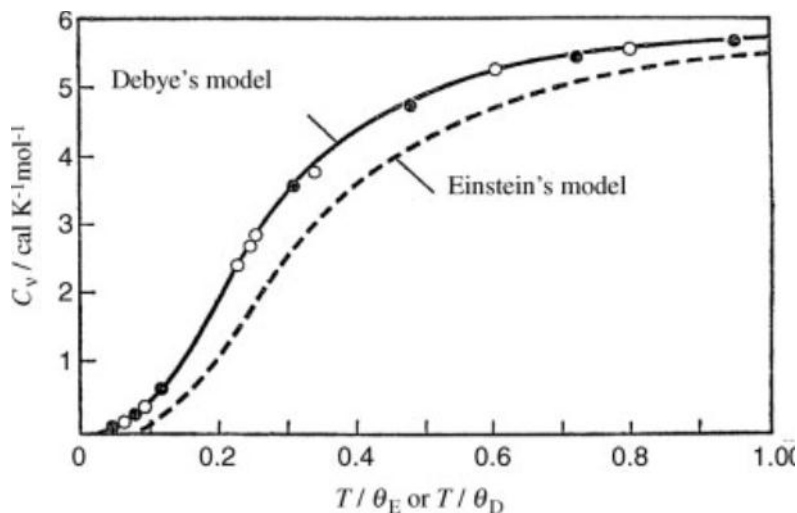


Figure 2-4: Theoretical heat capacity data calculated by Einstein’s and Debye’s models and compared with the experimental values of Al (white) and Cu (black) metals [29].



In recent years have accurate values from specific heat calorimetric measurements at low temperatures ( $T < 5$  K) revealed that Debye's equation for heat capacity does not fit the experimental results perfectly. It was also observed that Debye's temperature  $\theta_D$ , which according to his theory is constant, vary with temperature. This discrepancy in Debye's model may be explained on the base of his approximation made in treating solids as a continuous elastic media and neglecting the discreteness of the atoms [19].

## 2.2 DSC Q2000

Differential scanning calorimetry (DSC) has been used for more than thirty years to measure a wide variety of material properties, including heat capacity. DSC measurements are normally quite simple, fast and accurate, but heat capacity measurements usually require a minimum of three experiments and a normal accuracy provided is typically only  $\pm 10\%$  [17].

TA Instruments Q2000 Tzero™ DSC has developed and implemented an improved approach to make DSC measurements. This has made heat capacity measurements more easy and possible to measure in a single run and with an accuracy typically better than  $\pm 5\%$  [17].

### 2.2.1 Conventional DSC

The differential scanning calorimeter (DSC) is a technique that was developed by E. S. Watson and M. J. O'Neill in 1962 [33], where the term DSC initially was meant to describe an instrument that directly measured energy and allowed for precise heat capacity measurements [34]. It is now a fundamental tool in thermal analysis and precise measurement of heat capacities has distinctly been improved with modern DSCs [35]. DSC means the measurement of the change of the difference in the heat flow rate to the sample and to a reference sample while they are subjected to a controlled temperature program.

The heat capacity measurements in this report were performed on a DSC Q2000 (Tzero™ DSC-technology, TA Instruments Inc., USA). The Q2000 consists of three different main components; the instrument itself containing all the system electronics, the cell, which monitors the heat flow and temperature, and the cooling accessory [36].

In the cell, which is designed for both heating and cooling, are the sample and reference pan both situated on a thermoelectric disc surrounded by a furnace. Heat is transferred through the thermoelectric disc to both pans, and the differential heat flow to the pans is measured with the thermal equivalent of ohm's law as a base [37].

$$q_s = \frac{\Delta T_{rs}}{R_t} \quad (2.21)$$

This is a simplified model of the heat flow that does not take into account extraneous heat flow within the sensor or between the sensor and sample pan. A feature called Tzero™ takes into account exactly this, how DSCs always exhibit a substantial heat flow offset even without a sample present. This heat flow is strongly dependent on heating rate, temperature and other factors. To obtain good Cp results from an ordinary DSC it has been necessary to subtract an empty pan baseline run under identical conditions as for the experiment made. The instrument baseline means the residual heat flow signal of the DSC when operated empty.

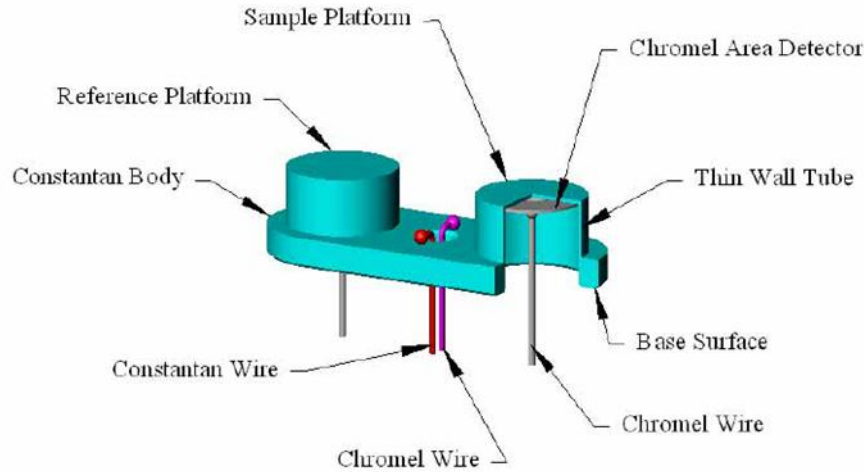


Figure 1: The constantan sensor, area thermocouple and Tzero™ thermocouple [38].

The cell sensor has two separated raised platforms to hold the sample and reference, which are connected by thin-walled tubes to the heating block (base) [39]. These thin-walled tubes create thermal resistances between the platforms and the base. In addition to the thermocouples on the underside of each platform measuring the temperature of the sample and reference, the Q2000 DSC provides a third chromyl thermocouple located between the reference and sample sensor, referred to as the Tzero™ thermocouple. This sensor acts like an independent measurement and control sensor and get the temperature at the base. This gives a thermal network model and a more complete heat flow equation (2.22), because it incorporates cell resistance and capacitance characteristics which were previously assumed to be negligible and accounts for the asymmetries in the cell.

$$q = -\frac{\Delta T_{rs}}{R_r} + \Delta T_0 \left( \frac{R_r - R_s}{R_r \cdot R_s} \right) + (C_r - C_s) \cdot \frac{dT_s}{dt} - C_r \frac{d\Delta T_{rs}}{dt} \quad (2.22)$$

The first term in (2.22) is the equivalent to (2.21). The second term accounts for the difference between the sample and the reference resistances, while the third term accounts for the difference in their capacitances. These terms have the biggest effect on the equation when the heat capacity of the sample is the dominant contributor to heat flow, which is during regions of the thermal curve. The fourth term on the other hand, which accounts for the difference between the sample and reference heating rate, has its largest impact during enthalpy events like melting.

This equation leaves out the pan heat flow effects, but this is accounted for when choosing a heat flow term. The Q2000 provide T1, T4 and T4P heat flows which accounts for pan effects. When measuring heat capacity only T4 and T4P heat flow are fit to use.

In this standard mode, heat flow is continuously converted to heat capacity as described in (2.23).

$$C_p = \frac{\text{Heat Flow} \left[ \frac{W}{g} \right]}{\text{Heating Rate} \left[ \frac{^{\circ}C}{min} \right]} \times K \text{ (Calibration Constant)} \quad (2.23)$$

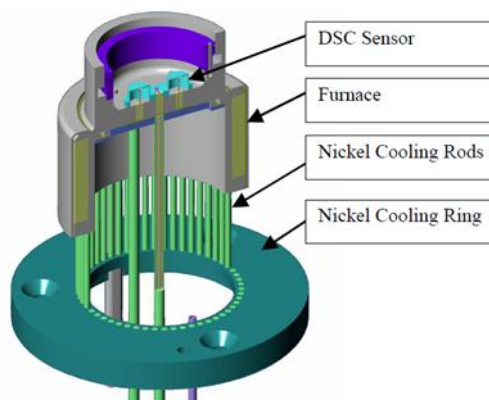


Figure 2: The furnace, cooling rods and cooling ring [40].

Surrounding the cell are the cooling rods and ring, and the furnace. An array of nickel cooling rods connects the silver furnace with the cooling ring, while the high thermal conductivity furnace uses rugged windings for enclosing the transducer [41]. Purge gas is here preheated before added into the sample chamber accurately dosed by digital mass flow controllers.

The cooling accessory elected for the device depends on the desired temperature range. The cooling accessory chosen was a liquefied nitrogen cooling system (LNCS), which allows automatic continuous temperature control within the range of  $-180^{\circ}\text{C}$  to  $550^{\circ}\text{C}$  [37].

### 2.2.2 MDSC

In the MDSC a more complex heating profile, or in other words temperature regime, is applied to the sample than is used in conventional DSC. It is an even more accurate method, and gives an accuracy of  $\pm 5\%$  as opposed to  $\pm 10\%$  in the conventional DSC method [17]. The conventional DSC method directly measures heat changes that occur in molecules during controlled increase or decrease in temperature. This method was initially proposed by Reading et al. [14], they applied a small sinusoidal modulation of a temperature superimposed onto an underlying linear heating rate. This gives a net effect so that the heat flow can be measured simultaneously with changes in heat capacity and is therefore very well suited for obtaining more accurate heat capacity results. This was added as an extension of the conventional DSC, and is a method recently developed to directly determine heat capacities for various materials isothermally and non-isothermally.

One of the major benefits with this technique is the ability to measure heat capacity in a quasi-isothermal mode, which means isothermal only with the exception of a small temperature modulation. In the MDSC, the standard DSC heat flow is called the total heat flow and contains the sum of all thermal transitions just as in the standard DSC. The heat capacity component is called the reversing heat flow and this signal contains the glass and melting transitions. The last component, the kinetic component, is called the nonreversing heat flow and contains the kinetic

events like curing, volatilization, melting and decomposition. These components are expressed respectively in equation (2.24).

$$\frac{dH}{dt} = C_p \frac{dT}{dt} + f(t, T) \quad (2.24)$$

Reversing heat capacity (MDSC mode) is measured in the same experiment used to measure DSC heat capacity and has therefore several significant advantages over just the DSC heat capacity measurement. Because of the way it is measured is it usually more accurate and reproducible, and the MDSC provides a check of the heat capacity as measured in the faster DSC single-run approach.

$$\textit{Reversing } C_p = \frac{\textit{Amplitude of Modulated Heat Flow} \times K_{C_p}(\textit{Calibration Constant})}{\textit{Amplitude of Modulated Heating Rate}} \quad (2.25)$$

By using amplitudes (total change) rather than absolute values for the heat flow and heating rate signals, the effect of baseline drift or curvature are eliminated. It means that runs, or experiments, are made over long periods (days) without any concerns for baseline drift, because the amplitude is not influenced by baseline.

### 2.3 Gas Adsorption in Porous Materials

Physical adsorption, or physisorption, can be described as a process where the adsorbed molecules dissolve in the solvent, but remain chemically unchanged [42]. In case of gas on solid adsorption, is the sorbent a solid material on which the physical adsorption occurs and the adsorbate a gas in adsorbed state. This process is a way of selectively store gases of interest. The gas molecules are weakly held at the surface of sorbents material by Van der Waals forces, typically at low temperatures and moderate pressures (<10 MPa), and when the system pressure is lowered or temperature is raised, the adsorbed gas molecules can be readily released. Furthermore this sorption process is fully reversible.

Several porous materials have been evaluated for selective gas adsorption [5, 43] including numerous types of carbonaceous materials and most recently, the new type, metal-organic frameworks (MOFs). It is the high surface area of very many MOFs, which can exceed 5000 m<sup>2</sup>/g (BET surface), in combination with micropores of diameters < 20 Å that leads to perfect conditions for physisorptive storage of small sorbent molecules, such as hydrogen, methane or carbon dioxide. Very promising hydrogen uptake values have been measured at low temperatures, but owing to the weak interaction of hydrogen with the framework, has the storage capacity for MOFs at room temperature not yet reached a good enough level for technological applications [44].

Gas sorption experiments published in [43] show that some MOFs and porous materials can selectively adsorb H<sub>2</sub> and CO<sub>2</sub> over N<sub>2</sub> and Ar. They also show adsorption capacities of the excluded gases almost equal to zero. Thus this was a selectivity attributed to the small aperture of the channels. This selective adsorption of H<sub>2</sub> over N<sub>2</sub> due to size exclusion was also observed in various porous materials. Another interesting ability is that MOFs selectively could adsorb O<sub>2</sub>, but not N<sub>2</sub> at low temperatures due to the pore size exclusion effect, even though the two molecules are similar in size. This indicates that although the pores size and shape of an adsorbent are the major factors in determining the adsorption selectivity of guest molecules, is the nature of the guest-surface interaction also important.

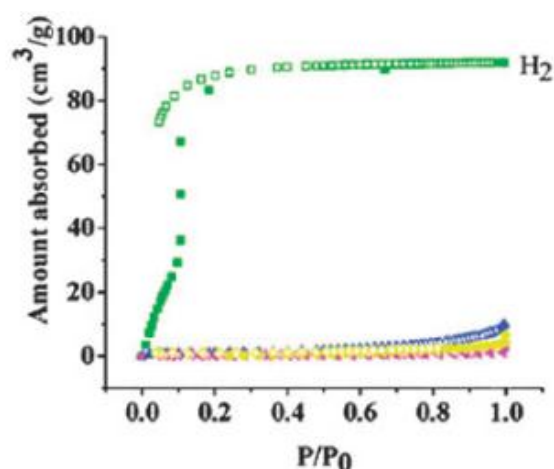


Figure 2-5: Gas adsorption/desorption isotherms of a Cu MOF ( Cu(fma)(4,4'-bpe)<sub>0.5</sub> ) at 77 K (N<sub>2</sub>, blue; Ar, red; CO, yellow) [43].

It has previously been demonstrated that for other microporous materials than MOFs, such as activated carbons or zeolites, that the amount of hydrogen adsorbed per unit mass is proportional to the adsorbent's specific surface area and pore size [3, 45, 46]. The strategies for improving the adsorption capacity has therefore involved increasing the BET specific surface areas and micropore volumes of the porous materials. It is also seen that narrower micropores have a larger influence on hydrogen adsorption characteristics, while larger pores are less significant [6]. MOFs have been stated as optimal candidates for hydrogen storage based on physisorption, because of their exceptionally high specific surface area and microporosity. On the other hand are these high storage capacities only reached at lower temperatures, because of the low adsorption enthalpy involved in physisorption. There are therefore directed great efforts towards the development of new materials showing higher adsorption enthalpies [45].

The most striking difference between materials such as activated carbons and MOFs is probably the total lack of non-accessible bulk volume in MOF structures. High surface areas are already known from activated carbons, but it is the absence of any dead volume in MOFs which on a weight-specific basis gives them the highest porosities and world record surface areas, and makes them quite useful for volume specific applications like adsorption [2]. Changing the array of metal clusters separated by organic linkers gives rise to different nanosize cages, or cavities, for selectively accommodating adsorbed molecules in MOFs. However, the decrease of hydrogen surface density for high surface area MOFs shows that the large surface areas in current MOFs are not effectively utilized for adsorbing hydrogen. The design of framework is therefore very important when maximizing hydrogen adsorption capacity on both gravimetric and volumetric basis [7].

### 2.3.1 Adsorption Models

To provide a representative link between process pressure and temperature with hydrogen uptake in an adsorbent is it necessary with a correlation between the two. It is rather important to understand the dynamic thermal behavior of cryo-adsorption storage, especially during filling and discharging operations, when studying hydrogen storage. The most common models used for the gas uptake are the Langmuir model and the BET adsorption isotherms [3]. The Langmuir model is more applicable for monolayer adsorption, while the BET model is an extension of the Langmuir model and assumes multilayer adsorption.

#### 2.3.1.1 Langmuir Method

Langmuir published in 1916 [47] and 1918 [48] a theory verified through a series of experiments. The theory is based on a kinetic model of the adsorption process, and several other assumptions. Firstly, that adsorption only occurs at a limited number of specific areas and that the saturation coverage corresponds to a complete occupancy of these areas. Secondly, that adsorption is restricted to a single monolayer, and the adsorption energy constant. Thirdly, that the molecules or atoms adsorbed do not undergo a phase transition, and that a dynamic equilibrium is reached

between the gas phase and the adsorbed state when the rates of adsorption and desorption are equal. Finally, that the interaction between adjacent adsorbed molecules or atoms is negligible, and that the probability for an adsorption/desorption in adjacent areas is independent of the other probabilities [3, 49].

### *2.3.1.2 BET Method*

BET method is a standard procedure for measuring surface areas in different materials, and is obtained by applying the theory of Brunauer, Emmet, and Teller [50] to nitrogen adsorption isotherms measured at 77 K. The BET equation reduces to the Langmuir equation by putting the finite number of molecular layers,  $N = 1$ . This would mean that applied to the monolayer region of adsorption isotherms for  $N_2$  at 77 K that both equations should lead to the same result. However, there is no general agreement between both equations concerning their application and derived surface area values [49]. The method gives possibility to compare the surface areas among different porous materials and also among benchmark materials from the literature.

The comparison is an advantage, but the method is based upon several assumptions [51], some of them very relevant with respect to metal-organic frameworks. The BET analysis assumes that adsorption occurs by multilayer formation, and that the number of layers adsorbed is infinite at the saturation pressure. In other words it assumes that the adsorption occurs as if on a free surface [52].

This assumption may break down, because it has been suggested that the adsorption in MOFs occurs through a pore-filling mechanism rather than by layer formation. However, the positions of the metal-organic framework atoms are known from crystallography, and this makes it possible to calculate the materials “accessible” surface area by making it a geometrical problem, in contrast to the BET method. The surface area defined as “accessible” is calculated by considering an adsorbate molecule and its center of mass rolling along the surface of the material in question. This in turn may give the incorrect surface area because the actual MOF can have defects caused by its synthesis, such as portions of the crystal collapsing.

Using molecular modeling to calculate nitrogen adsorption isotherms for a series of MOFs can provide a definitive test proving the BET methods reliability. The molecular modeling provides simulated isotherms which can be used to calculate the surface areas by using both methods, the Bet method and geometrically. These two methods can then be compared, because the same precisely known crystal structure is used. A study done in 2007 [51] show that the BET theory applied to experimental nitrogen isotherms is a valuable method for characterizing porous, crystalline materials. It is even valuable for MOFs, which have surface areas of thousands of  $m^2/g$  with pores that are the opposite of the flat surface areas used in deriving the BET theory.



### 2.3.2 Porous Materials

The best candidates for storing hydrogen in molecular form could be classified in two groups: Carbon materials and metal-organic frameworks [3]. The focus in this present work is measuring heat capacities of the compounds Cu- btc, Fe-btc and MIL-100 MOFs and AC-Norit R0.8 at cryogenic temperatures.

#### 2.3.2.1 Activated Carbon Norit R0.8

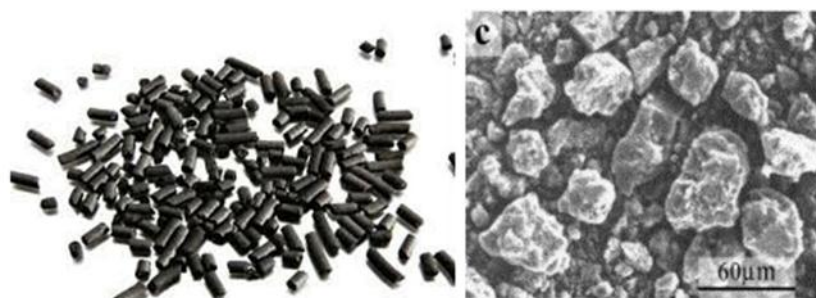


Figure 2-6: (Left) Norit R0.8 pellets. (Right) Scanning electron micrographs of activated carbon Norit R0.8 with a magnification of  $\times 500$  [53].

Microporous activated carbons used at 77 K appear as a very good candidate for hydrogen adsorptive storage [54], due to their microporous characteristics and accessibility at industrial level, and low cost. Activated carbon type Norit R0.8 is a steam activated extruded carbon produced by steam activation of peat under carefully controlled conditions. The adsorbent has a BET surface area of  $1385 \text{ m}^2/\text{g}$  and a bulk density of  $0.4 \text{ g/ml}$  [3]. It offers excellent adsorption properties and is often used for removal of impurities from water and industrial process applications [55].

Previous publications have used this material in hydrogen storage tests [56] and corresponding heat capacity measurements [3]. This publication shows specific heat capacity measurements with rather low values,  $0.15 \text{ J/g K}$  around 273 K. This is rather low considering activated carbon consisting mainly of carbon (graphite) and should therefore have specific heat capacity values similar to those of carbon.

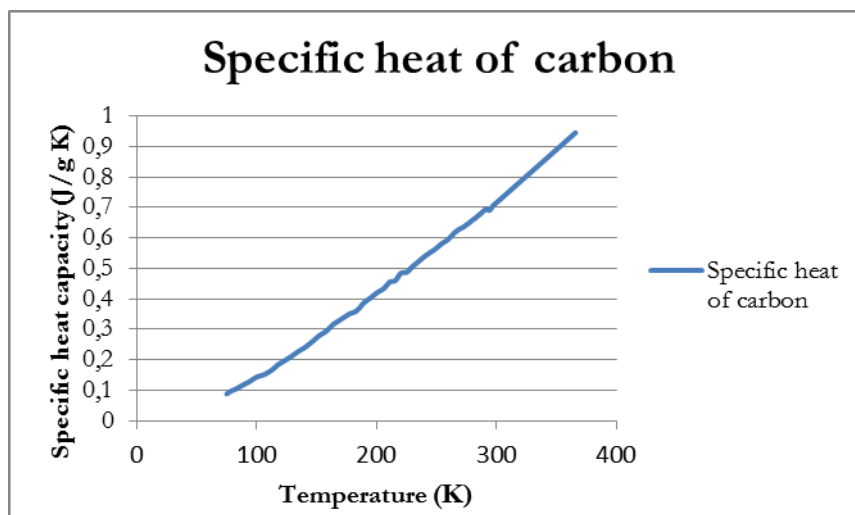


Figure 2-7: Specific heat capacity of carbon (graphite) [57].

Carbon's specific heat capacity at 273 K is about 0.64 J/g K [19], which is more than four times bigger than 0.15 J/g K. New specific heat capacity measurements for AC-Norit R0.8 would therefore be preferable to either prove or disprove this hypothesis.

### 2.3.2.2 Metal-organic Frameworks (MOFs)

MOF is a diverse and rapidly growing class and can be very useful in gas storage, in this context hydrogen storage [4-8]. The material was already mentioned by Tomic in 1965 [58]. However when O. M. Yaghi and his coworkers published the structure of MOF-5 (IRMOF-1) in late 1999, [59] and in 2002 published the concept of reticular design with totally different carboxylate linkers, [60-62] the field was again lighted interest upon. Nowadays there are several hundred different types of MOFs identified.

The metal-organic frameworks are crystalline compounds that consist of metal-carboxylate units, metal ions and organic linkers, thereby its first term “metal-organic”. These metal ions are coordinated to rigid the organic molecules to form one-, two-, or three-dimensional structures that can make the framework very porous, as described by its second term [63]. It is further shown that MOFs specific properties and structure depends strongly on the type of metal and linker chosen. This is used during the syntheses of MOFs, where it is possible to design or tailor the porosity of novel compounds from micro to nanopore scale. This self-assembly of metal-ions, acting like the coordination centers, linked with different polyatomic organic bridging ligands, together with the tailored porosity, results in robust solids with high thermal and mechanical stability [2].

In spite of versatile advantages of porous MOFs, which include tailor-made pore structures controllable porosity by change of organic ligands and metal subunits, most of the MOFs suffer from a lack of hydrothermal stability. Structural damage to a MOF that can be caused by moisture at processing conditions or during regeneration will strongly limit the utilization of a MOF as a sorbent for industrial applications [64].

The research activities done the last years on these materials, because of their combination of unbelievable levels of porosity, surface area, pore size and wide chemical inorganic-organic composition, has brought over 1000 publications on “metal-organic frameworks” and “coordination polymers” per annum [2].

### 2.3.2.2.1 Cu-btc

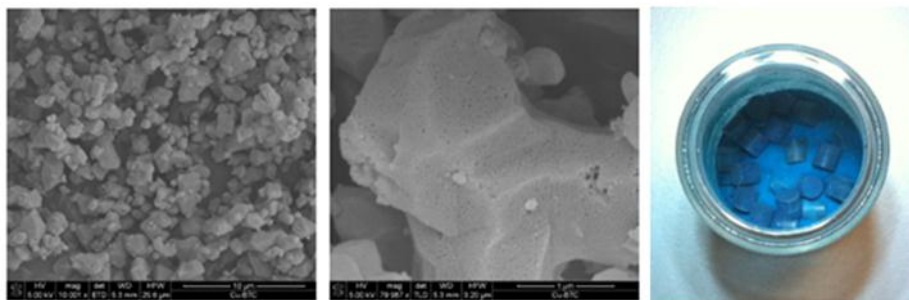


Figure 2-8: (Left) SEM images of Cu-btc [65]. (Right) Cu-btc pellets.

Copper(II) benzene-1,3,5-tricarboxylate,  $\text{Cu}_3(\text{btc})_2(\text{H}_2\text{O})_3$ , HKUST-1 or Cu-btc is a coordination polymer with small pores and so-called open metal-sites, i.e. metal centers with unsaturated coordination position. It is a copper based MOF that was first reported in 1999 by Williams and co-workers. The compound has a 3D face-centered-cubic crystalline structure assembled from dimeric cupric tetracarboxylate units, where each copper atom is coordinated by four oxygens coming from the benzene-1,3,5-tricarboxylate (denoted btc) linkers, and by one water molecule [66]. The adsorbent has a BET surface area of  $1154 \text{ m}^2/\text{g}$  and a bulk density of  $0.485 \text{ g/ml}$  [3].

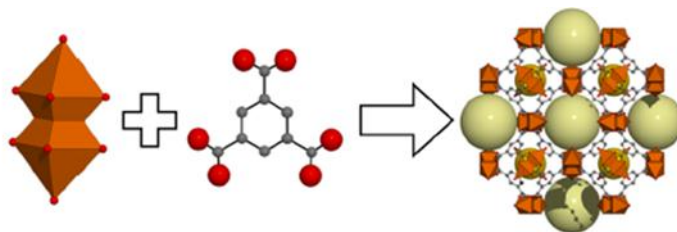


Figure 2-9: (Left) The metal complex (orange) consists of two copper atoms coordinated by ten oxygen atoms (red). Middle: the metal complexes are interconnected by BTC ligands (C: dark gray). (Right) Structure of Cu-BTC with pore diameters of  $5\text{\AA}$  (dark yellow sphere) and  $9\text{\AA}$  (light yellow sphere) [65].

MOFs with coordinately unsaturated metal areas, which are also termed “open” metal sites, such as Cu-btc, have attracted a lot of interest because of experimental observations that show evidence for a relatively strong interaction of the adsorbed hydrogen molecules with the metal centers. Based on these observations, has it been proposed an increase of the density of accessible metal sites as a step forward in the development of MOFs with higher isosteric heats

of hydrogen adsorption, which is a postulation for efficient hydrogen storage at room temperature [44].

Focusing on Cu-btc MOFs, some heat capacity values have been published [3, 14]. The article measuring the heat capacity of Cu-btc with the chemical formula  $(\text{Cu}_2(\text{OH})(2,2'\text{-bpy})_2(\text{BTC}) \cdot 2\text{H}_2\text{O})_n$  [14], show a value about  $0.99 \text{ J/g K}$  around  $273 \text{ K}$ .

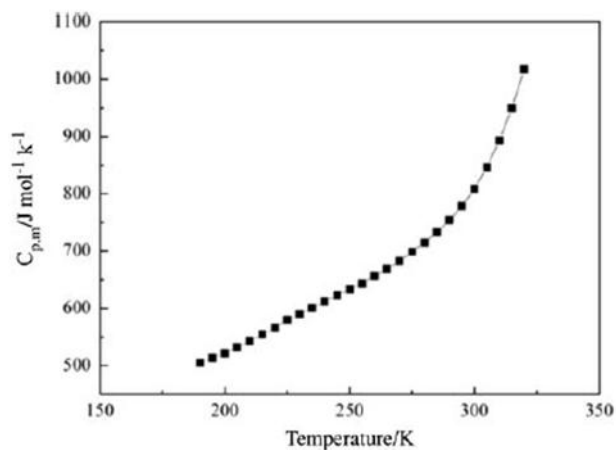


Figure 2-10:  $(\text{Cu}_2(\text{OH})(2,2'\text{-bpy})_2(\text{BTC}) \cdot 2\text{H}_2\text{O})_n$ , Cu-btc MOF heat capacity experimental data [14].

The article measuring specific heat capacity of  $\text{Cu}_3(\text{btc})_2(\text{H}_2\text{O})_3$  [3], show a value of  $0.55 \text{ J/g K}$  around  $273 \text{ K}$ . This value differs quite a lot from the other type of Cu-btc, which shows that the material's heat capacity depends rather much on its composition.

## 2.3.2.2.2 Fe-btc

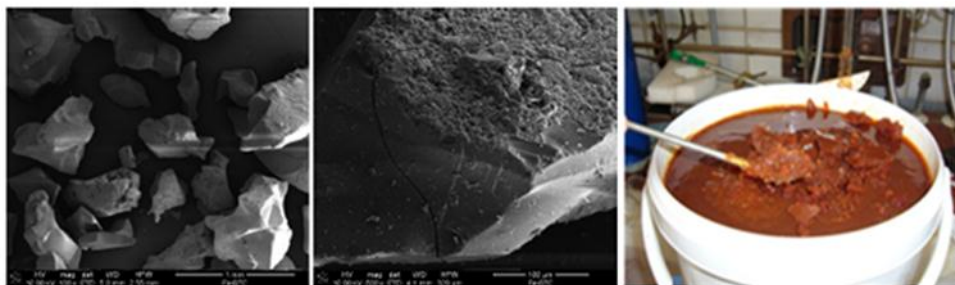


Figure 2-11: (Left) SEM images of Fe-btc [67]. (Right) Fe-btc-gel.

Ferric benzene-1,3,5-tricarboxylate (Fe-btc) may structurally and electrochemically be compared with the corresponding Cu-btc MOF. Investigations of iron-organic frameworks are less common compared with those of zinc and copper, etc. [14, 66, 68]. The main reason is that  $\text{Fe}^{2+}$  is air sensitive and readily changes into a stable polymeric hydrous iron oxide even on a strongly environment [69], whereas alkalescency is favorable for the construction of frameworks with high dimensionalities. The adsorbent has a BET surface area of  $772 \text{ m}^2/\text{g}$  [67].

## 2.3.2.2.3 MIL-100 (Fe)

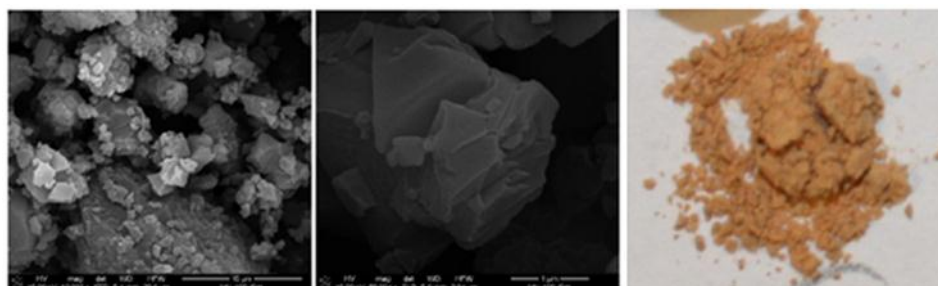


Figure 2-12: (Left) SEM images of MIL-100(Fe) [67]. (Right) MIL-100(Fe) material powder.

Up to now, several examples with MIL-100 structure, mesoporous MOFs built up from oxocentered trimers of  $\text{M}^{\text{III}}\text{O}_6$  octahedra ( $\text{M}=\text{Fe}, \text{Cr}, \text{Al}$ ) and trimesate moieties, have been reported (MIL stands for Materials of Institut Lavoisier). These solids exhibit very large pores, high surface areas around  $2000 \text{ m}^2/\text{g}$ , and a significant number of lewis metal sites [70]. MIL-100(Fe) or  $\text{Fe}^{\text{III}}_3\text{O}(\text{H}_2\text{O})_2\text{F}\cdot\{\text{C}_6\text{H}(\text{CO}_2)_3\}_2\cdot n\text{H}_2\text{O}$  ( $n \sim 14.5$ ) is an iron(III) benzene-1,3,5-tricarboxylate built up from trimers of iron octahedra sharing a common vertex  $\mu_3\text{-O}$ . The trimers are then linked by the benzene-1,3,5-tricarboxylate moieties, which is the same linker used in Cu- and Fe-btc. The trimers are linked in such a way that this leads to the formation of

hybrid supertetrahedra which further assemble into a zeolitic architecture of the MTN type (Figure 2-13). The adsorbent has a BET surface area of  $1677 \text{ m}^2/\text{g}$  [67].

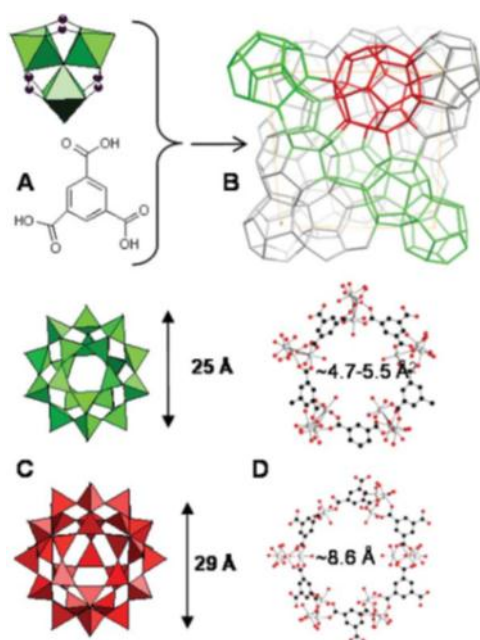


Figure 2-13: Structure of MIL-100(Fe). (A) A trimer of iron octahedra and trimesic acid. (B) Schematic view of one unit cell of MIL-100(Fe). (C) the two types of cages in polyhedral mode. (D) Pentagonal and hexagonal windows in balls and sticks (Fe: grey; O: red; C: black) [67].

## 2.4 Thermodynamics of the Test Sample

The thermodynamics of the test sample during a measurement cycle depends on several assumed scenarios. To better understand potential deviations in the measured heat capacity values, are the thermodynamics behind several thought scenario presented here.

The sample is prepared and encapsulated under following conditions; relative humidity (RH) 25 %, temperature 23 °C and atmospheric pressure. It is then cooled down to -180 °C, before it is heated up to 150 °C with a heating rate of 2 °C/min. The sample is activated with nitrogen gas as the purge gas, and the actual measurement is executed with helium flowing through the cell chamber. A detailed measurement description follows in chapter 0. The different cases investigated are the following;

### 2.4.1 Case 1 – Air

The whole sample (40  $\mu$ l) is filled up with air at ambient conditions. The Table 2.1 tabulates the anticipated air composition under ambient conditions together with the respective partial pressures and molar masses for the different gases in air.

Table 2.1: The air composition at atmospheric pressure, RH 25 % and 23 °C [71].

Gas type	Composition in air (P=1 atm, T = 23 °C)	P <sub>i</sub> ( T = 23 °C )	M <sub>i</sub> ( P=1 atm, T = 23 °C )
N <sub>2</sub>	77.428 %	0.785 bar	20.967 g <sub>-gas</sub> /mol <sub>-air</sub>
O <sub>2</sub>	20.846 %	0.211 bar	7.365 g <sub>-gas</sub> /mol <sub>-air</sub>
Ar	0.993 %	0.010 bar	0.547 g <sub>-gas</sub> /mol <sub>-air</sub>
H <sub>2</sub> O	0.693 %	0.007 bar	0.078 g <sub>-gas</sub> /mol <sub>-air</sub>
CO <sub>2</sub>	0.04 %	0.0004 bar	0.0267 g <sub>-gas</sub> /mol <sub>-air</sub>

The air is assumed to behave like an ideal gas, following the ideal gas law ( $PV=nRT$ ). This makes the pressure increase linearly with increasing temperature, since all the other properties are remained constant. Figure 2-14 show how the total air pressure and the partial pressures for the air compounds increase linearly with increasing temperature during an experiment run.



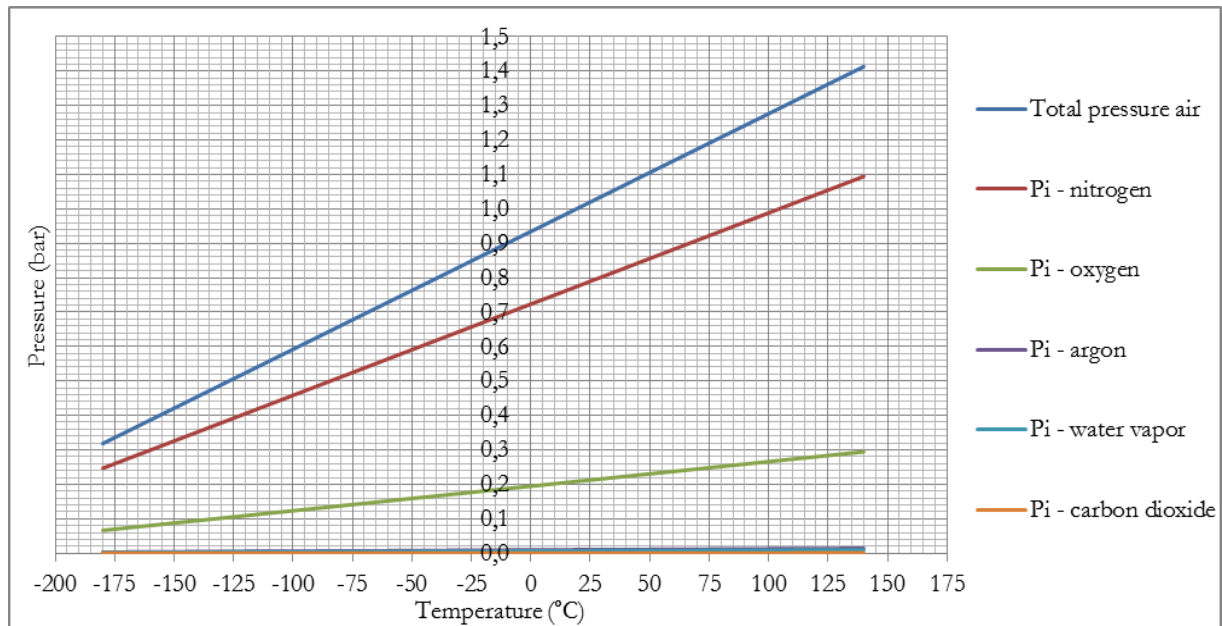


Figure 2-14: Total and partial pressure for the air and the different compounds in the sample, respectively.

The enthalpy change for air in the sample is plotted with temperature in Figure 2-15 to point out prospective enthalpy changes, which again would give sudden heat capacity changes for the gas. The figure does not show any big enthalpy change within the experimental temperature range, and the enthalpy increases with increasing temperature. All of the principal compounds have a boiling point lower than the temperature range in question, the gases remain therefore in the same physical state throughout an experimental run ( $N_2$ :  $-195.9\text{ }^\circ\text{C}$ ,  $O_2$ :  $-183\text{ }^\circ\text{C}$ ,  $Ar$ :  $-185.9\text{ }^\circ\text{C}$ ). However, the boiling point of both water vapor and carbon dioxide are within the temperature range, but they form a very small percentage of the air composition, and their enthalpy change poses no significant difference on the total air enthalpy curve.

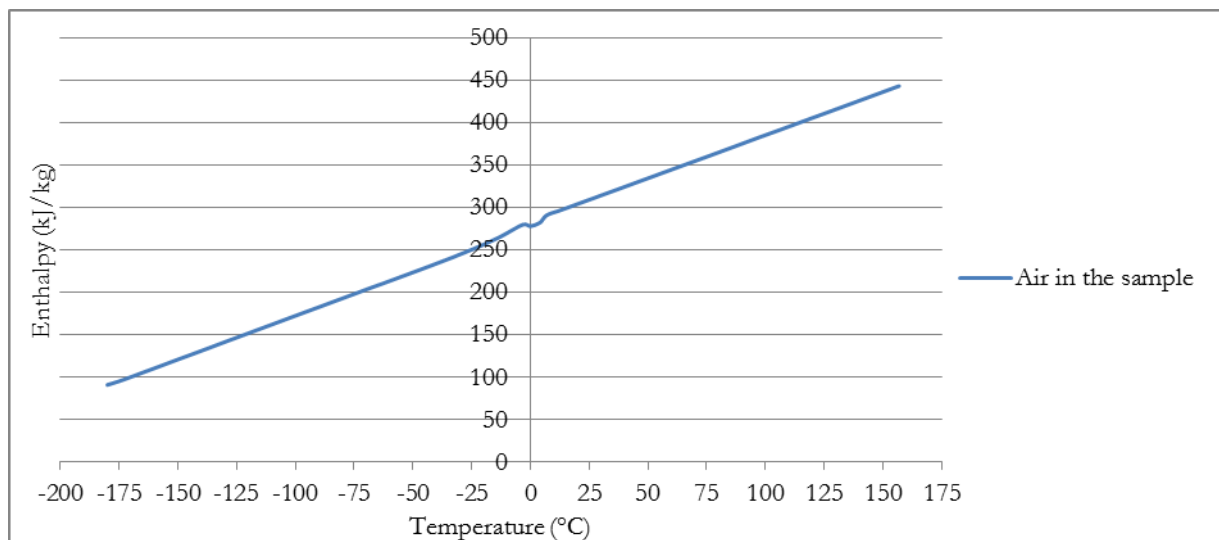


Figure 2-15: The enthalpy behavior for the humid air present in the sample [72].



### 2.4.2 Case 2 – N<sub>2</sub>

The whole sample (40  $\mu$ l) contains only dry N<sub>2</sub> (99.999% purity) after the activation, because the air contribution during the sample encapsulation is assumed negligible.

### 2.4.3 Case 3 - He

The whole sample (40  $\mu$ l) contains only helium (99.999% purity) owing to the lid not being air tight after the encapsulating. Helium then replaces all of the other inert gases in the sample during the experimental run.

In the second and third case, is the behavior of the gases also assumed to follow the ideal gas law. Thus, the pressure curve during these experiments will have the same curve as the total air pressure curve in Figure 2-14, because the remaining variables for simplicity are presumed constant in these cases as well.

The enthalpy change in the three first scenarios is plotted together with temperature in Figure 2-16. The figure does not show any big enthalpy change or phase transition within the experimental temperature range, and the enthalpy of the additional gases in the sample increases with increasing temperature. Nitrogen and helium both have boiling points lower than the temperature range in question, and the gases therefore remain in the same physical state throughout an experimental run (N<sub>2</sub>: -195.9 °C, He : -269 °C).

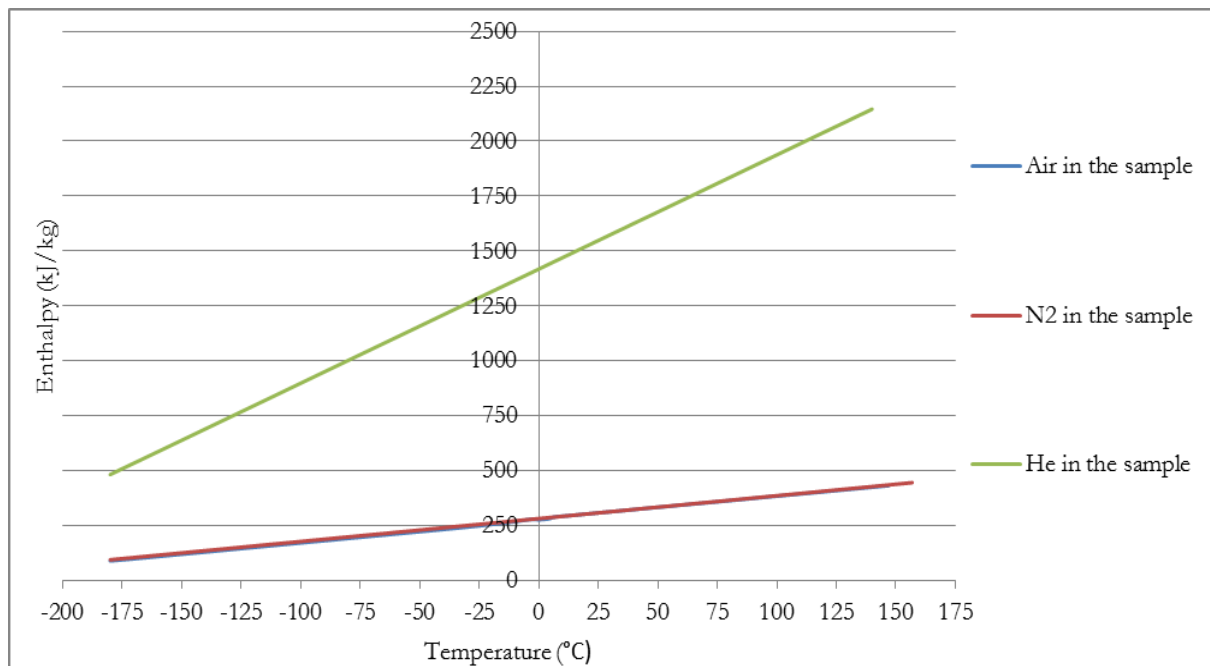


Figure 2-16: The enthalpy behavior for the different gases that can be present in the sample [72].

#### 2.4.4 Case 4 – Air and Water Adsorption

The material has adsorbed 0.015 g- H<sub>2</sub>O/ g-dry material from the water vapor present in the surroundings, and the rest of the sample (40 µl) is filled with air from case 1.

The amount of water adsorbed depends on several factors; the time the sample is exposed to air, the air's relative humidity (RH), the material's BET specific surface area, the water's partial and saturation pressure ratio ( $p/p_0$ ), and the water content in the sample after ended activation. The presumed water adsorption factor for the material used in this work was presumed on the basis of a study made on MIL-100(Fe) as a water adsorbent [64].

Based on this published study, MIL-100(Fe) BET specific surface area 1677 m<sup>2</sup>/g (see chapter 2.3.2.2.3), one minute air exposure, water partial pressure and water saturation pressure ratio  $p/p_0 = 0.25$ , and no water content after activation, was the water adsorption factor guessed to be  $Q_{ads} = 0.015$  g-H<sub>2</sub>O/g-dry sorbent.

The air in the sample has the same assumed behavior as in case 1. However, the behavior of the water vapor adsorbed in the sample was more difficult to anticipate.

As a starting point was the definition of phase change adopted; phase change requires molecular interaction. The adsorbed water molecules are connected separately to the material's molecular surface, because of the adsorbing Van der Waal forces exceeding the kinetic forces among the water molecules. This means that the water molecules have no actual interactions between them when adsorbed, and the most adjacent theory on its behavior would be that they are kept in a so called vapor phase throughout the whole experimental temperature range. Seeing that the water adsorbed does not undergo any phase transition, neither will this enthalpy curve consist of any sudden change. This is nothing more than a presumption on the water behavior, and should be further investigated.

The most probable scenario is a combination of case 1 and 4.

## 2.5 Theoretical Summary

The theory of specific heat in solids shows that specific heat capacity for a material normally increases with increasing temperature, due to the specific heat capacity being a function of its own substance structure. More precisely, it depends on how many degrees of freedom available in the substance particles, where a degree of freedom is any form of energy in which heat transferred into an object can be stored.

Debye heat capacity model is nowadays the best theoretical model for heat capacity in solids. Even though newer research has revealed some discrepancy in the model at low temperatures and that Debye's temperature is not a constant, but varies with temperature.

The equipment most suitable for experimental heat capacity measurements is a differential scanning calorimeter (DSC), where TA Instruments has provided NTNU with a DSC Q2000. This instrument provides a modulated temperature method which gives quite accurate heat capacity results. The inaccuracy is exclaimed to be 5%.

The amount of hydrogen adsorbed per unit mass is proportional to the adsorbent's specific surface area and pore size. Very many MOFs, which can exceed 5000 m<sup>2</sup>/g (BET surface), in combination with micropores of diameters < 20 Å, leads therefore to perfect conditions for physisorptive storage of small sorbent molecules, such as hydrogen.

Gas sorption experiments done [43] show that some MOFs and porous materials can selectively adsorb H<sub>2</sub> and CO<sub>2</sub> over N<sub>2</sub> and Ar, and that the adsorption capacities of the excluded gases almost equal to zero. Although the pores size and shape of an adsorbent are the major factors in determining the adsorption selectivity of guest molecules, is the nature of the guest-surface interaction also important.

The enthalpy change for each gas within the experimental temperature ratio is the most relevant property to plot with temperature, because regarding the definition of heat capacity is it with a fixed temperature the only property that can influence the measured heat capacity value of the material. The thermodynamics of the test sample during a measurement cycle depends on four assumed scenarios, where each scenario contains different inert gas types. None of the scenarios have any sudden enthalpy changes on their enthalpy curves.

The most probable scenario is a combination of case 1 and 4.

### 3 Experimental

#### 3.1 Equipment

Heat capacity measurements were performed on DSC Q2000 (T-zero DSC-technology, TA Instruments Inc., USA). See chapter 2.2 for a detailed description of the instrument. A mechanical cooling system with liquefied nitrogen (LNCS) was used for the experimental measurement.



Figure 3-1: A differential scanner calorimeter (DSC) Q2000 TA Instruments Inc [37].

The types of pans and lids used were Tzero™ pans (PN 901683.901) and Tzero™ hermetic lids (PN 901684.901). The Tzero™ press had two sets of crimping parts for encapsulating the sample cups, blue top and bottom parts, used for hermetic sealing, and black top and bottom parts, used for compressing the sample.



Figure 3-2: (Left) The Tzero™ press with its corresponding encapsulation parts [37]. (Right) An encapsulated sample with Tzero™ pan and hermetic lid.

Sample mass was weighed on a Mettler Toledo excellence plus ® with an accuracy of  $\pm 0.01$  mg.

## 3.2 Procedures

### 3.2.1 Sample Preparation

The sample pan was filled up with material powder, and the pan and lid compressed with black Tzero™ press parts to 45° of the press' maximum. The lid was then straitened, before the sample was encapsulated and sealed with the blue Tzero™ press parts. The encapsulation was performed after the activation for the activated samples and after 24 hours in ambient surroundings for the inactivated samples.

The sample crimping is very important regarding the accuracy of the heat capacity measurements. Firstly, the object is to compress the material and obtain a very good thermal contact with the cup bottom. Secondly, to get the sample pan tightly sealed with a hermetic lid to prevent volatiles from the sample being released. It is an advantage using a powder material, and packs it densely in a Tzero™ pan. However, the thermal contact is not only important between the sample material and the bottom of the cup, but also the contact surface area between the pan bottom and the sensor. This is why Tzero™ pans are used in heat capacity measurements, because of their flat pan bottom. These considerations together with a very clean sensor surface give the most accurate result values.

### 3.2.2 Activation

Four different materials, Cu-btc, Fe-btc, MIL-100(Fe) and AC Norit 8.0 were measured both activated and inactivated. The activation procedure was mainly a dehumidification process of the samples, avoiding the influence of adsorbed water in the measurements. Where the inactivated samples on the other hand were mistreated and exposed to a humid atmosphere ( $\varphi = 23\text{--}26\%$ ,  $T \approx 23^\circ\text{C}$ ).

The activation process was performed based on experience from other activations made on the materials [7, 45]. The samples were heated up to 150 °C under vacuum, 6 – 8 Pa (the last three activations about 1 Pa), for a minimum of 12 hours, often more. The activation equipment consisted of small pipes, with four end caps, connected to a vacuum pump and a dry nitrogen gas tank (99.999%purity), which was used as purge gas before opening the caps after ended activation.

The metal end caps contained one sample in each one. The pipe set-up was surrounded by a heating band, and the whole installment was covered by isolation.



Figure 3-3: The activation set-up. (Left) Activation in process with heating band, isolation and connected to the vacuum pump. (Right) Show the pipe set-up with its corresponding four metal end caps.

### 3.2.3 Method for Measurement and Calibration

Dry nitrogen gas with high purity (99.999%) was used as base purge gas (1 bar) and helium gas with high purity (99.999%) was used as purge gas (25 ml/min) through the DSC cell. The temperature scale of the instrument was initially calibrated in the standard DSC mode, using the extrapolated onset temperatures of the melting indium (156.61°C) at a heating rate of 10°C/min. The energy scale was calibrated with the heat of fusion of indium (28.45 J/g). The heat capacity calibration was made by running a standard sapphire ( $\alpha\text{-Al}_2\text{O}_3$ ) at the experimental temperature (-180°C – 150°C).

The calibration method and the experimental method, a MDSC technique, were performed at the same conditions as follows: (1) sampling interval at 1.00 s/pt.; (2) zero heat flow at the average temperature of the desired temperature range for the experiment (-15°C); (3) equilibrate at the minimum temperature of the range (-180°C); (4) isothermal for 5.00 min; (5) modulated temperature amplitude of +/- 1°C every 40 seconds; and (6) temperature ramp at 2°C/min until it reached the maximum temperature of the experiment (150 °C) [10-15]. A complete and detailed description of the measurement and calibration methods is found in the attached appendix I.

The masses of the reference and sample pans with lids were within  $52.55 \pm 0.05$  mg and  $52.25 \pm 0.05$  mg.

### 3.3 Materials Investigated

All the details over the samples measured are found in the sample list in appendix II.

There are performed samples with activated and inactivated material with to different temperature ranges, and two different activation vacuum pressures.

**Table 3.1: Experimental matrix over measurements performed.**

Material	Inactivated	Activated (6-8 Pa, 150°C)	Activated (1 Pa, 150°C)	-180°C to 150°C	-180°C to 20°C
<b>Sapphire</b> ( $\alpha$ -Al <sub>2</sub> O <sub>3</sub> )	4 samples + 1 test	-	-	4 samples + 1 test	-
<b>Norit R0.8</b>	6 samples; 2 set	7 samples; 2 set	-	6 samples;2 set A 3 samples;1 set IA	3 samples;1 set IA
<b>Cu-btc</b>	9 samples; 3 set	6 samples; 2 set	4 samples; 1 set	3 samples;1 set A 3 samples;1 set IA	7 samples;2 set A 6 samples;2 set IA
<b>Fe-btc</b>	6 samples; 2 set	3 samples; 1 set	3 samples; 1 set	3 samples;1 set A 3 samples;1 set IA	4 samples;1 set A 3 samples;1 set IA
<b>MIL-100(Fe)</b>	6 samples; 2 set	7 samples; 2 set	4 samples; 1 set	3 samples;1 set A 3 samples;1 set IA	8 samples;2 set A 3 samples;1 set IA

## 4 Results and Discussion

### 4.1 Calibration with Sapphire ( $\alpha\text{-Al}_2\text{O}_3$ )

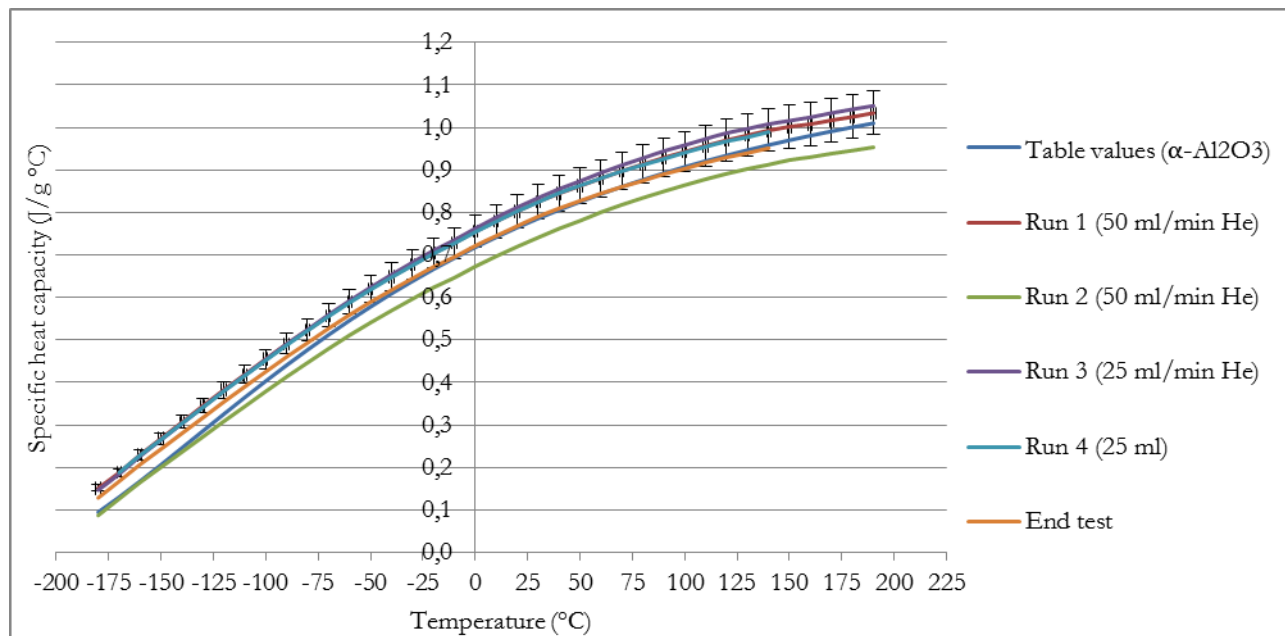


Figure 4-1: Heat capacities of standard sapphire ( $\alpha\text{-Al}_2\text{O}_3$ ). Experimental values for calibration (Run 1-4), tabulated values (blue) [18], and a test run after ended use of the DSC (orange).

Figure 4-1 show the four heat capacity calibration runs performed with sapphire ( $\alpha\text{-Al}_2\text{O}_3$ ) together with the tabulated reference values for sapphire [18], and a test run where the heat capacities of sapphire were measured over again after all the porous materials had been measured.

The heat capacity measurements were repeated four times under the same conditions, with the exception of the helium mass flow change in the cell chamber. The emphasis of these measurements was to assess the reproducibility and ensure accuracy of the measured data using MDSC (Q2000). The standard deviations for standard sapphire were below 0.044 accounting for every run, but looking at the graph, run 2 deviates from the other heat capacity values. Taking under consideration the Chauvenet's criterion the second run does not deviate severe enough to rule out the values. However, it is known from the instructions of these measurements that when using helium as a cell purge gas it is only to be used about 25 ml/min, run 2 was therefore excluded from the analysis of the calibration, and the standard deviations were below 0.028. Compared to other heat capacity studies on MOFs [10-14], it show a reasonably good reproducibility in the temperature range from -180 to 140°C.

A heat capacity calibration test was executed after ended experiments. This test showed good results, still within the 5% acceptable inaccuracy range of the reference values. This demonstrated the fact that the instrument is working as it should, since it continued to measure exact heat capacities for the reference material used for calibrating it.



## 4.2 Activated Carbon Norit R0.8

The heat capacities of activated samples as a function of temperature are shown in Figure 4-2. There were made two activation sets, each with three samples, activated under the same conditions.

The experimental values from the inactivated samples are shown in Figure 4-3. The inactivated material's heat capacities are plotted together with the activated sample values (black), which makes it easier to discover obvious distinctions between the activated and inactivated material values. There were as well made two different sets of inactivated samples, with three samples in each set, both exposed to normal humidity at room temperature.

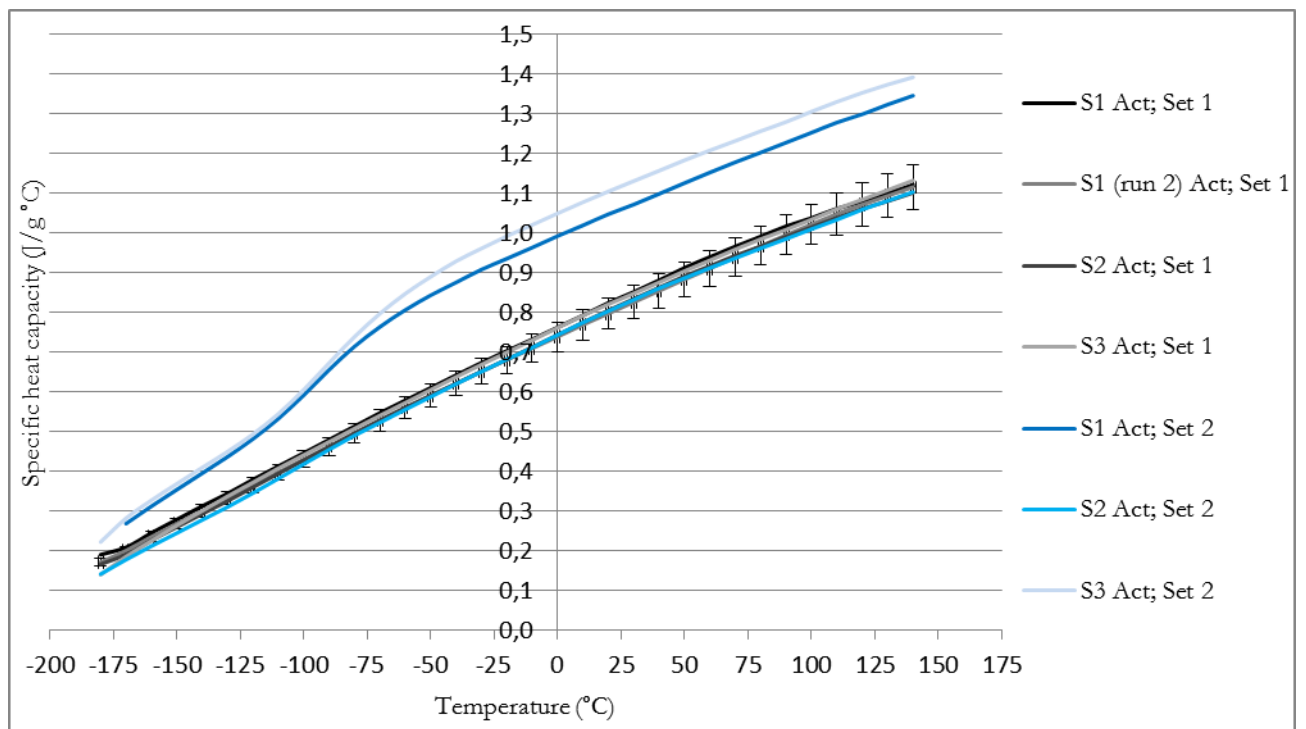


Figure 4-2: Heat capacities of AC Norit R0.8 activated samples (1. activation – black; 2. activation – blue).

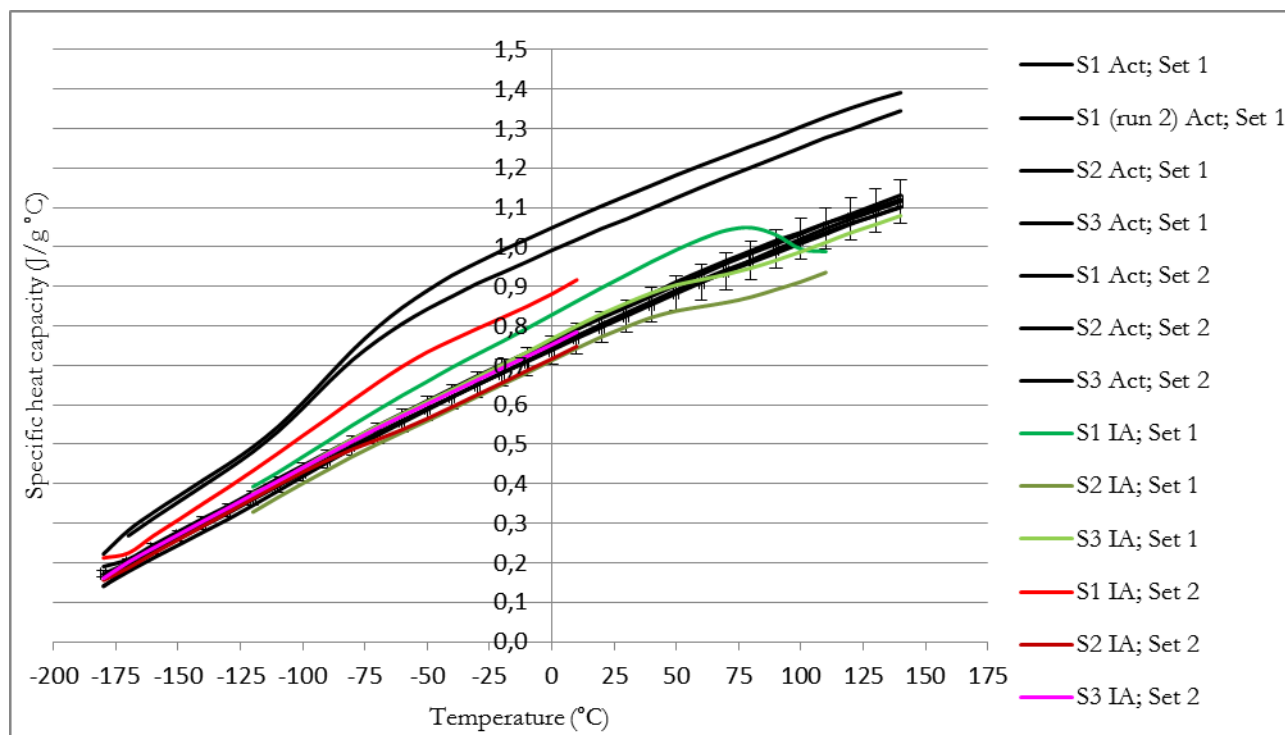


Figure 4-3: Heat capacities of AC Norit R0.8 inactivated samples (1. set – green; 2. set – red); activated samples (black).

From Figure 4-2, it can be seen that the heat capacities of the samples increase with increasing temperature in a smooth and continuous manner in the experimental temperature range, in accordance with the theory of specific heat of solids in chapter 2.1. With the exception of the two curves from the second activation set, have all the activated samples heat capacities within a 5% error bar. These two curves, which deviate from the majority, have higher heat capacities than the other sample values, both the activated and the inactivated. Implicating knowledge from experience, are these heat capacities presumed to be incorrect and left out in further presentation of the heat capacity measurement results. This is due to the fact that the inactivated samples should consist of more water in their framework than the activated samples, and therefore have higher  $C_p$  values.

This 5% deviation for the other activated material values might come from different error sources like the sample preparation, sample activation or from an instrumental error source. Regarding the study of each error source in chapter 4.7, is the most probable cause behind the variance within the bulk, and the variance between the two activated sample curves and the rest of the heat capacities, inaccuracies in the activation process.

It can be expected that the inactivated heat capacities in Figure 4-3 in general are higher than the activated material's heat capacities. This is due to the activation process, which principally is performed to dehumidify the material and replace the air in the sample with  $N_2$ . Nitrogen is according to studies on adsorption in porous materials [43] hardly adsorbed by the sample. Further, the thermodynamics of case 2 (chapter 2.4.2), show that the nitrogen in the sample does not undergo any phase change within the experimental temperature range and therefore does not

have any sudden heat capacity changes. Accordingly, demonstrates the uncertainty analysis for the different thermodynamic scenarios (chapter 5.5), that the biggest heat capacity influence most probably will come from a significant water concentration in the material framework, and not nitrogen present in the sample. The anticipated higher water concentration in the inactivated material's framework than in the activated material is therefore assumed to give higher heat capacities, because water has high  $C_p$  values [73]. This leaves water contribution in the framework to be the most likely difference between the inactivated and activated experimental values.

The green curves from Figure 4-3 can indicate some anomalies around 100°C, which very likely are due to water, even though the heat capacities are not higher than the bulk of the activated sample's values for every one of the curves. The variance between the green curves may be caused by a difference in the water adsorption in every sample, due to indifferences in the sample preparation and material handling. The red curves from the second set of inactivated samples follow most probably the same reasoning.

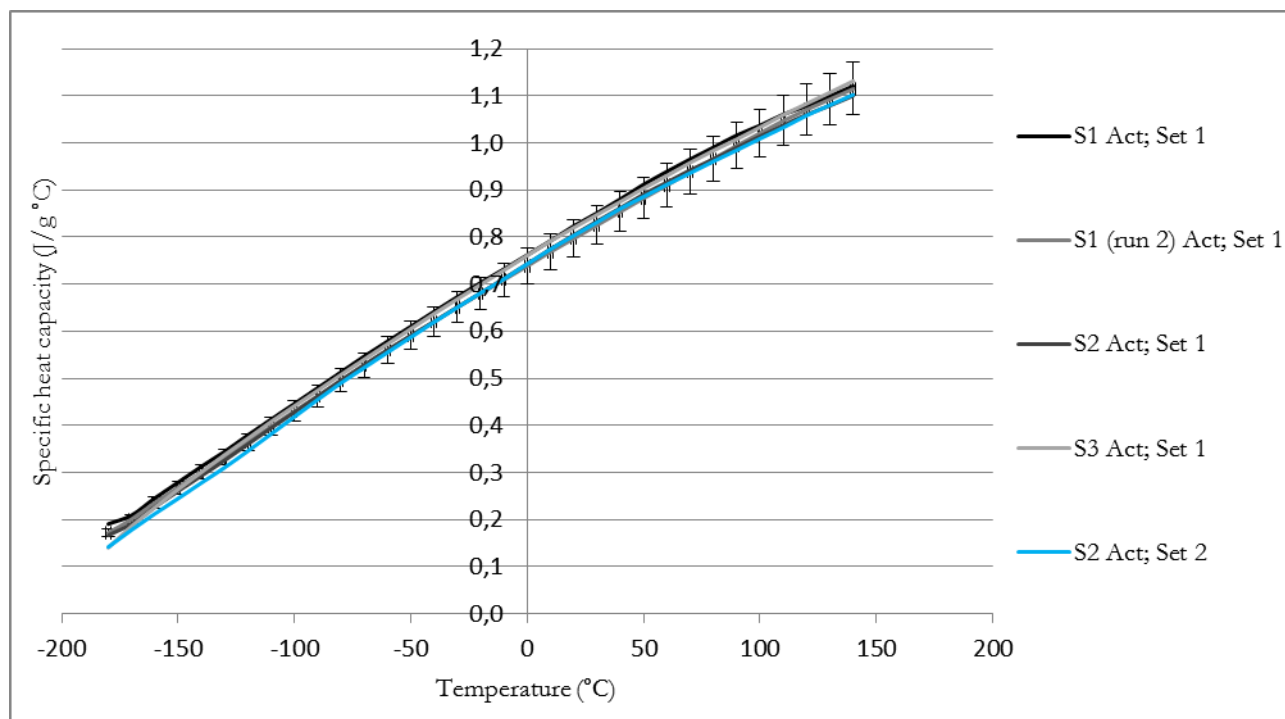


Figure 4-4: Heat capacities of AC Norit R0.8 selected activated samples (1. activation – black; 2. activation – blue).

The heat capacities of the selected samples are shown in Figure 4-4, and the data of the selected experiments and the standard deviation for the respective samples are given in Appendix III. The experimental standard deviations below 0.02 are obtained and show compared to other heat capacity studies on MOFs [10-14] reasonably good reproducibility in the temperature range from -180°C to 140°C.

The heat capacities of the average sample are fitted to the following polynomial equation of heat capacities ( $C_p$ ) with temperature ( $x$ ) going from  $-180^\circ\text{C}$  to  $140^\circ\text{C}$ .

$$C_p \left[ \frac{\text{J}}{\text{g K}} \right] = 0.75058 + 2.97345 \cdot 10^{-3} X - 2.11335 \cdot 10^{-6} X^2 - 6.59476 \cdot 10^{-10} X^3 - 1.0895 \cdot 10^{-11} X^4 - 1.15506 \cdot 10^{-13} X^5 \quad (4.1)$$

The correlation coefficient of the fitting,  $R^2 = 0.999993$ .

Looking into earlier published data on heat capacities for activated carbon is it overall most common referring to the heat capacities for carbon (graphite) as reference, since activated carbon Norit R0.8 is a microporous carbon material. The theoretical heat capacities of carbon according to the Debye model is graphed together with the reference heat capacities of carbon (graphite) [57], the measured values of AC Norit R0.8, and published data [3] in Figure 4-6. The theoretical heat capacities are calculated by means of the Debye temperature of carbon (graphite) as a function of temperature in combination with the Debye heat capacity model, Figure 4-5.

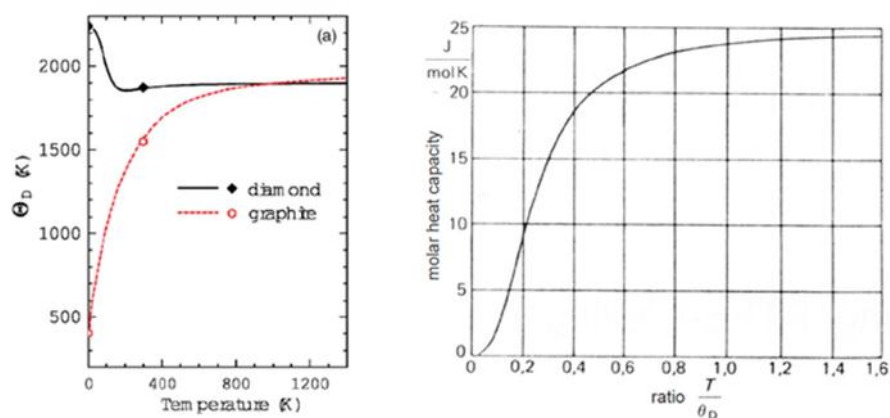


Figure 4-5: (Left) Debye temperature for carbon (graphite and diamond) varying with temperature [74]. (Right) Molar heat capacities for solids according to the Debye function [26].

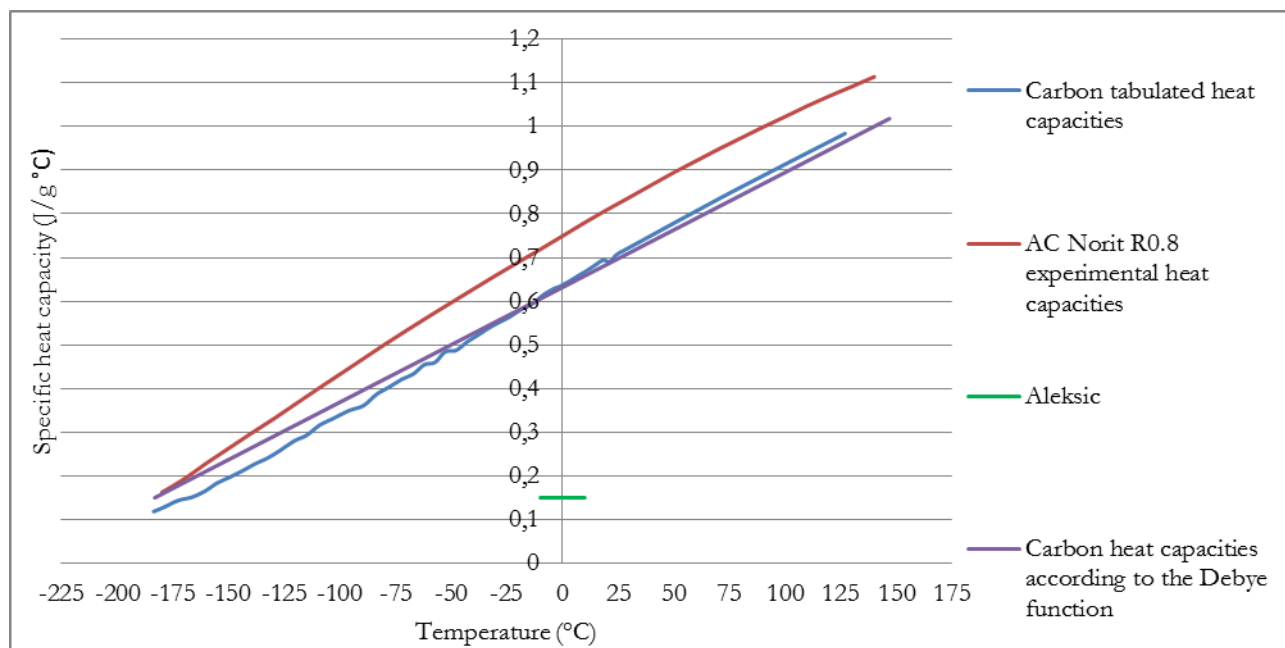


Figure 4-6: Activated carbon Norit R0.8 heat capacities from different references; measurements from this report (red), carbon (graphite) values [57] (blue), measurements made in earlier study [3] (green), and heat capacities according to the Debye function[26, 74] (purple).

Figure 4-6 show a relatively good coherence between the experimental heat capacities for Norit R0.8 and the reference values for carbon (graphite). The two graphs have somewhat the same slope, where the experimental data is displaced almost parallel to the reference values, only higher up on the heat capacity scale. However, higher  $C_p$  values can be expected for AC Norit R0.8, because it has a higher surface area and therefore is a better water adsorbent. This has probably led to some existing water in the framework influencing the results. The published results by Aleksic on the other hand, lack coherence with our values, as was anticipated earlier. Based on the tabulated heat capacities for carbon and the good reproducibility of the different measurements in Figure 4-4, is it possible to reject the other published results, and trust our experimental values.

### 4.3 Cu-btc

The heat capacities of Cu-btc as a function of temperature are shown in Figure 4-7. There were made three activation sets, each with minimum three samples each. All three sets were activated under the same conditions, with the exception of the vacuum pressure being lower under the third activation.

The experimental values from the inactivated samples are shown in Figure 4-8. The inactivated material curves are plotted together with the activated sample values (black), which makes it easier to discover obvious distinctions between the activated and inactivated material values. There were as well made three different sets of inactivated samples, with three samples in each set. The first two were exposed to normal humidity at room temperature, while the third set were material taken directly from the storage box, still having a dark blue color as a sign of low water content in its framework.

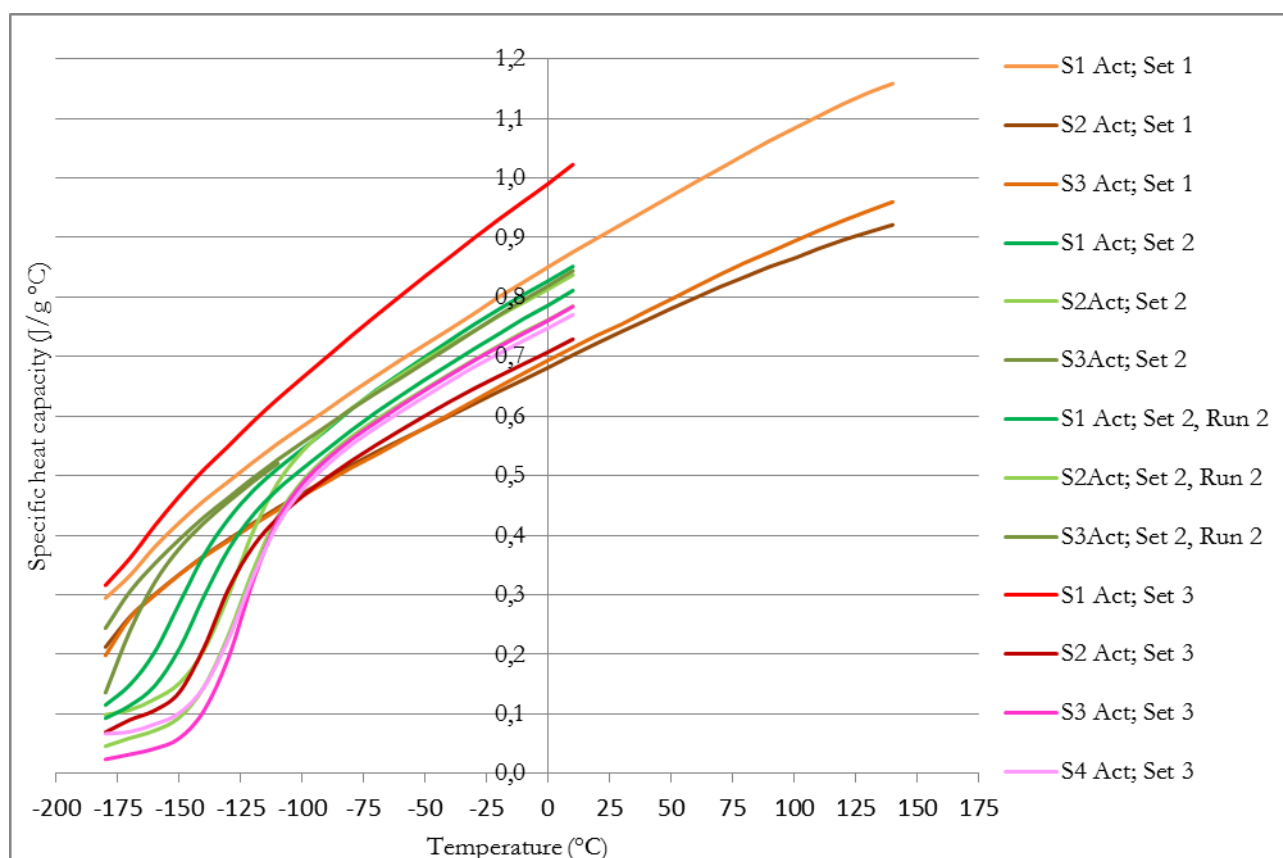


Figure 4-7: Heat capacities of Cu-btc activated samples (1. activation – orange; 2. activation (1. and 2. run) – green; 3. activation – red).

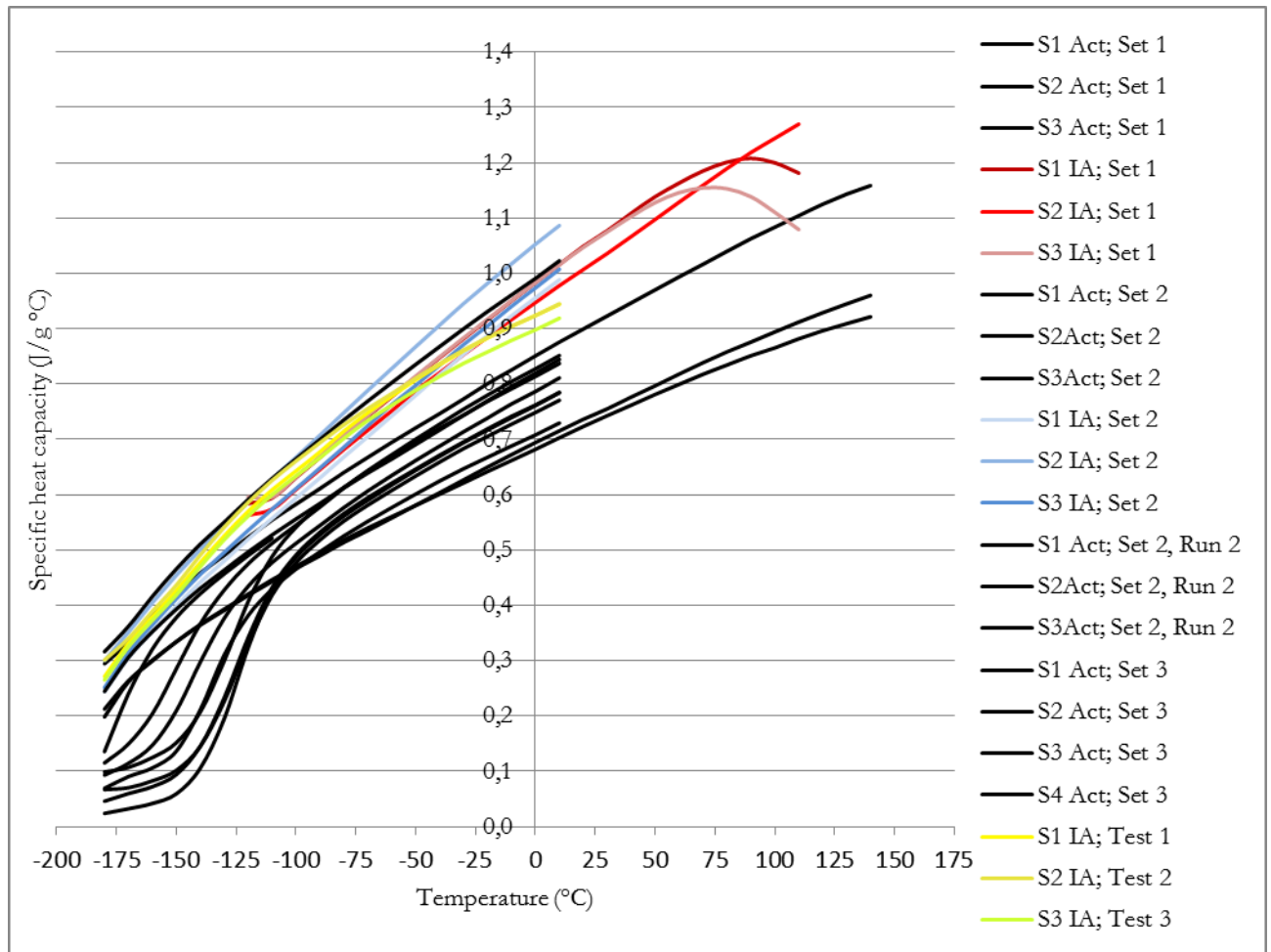


Figure 4-8: Heat capacities of Cu-btc inactivated samples (1. set – red; 2. set – blue; test set – yellow/green); activated samples (black).

All heat capacities for the inactivated samples in Figure 4-8 are higher than the majority of the activated material's heat capacities. This trend is assumed to follow the same explanation that was given to explain this same tendency in the heat capacity curves for activated carbon Norit R0.8, see chapter 4.2.

The red curves from Figure 4-8 indicate some anomalies around 100°C, which very likely are due to water. The variance between the different inactivated material curves may be caused by a variance in the water adsorption in every sample, due to indifferences in the sample preparation and material handling.

From Figure 4-7, it can be seen that the heat capacities of the samples increase with increasing temperature, in accordance with the theory of specific heat of solids. Some of the curves increase in a smooth and continuous manner in the experimental range, while the bulk of the sample curves have an abnormal transition part between -180°C and -100°C. This anomaly has so far not been possible to provide a background for. It has on the other hand been possible to rule out some of the possibilities causing this deviation in the curves.

The four different scenarios from chapter 2.4 are used as a starting point for further investigation. The first step was to investigate the inert gases in the sample, and the impact they could have on the measured heat capacities, such as prospective phase changes which provoke relatively high heat changes in the sample. Based on these scenarios the influential gases in question were nitrogen, oxygen, argon, carbon dioxide, water vapor and helium. Nitrogen, oxygen, argon, and helium have boiling points lower than the experimental temperature range, which means that any sudden change in heat capacity, as seen from Figure 4-7, cannot be caused by any of these gases. In other words, they do not undergo any phase transitions within this temperature range and therefore do not have any change in their own heat capacity curve which can influence the material's heat capacity.

Carbon dioxide and water vapor on the other hand, both have boiling points within the temperature change in question. However, they form a very small percentage of the air composition, and their enthalpy change poses no significant difference on the total air enthalpy curve. Yet, the impact the latent heat of vaporization for the gases would have had on the Cu-btc sample's heat change was calculated. The transition range constituted a change in heat capacity of approximately 0.4 J/g K over a 40 K temperature interval, which gave a heat change of 0.24 J. The energy change from the existing mass of carbon dioxide sublimating forms 0.01% of the heat change that gives the curve transition. The energy change from the existing water mass evaporating amounts to the same percentage, 0.01%, of the heat change that gives the curve transition. This eliminates the possibility that the carbon dioxide or the water vapor content in air provided the anomaly in the heat capacity curves. This is in coherence with the thermodynamics presented in chapter 2.4.

The water content will undergo two phase transitions within the temperature range according its water phase diagram, but neither one would have any significant difference on the material's heat capacity, see chapter 2.4.1 and 5.5.1.

The amount of water adsorbed by the material could be crucial. Two matters were taken into account. Firstly, if the water vapor adsorbed in the sample would undergo any phase change, which would lead to a heat capacity change. Secondly, if the water vapor adsorbed in the sample could be the reason behind the sudden heat capacity change for the activated Cu-btc sample. It is seen from the theory in chapter 2.4.4 that the water adsorbed does not undergo any phase change. It remains in the same gas phase, and therefore does not have any sudden heat capacity changes within the experimental run that would influence the material's heat capacity. However, this is only a presumption of the water behavior, and should be investigated further. Further on is it very peculiar that this curve transition on the activated sample curves is not present in the heat capacity curves for the inactivated Cu-btc samples in Figure 4-8. The inactivated material did not undergo an activation to remove the water content in the sample material, and should therefore have shown the same anomaly if it actually was caused by water in the sample.

There are still some theories that support the fact that these deviation were caused by water. A chemical reaction between the water molecules and the material could come into being with increasing temperature, even though this probably would be visible in the inactivated sample values as well. An oxidation film arising on the activated material during activation is another



theory, which was not present on the inactivated material, which broke and caused this severe shift in heat capacity.

Other explanations could be that the materials in question in this work actually contaminated each other's activation, even though the parts were washed thoroughly every time. That there was a structural shift within the material at low temperatures, which was only seen, or possible on activated material, or that the organic linkers changed with low temperatures. These would all be interesting theories to investigate further, especially if there was a problem in the actual activation procedure or a chemical variation in the material in question.

The most likely error causing this abnormality based on this argumentation and the investigation presented in chapter 4.7, was the activation of the samples, because the heat capacities for the inactivated samples increase in a smooth and continuous matter. The only exceptions are some anomalies around 100 °C for some of the inactivated sample curves, which would be natural to assume as mentioned, was due to a change of water in the framework.

The different activated samples were opened and compared, to see if the color could explain the evident deviation on some of the graphs. The three first samples in Figure 4-9 have the respective three first curves in Figure 4-7, which all have values without the inexplicable transition at low temperatures. The following three samples have the three first sample curves from the second activation set in Figure 4-7, where all curves show the same anomaly around -160 °C, but to different extents.

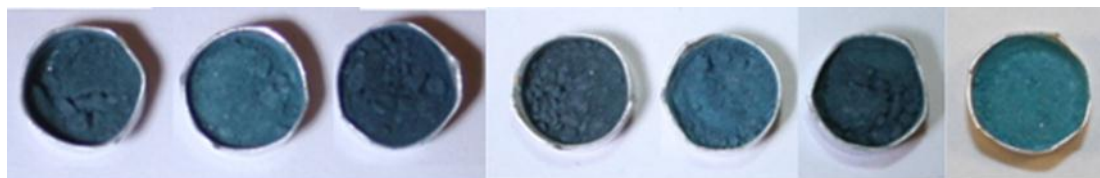


Figure 4-9: Cu-btc activated samples; the three from the left are set 1, the next three are set 2, all in chronological order according to the experimental sequence, and the last one is an inactivated sample.

The colors of the different samples, which in Figure 4-10 are more evident, are all quite different from each other, and a clear pattern between the color of the Cu-btc material and the curves with and without the deviation is not possible to easily point out. What on the other hand is easier to discover is the evident difference between the color of ideal Cu-btc material and this work's activated sample material. It is seen from Figure 4-10 that the six samples in the middle are much greener than the clear deep blue color of the ideal Cu-btc sample on the left. The indications from this observation are difficult to state what are, other than that the activation procedure probably contaminates the Cu-btc in some way. It is also difficult to know why the activation of some samples give a deviation or transition on the heat capacity graph, while other samples show smooth and continuous curves without anomalies. This is a challenge for further investigation.

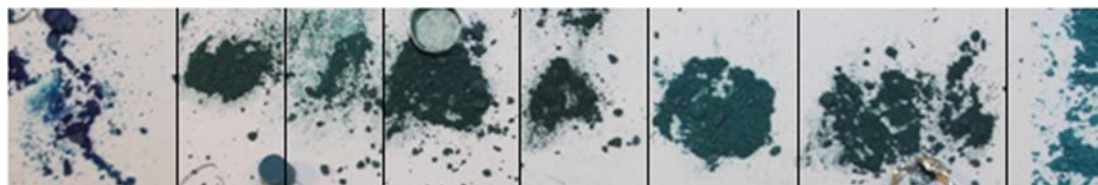


Figure 4-10: Cu-btc activated samples; the first one from the left are a correctly activated sample, the next three are set 1, then the following three are set 2, all in chronological order according to the experimental sequence, and the last one an inactivated sample.

The first red curve from the third activation set in Figure 4-7 has higher heat capacities than the other sample values, both the activated and the inactivated. Implicating the knowledge from experience, that the inactivated samples should consist of more water in their framework than the activated samples and therefore have higher  $C_p$  values, and seeing that the greater part of the curves have heat capacities more or less within a reasonable range, are this sample's values presumed to be incorrect and left out in further presentation of the heat capacity measurement results. The curves which contain the transition at low temperatures are also left out of the representation of the Cu-btc heat capacity measurement results. They are assumed to give incorrect heat capacity values for Cu-btc. Even though the possibility that the curves with the transition are giving the right results for the sample's heat capacities exists, are knowledge from experience and other published heat capacities of MOFs [10-14] considered to be a good enough reason to choose the activated sample values without the deviation to be the approximately correct heat capacities for the Cu-btc material.

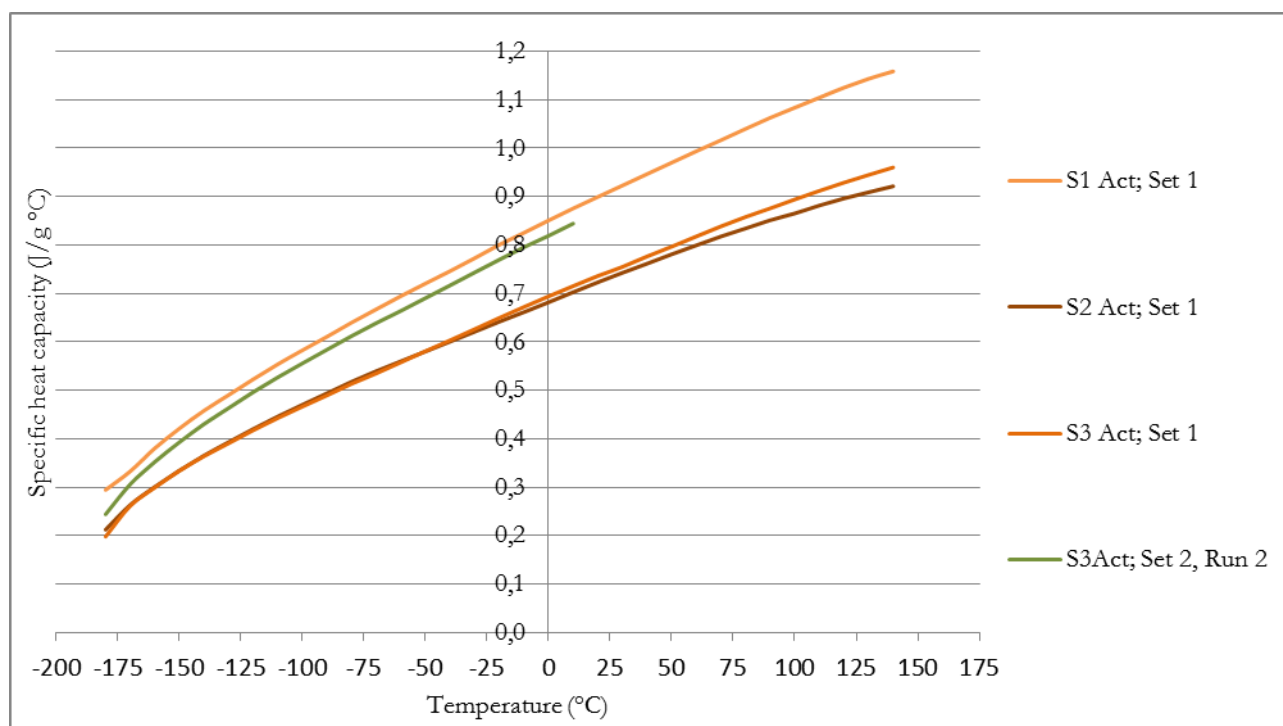


Figure 4-11: Heat capacities of Cu-btc selected activated samples (1. activation – orange; 2. activation – green).

The heat capacities of the selected samples are shown in Figure 4-11, and the data of the selected experiments and the standard deviation for the respective samples are given in Appendix IV. The experimental standard deviations below 0.13 are obtained and show compared to other heat capacity studies on MOFs [10-14], reasonably good reproducibility in the temperature range from -180°C to 140°C.

The heat capacities of the average sample are fitted to the following polynomial equation of heat capacities ( $C_p$ ) with temperature ( $x$ ) going from -180°C to 140°C.

$$C_p \left[ \frac{J}{g K} \right] = 0.75348 + 2.09366 \cdot 10^{-3} X - 1.77581 \cdot 10^{-6} X^2 - 3.12326 \cdot 10^{-10} X^3 - 2.34765 \cdot 10^{-11} X^4 + 2.81617 \cdot 10^{-13} X^5 \quad (4.2)$$

The correlation coefficient of the fitting,  $R^2 = 0.999642$ .

The theoretical heat capacities of copper according to the Debye model is graphed together with reference heat capacities of copper, the measured values of Cu-btc, and published data [3, 14] in Figure 4-12. The theoretical heat capacities are calculated by means of the Debye temperature of copper in combination with the Debye heat capacity model, Figure 4-5.

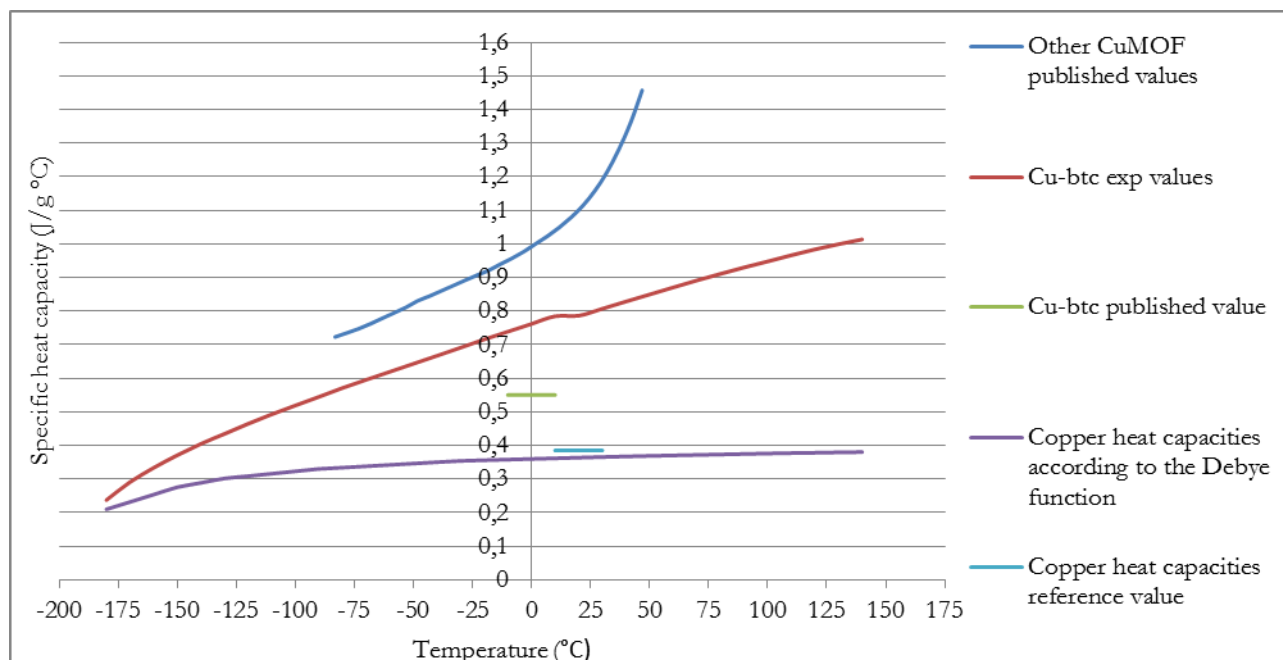


Figure 4-12: The Cu-btc experimental results (red) compared to other published values for both the same Cu-btc material (green) and another CuMOF [14] (blue), and compared to theoretical Cu values (purple and turquoise).

Figure 4-12 show no coherence between the experimental heat capacities for Cu-btc and the other published data. The measurements made by L. Song [14] are on a different CuMOF than the one investigated in this work. The fact that these measurements differ so much from each other support the theory that the heat capacity depends a lot on the material structure and organic ligand more than its metal compound. The published results by Aleksic [3] on the other hand, lack coherence with our values even though it is the exact same material measured. This might be due to an improved measurement procedure in this investigation.

#### 4.4 Fe-btc

The heat capacities for Fe-btc as a function of temperature are shown in Figure 4-13. There were made two activation sets, each with three or four samples. Both sets were activated under the same conditions, with the exception of the vacuum pressure being lower under the second activation.

The experimental values from the inactivated samples are shown in Figure 4-14. The inactivated material curves are plotted together with the activated sample values (black), which makes it easier to discover obvious distinctions between the activated and inactivated material values. There were as well made two different sets of inactivated samples, with three samples in each set. The samples were exposed to normal humidity at room temperature.

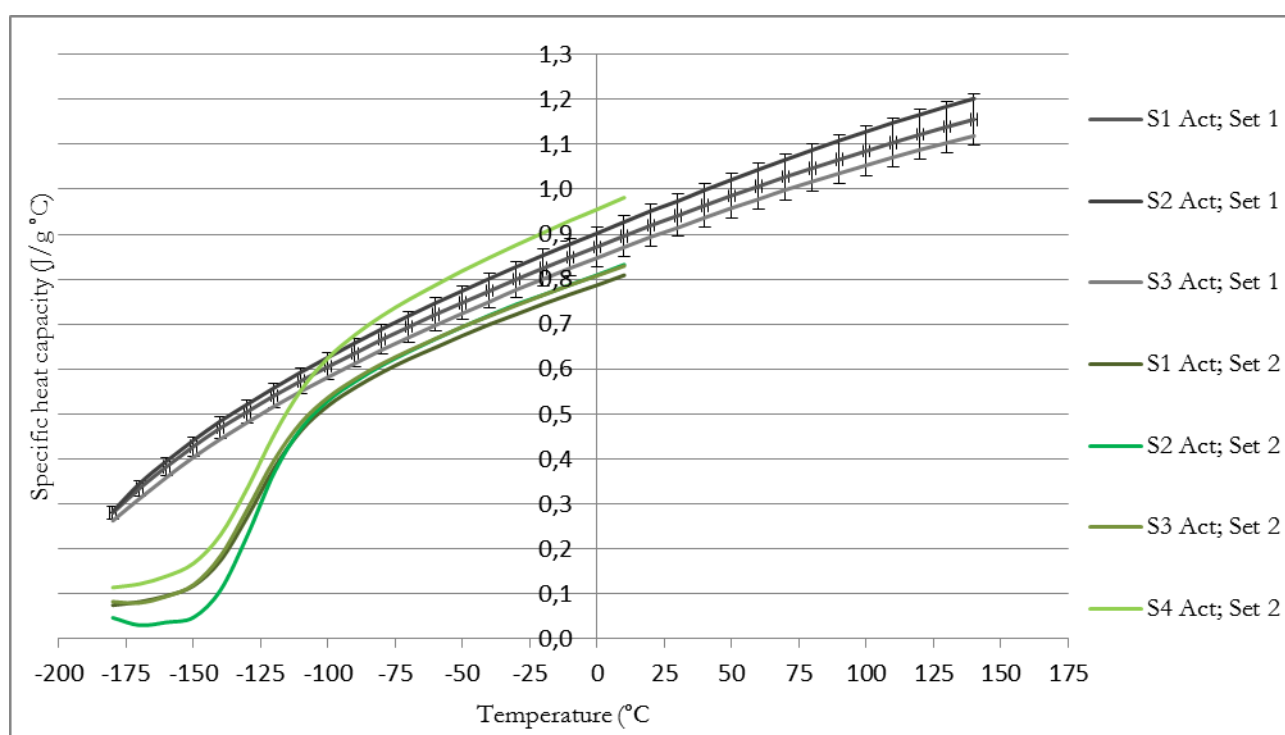


Figure 4-13: Heat capacities of Fe-btc activated samples (1. activation – black; 2. activation – green).

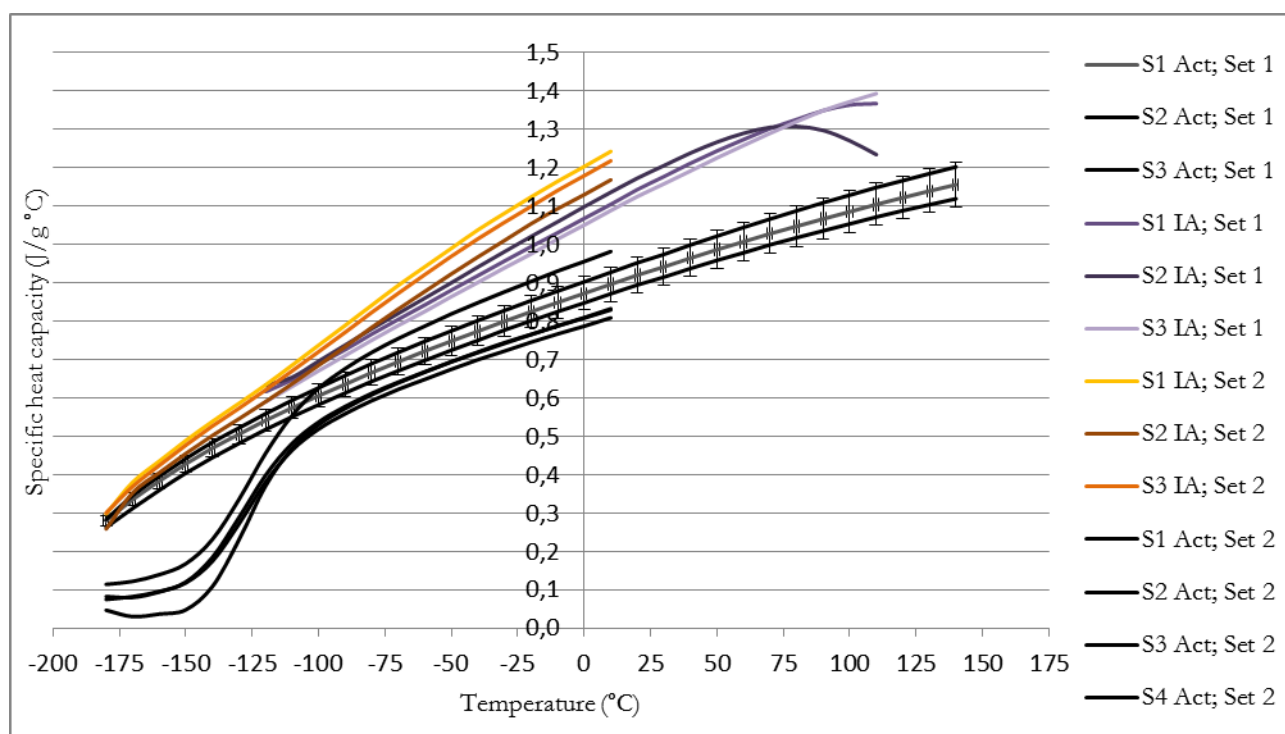


Figure 4-14: Heat capacities of Fe-btc inactivated samples (1. set – purple; 2. set – orange); activated samples (black).

All heat capacities for the inactivated samples in Figure 4-14 are higher than the activated material's heat capacities. This trend is assumed to follow the same explanation that was given to explain this same tendency in the heat capacity curves for activated carbon Norit R0.8, see chapter 4.2.

The purple curves from Figure 4-14 indicate some anomalies around 100°C, which very likely are due to water. The variance between the different inactivated material curves may be caused by a variance in the water adsorption in every sample, due to indifferences in the sample preparation and material handling.

From Figure 4-13, it can be seen that the heat capacities of the samples increase with increasing temperature, in accordance with the theory of specific heat of solids. One half of the curves increase in a smooth and continuous manner in the experimental range, while the other half have an abnormal transition part between -180°C and -100°C. This anomaly seems very similar to the deviation found on several of the Cu-btc activated sample curves. As a consequence of the measurements being performed under the exact same conditions and the sample preparation being identical for every experiment, are the argumentation behind these sudden changes in heat capacity assumed to be the same as for the changes in the Cu-btc heat capacities. See chapter 4.3 for a complete analysis of the sudden heat capacity change.

The different activated samples were opened and compared, to see if the color could explain the evident deviation on some of the graphs. The three first samples in Figure 4-15 have the respective three first (black) curves in Figure 4-13, which all have values without the inexplicable transition at low temperatures. The following four samples belong to the last four (green) sample

curves from the second activation set in Figure 4-13, where all curves show the same anomaly around  $-160^{\circ}\text{C}$ , but to different extents.



Figure 4-15: Fe-btc activated samples; the three from the left are set 1, and the last four set 2, all in chronological order according to the experimental sequence.

The colors of the different samples show that the first activation gave a darker black color to the samples, while the second activation gave the samples a more dark brown color. Comparing these colors to the red-brown color of the inactivated material in Figure 4-16, demonstrates that the samples have been activated, but not the level of success. It seems like the first activation is more successful, because of the darker color on all samples. This would be in good coherence with the respective heat capacity graphs. However, there is no certainty on the matter, only vague assumptions based on personal experience.



Figure 4-16: Fe-btc activated samples; the difference between the 1. set (up) and the 2. set (down). (Right) The Fe-btc inactivated gel.

The curves which contain the transition at low temperatures are therefore left out in further presentation of the heat capacity measurement results. Even though the possibility of the curves with the transition being the right results for the sample's heat capacities exists, are knowledge from experience and other published heat capacities of MOFs [10-14] considered to be a good enough reason to choose the activated sample values without the deviation part to be the approximately correct heat capacities for the Fe-btc material.

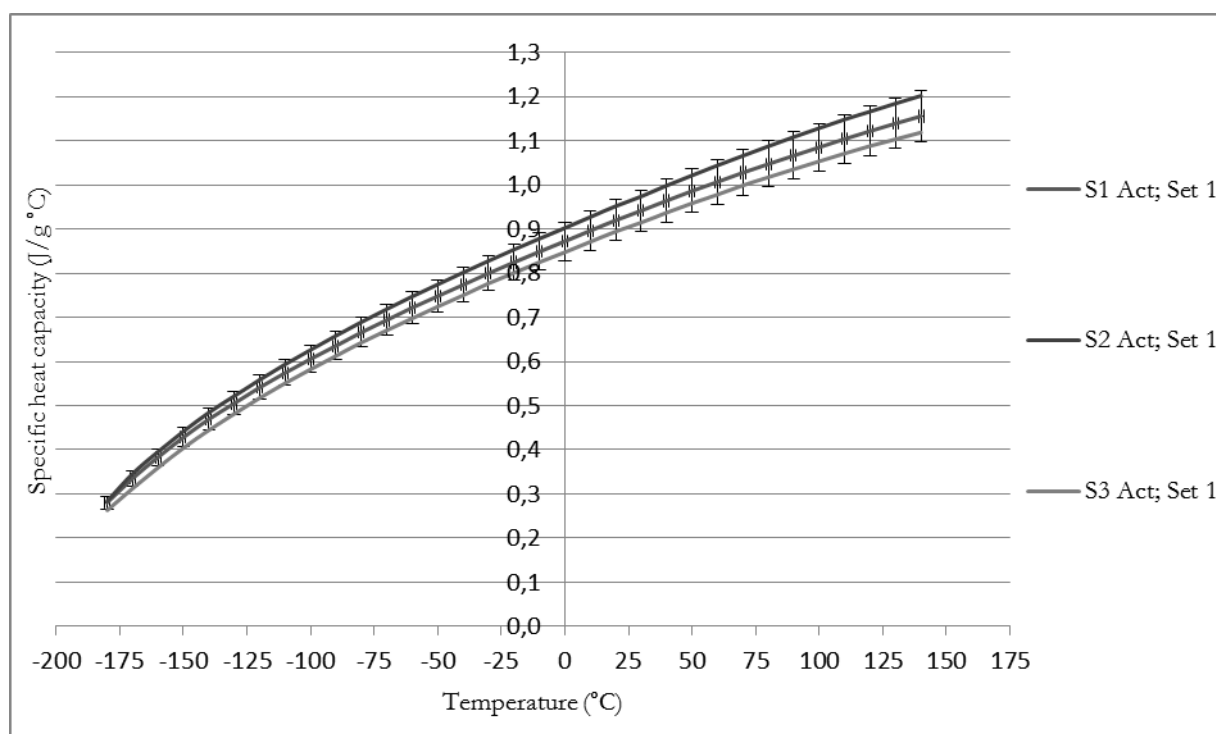


Figure 4-17: Heat capacities of Fe-btc selected activated samples (1. activation – black).

The heat capacities of the selected samples are shown in Figure 4-17, and the data of the selected experiments and the standard deviation for the respective samples are given in Appendix V. The experimental standard deviations below 0.04 are obtained and show compared to other heat capacity studies on MOFs [10-14], reasonably good reproducibility in the temperature range from -180°C to 140°C.

The heat capacities of the average sample are fitted to the following polynomial equation of heat capacities ( $C_p$ ) with temperature ( $x$ ) going from -180°C to 140°C.

$$C_p \left[ \frac{J}{g K} \right] = 0.87477 + 2.40197 \cdot 10^{-3} X - 2.24245 \cdot 10^{-6} X^2 - 1.13458 \cdot 10^{-9} X^3 - 4.82423 \cdot 10^{-11} X^4 + 2.57859 \cdot 10^{-13} X^5 \quad (4.3)$$

The correlation coefficient of the fitting,  $R^2 = 0.999994$ .

Published data on earlier measurements are not found. Heat capacity measurements for Fe-btc do not appear to have been determined previously.



## 4.5 MIL-100(Fe)

The heat capacities for MIL-100(Fe) as a function of temperature are shown in Figure 4-18. There were made three activation sets, with minimum three samples each. All three sets were activated under the same conditions, with the exception of the vacuum pressure being lower under the third activation.

The experimental values from the inactivated samples are shown in Figure 4-19. The inactivated material curves are plotted together with the activated sample values (black), which makes it easier to discover obvious distinctions between the activated and inactivated material values. There were made two different sets of inactivated samples, with three samples in each set, both were exposed to normal humidity at room temperature.

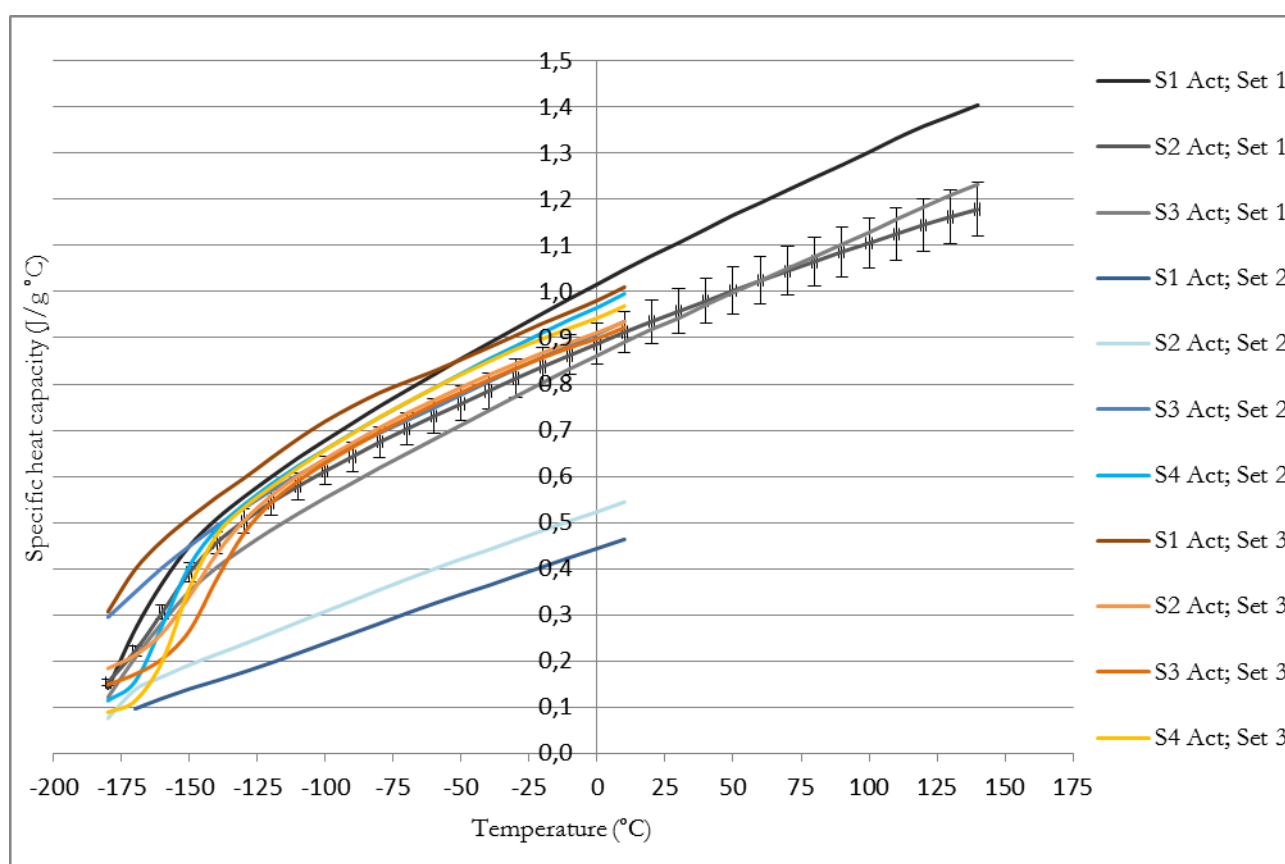


Figure 4-18: Heat capacities of MIL-100(Fe) activated samples (1. activation – black; 2. activation – blue; 3. activation – orange/yellow).

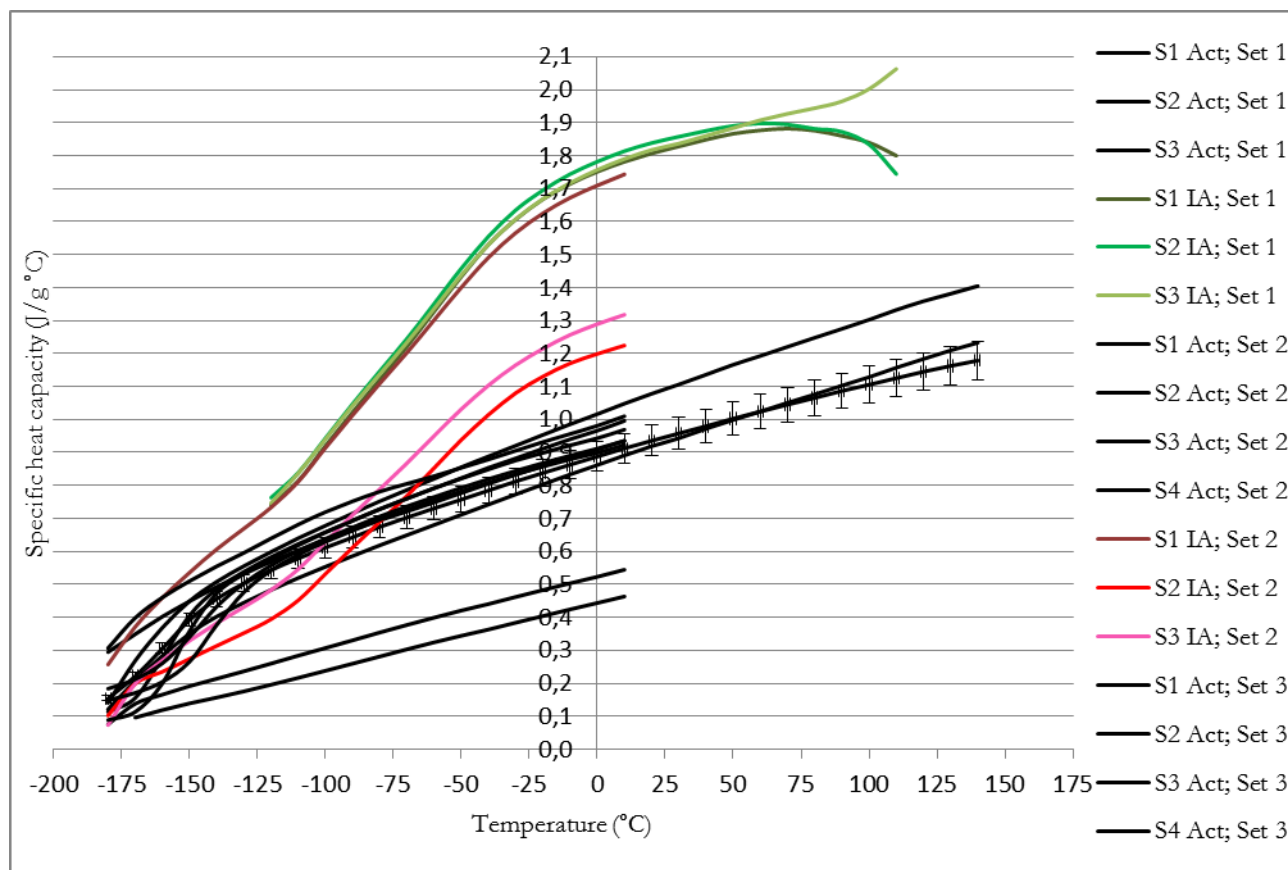


Figure 4-19: Heat capacities of MIL-100(Fe) inactivated samples (1. set – green; 2. set – red); activated samples (black).

Almost all heat capacities for the inactivated samples in Figure 4-19 are higher than the activated material's heat capacities. This trend is assumed to follow the same explanation that was given to explain this same tendency in the heat capacity curves for activated carbon Norit R0.8, see chapter 4.2.

The green curves from Figure 4-19 indicate some anomalies around 100°C, which very likely are due to water. The variance between the different inactivated material curves may be caused by a variance in the water adsorption in every sample, due to indifferences in the sample preparation and material handling.

From Figure 4-18, it can be seen that the heat capacities of the samples increase with increasing temperature, in accordance with the theory of specific heat of solids. Some of the curves increase in a smooth and continuous manner in the experimental range, while some of them have an abnormal transition part around -150 °C. This anomaly seems very similar to the deviation found on some of the Cu-btc activated material curves, but it seems like the dimension of the heat capacity change varies some. As a consequence of the measurements being performed under the exact same conditions and the sample preparation being identical for every experiment, are the argumentation behind these sudden changes in heat capacity assumed to be the same as for the changes in the Cu-btc heat capacities. See chapter 4.3 for a complete analysis of the sudden heat capacity change.

The different activated samples were opened and compared, to see if the color could explain the evident deviation on some of the graphs. The three first samples in Figure 4-20 have the respective three first (black) curves in Figure 4-18. The following four samples belong to the four (blue) sample curves from the second activation set in Figure 4-18. The last sample is an inactivated sample, to see the color difference and the degree of activation on the other activated samples.



Figure 4-20: MIL-100(Fe) activated samples; the three first ones from the left are set 1, the next four samples are set 2, all in chronological order according to the experimental sequence, and the last one is an inactivated sample.

The colors of the different samples, which in Figure 4-21 are more evident, show a variation between almost every sample. Figure 4-22 shows the color of the four samples from the third activation set in Figure 4-18, which are quite discolored in comparison to the other sets. Comparing the colors of the samples to their respective heat capacities does not give a clear coherence between color of the material and behavior of the curve. It is actually difficult to make out any theory on parallels between the two, but it seems more obvious that there is a problem with the activation of the material.



Figure 4-21: MIL-100(Fe) activated samples; the four first ones from the left are set 1, the next three samples are set 2, all in chronological order according to the experimental sequence, and the last one is an inactivated sample.



Figure 4-22: MIL-100(Fe) activated samples set 3, all in chronological order according to the experimental sequence.

The curves which contain the greatest heat capacity change at low temperatures are left out in further presentation of the heat capacity measurement results. This is due to the assumption that this is an incorrect curve over the material's heat capacities. Even though the possibility of the curves with the transition being the right results for the sample's heat capacities, are knowledge from experience and other published heat capacities of MOFs [10-14] considered to be a good enough reason to choose the activated sample values without the biggest deviation part to be the

approximately correct heat capacities for the MIL-100(Fe) material. The two blue curves in Figure 4-18 are also left out of the representation of the MIL-100(Fe) heat capacity measurement results, because they deviate quite a lot from the bulk of the samples.

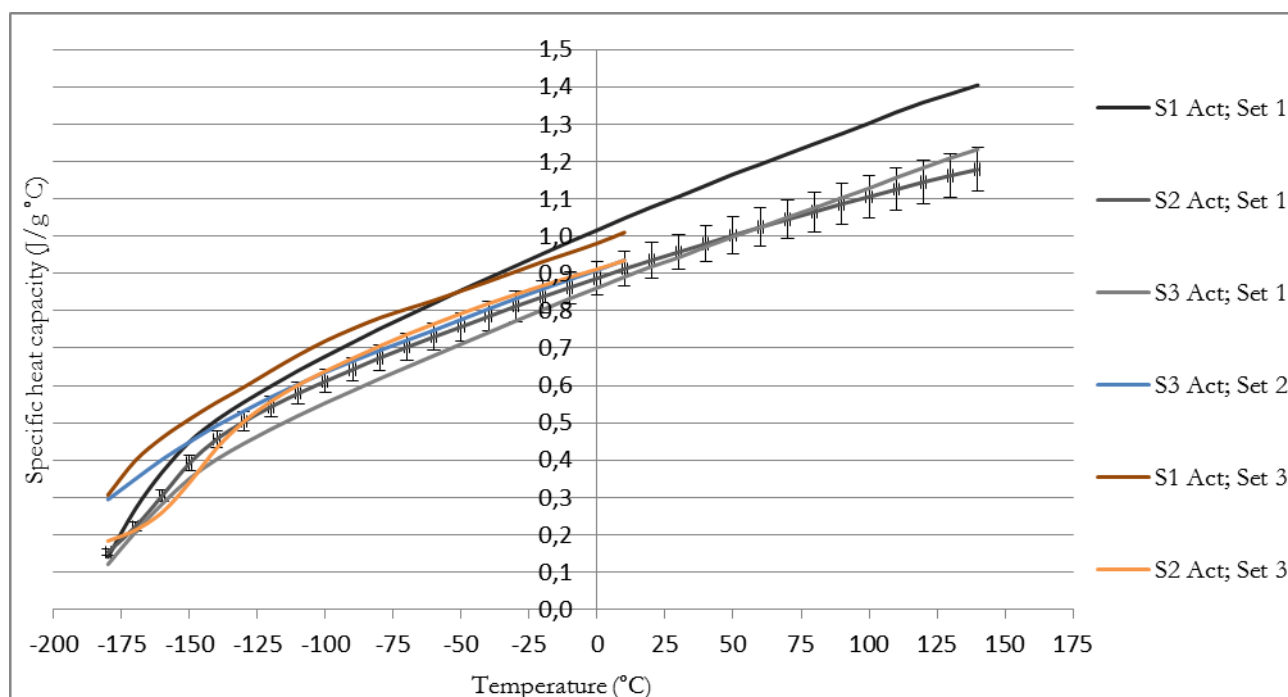


Figure 4-23: Heat capacities of MIL-100(Fe) selected activated samples (1. activation – black; 3. activation – orange/yellow).

The heat capacities of the selected samples are shown in Figure 4-23, and the data of the selected experiments and the standard deviation for the respective samples are given in Appendix VI. The experimental standard deviations below 0.13 are obtained and show compared to other heat capacity studies on MOFs [10-14], reasonably good reproducibility in the temperature range from -180°C to 140°C.

The heat capacities of the average sample are fitted to the following polynomial equation of heat capacities ( $C_p$ ) with temperature ( $x$ ) going from -180°C to 140°C.

$$C_p \left[ \frac{J}{g K} \right] = 0.92626 + 2.63184 \cdot 10^{-3} X - 4.8793 \cdot 10^{-7} X^2 - 3.84323 \cdot 10^{-11} X^3 - 1.15377 \cdot 10^{-10} X^4 + 6.2683 \cdot 10^{-13} X^5 \quad (4.4)$$

The correlation coefficient of the fitting,  $R^2 = 0.999953$ .

Published data on earlier measurements are not found. Heat capacity measurements for MIL-100(Fe) do not appear to have been determined previously.

## 4.6 Heat Capacity Measurements for all Porous Materials

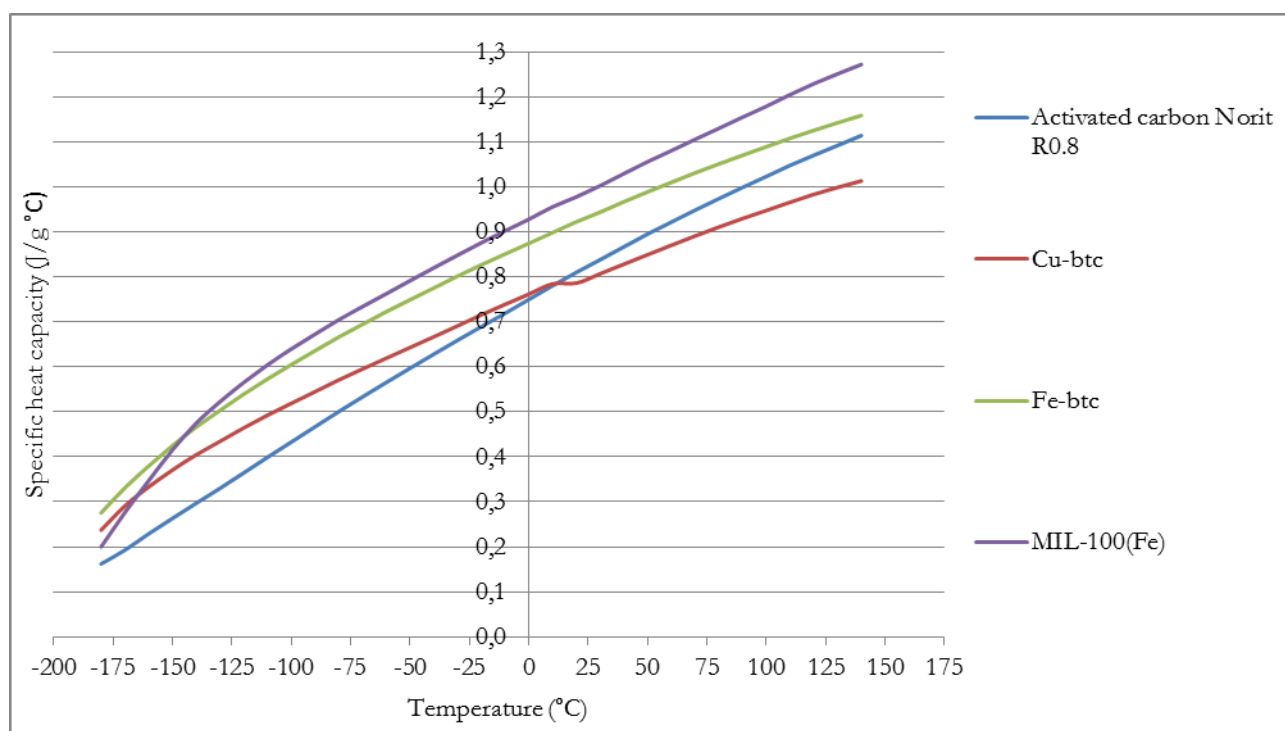


Figure 4-24: The average heat capacities from the selected measurement curves for each material measured.

Figure 4-24 shows the average heat capacities from the selected measurement curves for each material measured. It is seen that the three MOFs have somewhat the same slope, these MOFs are all compounds with the same organic linker, benzene-1,3,5-tricarboxylate (btc). The Fe-btc and MIL-100(Fe) have heat capacities within the closest range of each other. This may be because in addition to hold the same organic linker in their structure, are they both built up using Fe as their metal, so the structural composition is the only difference between the two.

## 4.7 Potential Error Sources Based on Experience

The pan and lid encapsulation is necessary for a tight and sealed sample. This is very important because volatilization during the measurement, which leads to a change in the sample mass, such as changes in the material framework's water content, will give incorrect and useless heat capacity values. Appendix II shows an overview over the sample masses after terminated experiments, and their mass deviations. The majority of the mass variances are below 1% of their original weight, but there are some mass changes as large as 4.26%. This may according to the manual be one of the reasons behind result variances. Studying the result curves and comparing them against their sample mass variances one can dimly perceive a pattern, where an increase in sample mass gives increased heat capacities and conversely. However, the results yields in some cases away from the pattern, which makes it difficult to establish a rule over the measurement behavior in the case of mass change.

For accurate  $C_p$  measurements are good thermal contact between the cups and the sensors very important. The sample and reference cups need to be clean and smooth on the bottom side, and the Tzero™ pans are therefore used because of their flat pan bottom. Also the sensor surface is required to be very clean. The handling of the samples is therefore very careful, and the samples are never touched, only prepared using tweezers and gloves. The sensor is also repeatedly cleaned with a special brush tailored for this exact purpose. However, some unevenness on some of the samples was difficult to avoid, and this was noted in the sample list, appendix II. The small differences noted were as far as the results observed without any noticeable impact on the heat capacity values. Even though it is not possible to see any obvious change in the results owing to the unevenness on some of the samples, it does not mean that it did not affect the results anyway, but it is more probable to anticipate that the inequality was too small to have any impact.

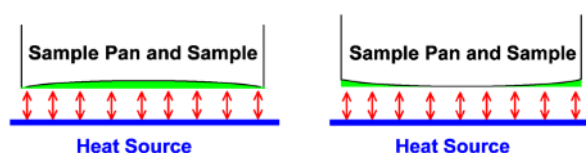


Figure 4-25: Effects from an uneven pan bottom after a poor sample preparation [75].

The sample preparation is rather important for obtaining accurate  $C_p$  results, to ensure fast internal heat transfer and good thermal contact between the material and its pan bottom. The material should be in a powder form which is densely packed by stapling it into its cup by using the lid and the Tzero™ sample press. Any contamination or poorly densely packing of the material can cause inaccuracies. Every part of the equipment used was thoroughly washed with distilled water before use and between every material change, and gloves were used if the sample were in contact with the hands. The noticeable poorly packed samples were as well noted in the sample list, appendix II. Comparing the samples in question with their respective curves does not show deviations in obvious coherence. However, it might be a small increase in their heat capacities compared to the other sample curves from the same set. On the other hand, this is a

very vague assumption to take, and these increases can very easily come from other error sources, or even be a combination of several.

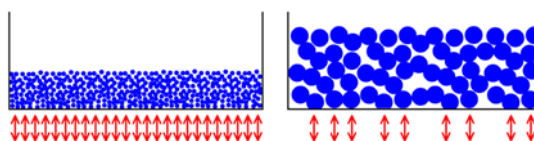


Figure 4-26: Effects from sample preparation, and how it affects the heat flow [75].

The cell needs to be clean to avoid any destabilization of the  $C_p$  curve. Thus, the cell chamber on the DSC was thoroughly cleaned by a TA Instruments technician before starting the measurements. Thereafter, the cell chamber was cleaned at regular intervals. The baseline was checked both before and after the measurement period to ensure the instruments accuracy. The baseline at start-up was straight and a part of the instrumental calibration, while the baseline at ended experiments was gently decreasing. This would normally have an influence on the heat capacities measured, since  $C_p$  is depending on the total heat flow, but the method used being MDSC, the reversed  $C_p$  is measured instead of the total  $C_p$  as normal in the conventional DSC method. Reversed  $C_p$  is depending on the amplitudes of the modulated heat flow and heating rate, and not the baseline [17]. Regardless of this statement, one cannot completely rule out the importance of a heat flow change, but it is without any doubt less important than it would have been using another measuring method.

Another disturbance to the results can be a dirty and imperfectly fitted cell lid. The cell lid was therefore cleaned and fitted to the cell chamber by the same TA Instruments technician before starting measurements. Subsequently, the cell lid is untouched. This does not rule out any interference on the result curve, but if they exist they should only appear at the very beginning of the curve as an interruption, not a transition. These indifferences are not observed.

It would evince traces of an inaccuracy of the autosampler in the same way as a defect with the cell lid would. The TA Instruments technician as well corrected the autosampler so that both reference and sample were placed perfectly on each pan in the cell. This correction might have diverted a little bit, but as far as the observed heat capacity graphs go, there is little insinuating of an impact from this.

There are two purge gases, one for the DSC cell (helium) and one for the LNCS flange (nitrogen). If the instrument is run without cell purge, the heat flow value will not be fully quantitative, as calibration depends upon flow rate of the cell purge. If it is run with no base purge it can be that there is some irreversible moisture condensation in the system. Since the cell purge, helium, has been on at all times, and this mass flow is automatically checked by the system and the experiment procedure aborted if the mass flow becomes lower than required, this cannot be a source of error. The base purge on the other hand has no security mechanism, and has unfortunately sometimes been forgotten to turn on during experiments. This is noted in the

sample list, appendix II. The first episodes with activated AC Norit R0.8 samples show a possibility for a correlation between the lack of purge gas and increasing heat capacities. However, due to a lack of consistency in the correlation and the fact that irreversible moisture condensation in the system would show unexpected peaks around 0 °C, this is highly unlikely. Peaks around 0°C, are in addition absent in every sample curve, if this proves a dry cell or not is difficult to state with certainty without further testing.

The modulation period is 40 sec, maybe it would be recommendable to work at a higher period than 40 sec, 60 sec e.g. to make sure that the sample can follow the modulation in the MDSC method.

The last potential error source considered was the actual instrument and its calibration being shifted. A heat capacity calibration with sapphire was executed, as well as indium calibration verification. The heat capacity calibration showed good results still inside of the 5 % acceptable inaccuracy range of the table values, and the indium verification was successful. This demonstrated at least the fact that the instrument is working as it should, and still measures exact heat capacities for the reference material used for calibrating it.





## 5 Uncertainty Analysis

The heat capacity is calculated by the DSC Q2000 instrument as a function of mass. In this section, the uncertainties on the heat capacity and mass will therefore be investigated and calculated.

### 5.1 Heat Capacity Uncertainty Analytical Calculation

The specific heat capacity can be defined by the following equation:

$$C_P = \frac{C_{P\ mat} \cdot m_{mat} + C_{P\ gas} \cdot m_{gas}}{m_{mat} + m_{gas}} \quad (5.1)$$

The specific heat capacity can be expressed as a function of the following variables:

$$C_P = f(C_{P\ mat}, C_{P\ gas}, m_{mat}, m_{gas}) \quad (5.2)$$

The expected uncertainty can be defined as:

$$\Delta C_P = \sqrt{\left(\frac{\partial C_P}{\partial C_{P\ mat}} \Delta C_{P\ mat}\right)^2 + \left(\frac{\partial C_P}{\partial C_{P\ gas}} \Delta C_{P\ gas}\right)^2 + \left(\frac{\partial C_P}{\partial m_{mat}} \Delta m_{mat}\right)^2 + \left(\frac{\partial C_P}{\partial m_{gas}} \Delta m_{gas}\right)^2} \quad (5.3)$$

Where the partial derivatives are respectively given by:

$$\frac{\partial C_P}{\partial C_{P\ mat}} = \frac{m_{mat}(m_{mat} + m_{gas})}{(m_{mat} + m_{gas})^2} \quad (5.4)$$

$$\frac{\partial C_P}{\partial C_{P\ gas}} = \frac{m_{gas}(m_{mat} + m_{gas})}{(m_{mat} + m_{gas})^2} \quad (5.5)$$

$$\frac{\partial C_P}{\partial m_{mat}} = \frac{C_{P\ mat}(m_{mat} + m_{gas}) - (C_{P\ mat} \cdot m_{mat} + C_{P\ gas} \cdot m_{gas})}{(m_{mat} + m_{gas})^2} \quad (5.6)$$

$$\frac{\partial C_P}{\partial m_{gas}} = \frac{C_{P\ gas}(m_{mat} + m_{gas}) - (C_{P\ mat} \cdot m_{mat} + C_{P\ gas} \cdot m_{gas})}{(m_{mat} + m_{gas})^2} \quad (5.7)$$

### 5.2 Sample Basis

To calculate several uncertainties in coherence with the experiments performed a reference sample is chosen, where its characteristics are chosen on the basis of the samples in question, in other words, more or less average properties.

Table 5.1: A sample used as a reference for uncertainty calculations.

Sample	Pan&Lid	Material	Total <sub>Before</sub>	C <sub>P</sub> lower value	C <sub>P</sub> higher value	Inner volume
Sx Act; Set x	52.35 mg	15 mg	67 mg	0.16 J/g K	1.27 J/g K	40 µl

### 5.3 Different Cases over the Inert Gases Present in the Sample

As presented in chapter 2.4 is it not known which inert gases that are present in the sample, but there is a limited amount of gases that can be present. The different cases, which are the same used in chapter 2.4, are the following:

- **Case 1:** The whole sample (40  $\mu\text{l}$ ) is filled with air ( $p = 1 \text{ atm}$ ,  $T = 23^\circ\text{C}$ ,  $\text{RH} = 25\%$ ,  $\rho_{\text{air}} = 1.0983 \text{ kg}/\text{m}^3$ ) having the assumed composition;  $\text{N}_2$  : 77.428%,  $\text{O}_2$  : 20.846%,  $\text{Ar}$  : 0.993%,  $\text{H}_2\text{O}$  : 0.693%, and  $\text{CO}_2$  : 0.04%.
- **Case 2:** The whole sample (40  $\mu\text{l}$ ) is filled with  $\text{N}_2$ .
- **Case 3:** The whole sample (40  $\mu\text{l}$ ) is filled with He.
- **Case 4:** The material has adsorbed 0.015 g-  $\text{H}_2\text{O}$ / g-dry material, and the rest of the sample (40  $\mu\text{l}$ ) is filled with air from case 1.

These cases will all have different uncertainties, and the  $dC_p$  will be calculated for each case. The most probable scenario is assumed to be a mix of 1 and 4.

### 5.4 Variations of the Different Parameters

#### 5.4.1 Estimation of $\Delta m_{\text{mat}}$

The  $m_{\text{mat}}$  is not directly measured, but extracted from the following equation:

$$m_{\text{mat}} = m_{\text{total}} - m_{\text{pan\&lid}} \quad (5.8)$$

This gives the following uncertainty on the  $m_{\text{mat}}$ , with the partial derivatives being 1 and -1, respectively:

$$\Delta m_{\text{mat}} = \sqrt{(\Delta m_{\text{total}})^2 + (\Delta m_{\text{pan\&lid}})^2} \quad (5.9)$$

The observed mass accuracy when weighed with a Mettler Toledo excellence plus  $\text{\textcircled{R}}$  and taking into account the uncertainties in temperature and destabilizations of the weight, is  $m_{\text{pan\&lid}} = 52.35 \pm 0.01 \text{ mg}$ . The  $m_{\text{total}}$  is weighed both before an experiment and after, the deviations results are noted in the sample list attached in appendix II, and the “worst case scenario” gives an uncertainty of 4.26% mass increase or decrease. The total mass is assumed to be  $m_{\text{total}} = 67 \pm 3 \text{ mg}$  based on the “worst case scenario”.

$$\Delta m_{\text{mat}} = 3 \text{ mg.}$$

### 5.4.2 Estimation of $\Delta m_{\text{gas}}$

This value  $\Delta m_{\text{gas}}$  is a factor that depends on the surrounding conditions of the sample and the assumed case.

- **Case 1:** In this scenario is the uncertainty value of the  $m_{\text{air}}$  depending on the temperature, pressure and relative humidity of the surroundings when encapsulating the sample. From Molière's diagram over humidity in air [76] is temperature varied from 22°C to 24°C, the relative humidity varied from 22% to 27%, and the pressure held constant to 1 atm. This gave a density varying from 1.0857 kg/m<sup>3</sup> to 1.1111 kg/m<sup>3</sup>. This gives a reasonable estimated  $m_{\text{air}} = 0.0439 \pm 0.0005$  mg.

$$\Delta m_{\text{air}} = 0.0005 \text{ mg}$$

- **Case 2:** This value depends on the temperature and pressure of nitrogen flowing into the sample. The nitrogen is added to the sample right after it's activation. An estimation of the  $\Delta m_{\text{N}_2}$  is reasonable to calculate based on the density slightly varying with the fast temperature change after the activation. A rational guess would be choosing densities from 0.9754 kg/m<sup>3</sup> (at 350 K) to 1.1380 kg/m<sup>3</sup> (at 300 K) using the ideal gas law. This gives the following inert gas mass in a 40  $\mu\text{l}$  sample;  $m_{\text{N}_2} = 0.042 \pm 0.004$  mg.

$$\Delta m_{\text{N}_2} = 0.004 \text{ mg}$$

- **Case 3:** In this scenario helium is entering into the sample because of the lid not being airtight. The  $m_{\text{He}}$  will therefore slightly vary with temperature, due to the density changing as a function of temperature. The different densities chosen are based on the experimental temperature range (-180°C to 140°C), 0.4878 kg/m<sup>3</sup> (at 100 K), and 0.1220 kg/m<sup>3</sup> (at 400 K) using the ideal gas law. This gives the following inert gas mass in a 40  $\mu\text{l}$  sample;  $m_{\text{He}} = 0.012 \pm 0.008$  mg.

$$\Delta m_{\text{He}} = 0.008 \text{ mg}$$

- **Case 4:** This value depends on both the air mass value from case 1, and the adsorbed water mass in the material. The water adsorption is a guessed factor based on several different factors, see chapter 0 for a more detailed explanation of the estimation. Calculating the uncertainty on this factor will not be highly unreliable because of all the guessed assumptions that are made deciding the magnitude of this factor. There are very little published data concerning the properties of the MOFs measured, and due to this lack of information on the water adsorption rate for the different materials is this factor held constant and left out of the uncertainty calculations. However, it is suggested to do further investigations on the adsorption rate of water vapor, seeing how this can have quite a large impact on the measured heat capacity.

The inert gas mass is then extracted from the following equation:

$$m_{\text{gas}} = m_{\text{air}} + m_{\text{H}_2\text{O}}(g) \quad (5.10)$$

This gives the following uncertainty of  $m_{\text{gas}}$ , with both of the partial derivatives being 1:

$$\Delta m_{\text{gas}} = \sqrt{(\Delta m_{\text{air}})^2 + (\Delta m_{\text{H}_2\text{O}(g)})^2} \quad (5.11)$$

The variation of the air mass is assumed to be the same as in case 1, while the mass for the water vapor is estimated to have the same variance percentage as the material mass,  $m_{\text{H}_2\text{O}(g)} = 0.022 \pm 0.05 \text{ mg}$ .

$$\Delta m_{\text{gas}} = 0.05 \text{ mg}$$

### 5.4.3 Determination of $\Delta C_{\text{P mat}}$

Performance of the instrument (DSC Q2000), using the MDSC method, is reported by TA Instruments [17] to be 5%. Aluminum heat capacity from the pan and lid is already accounted for in the instrumental inaccuracy. Thus, owing to internal routines in the instrument, and the fact that a sensitivity analysis is not performed on the instrument, it is assumed that this uncertainty error is 5% of the correct heat capacity value of the material. The sensitivity analysis of the instrument is not executed partly due to the time perspective of this work, but also a settlement of it being unneeded because of unsatisfactory measurement results. However, it would for further investigations on the matter be natural to look into how much an error of the pan and lid mass input constitute on the output heat capacity value.

Since the heat capacity varies quite a lot with temperature, will the 5% error give larger deviations at high heat capacity values than with lower values. This gives two different heat capacity uncertainty cases;  $\Delta C_{\text{P mat lower}}$  and  $\Delta C_{\text{P mat higher}}$ .

$$\Delta C_{\text{P mat lower}} = 0.008 \text{ J/g K}$$

$$\Delta C_{\text{P mat higher}} = 0.07 \text{ J/g K}$$

### 5.4.4 Estimation of $\Delta C_{\text{P gas}}$

This value  $\Delta C_{\text{P gas}}$  is reflecting the fact that the actual specific heat capacity of the inert gases in the sample varies with temperature, where constant values were used in this calculation.  $\Delta C_{\text{P gas}}$  depends on the different possible cases of the inert gases content in the sample.

- **Case 1:** The value  $C_{\text{p air}}$  used is 1.007 J/g K. This heat capacity value varies with temperature [77], it also depends on the air's relative humidity, using the tabulated values a variance assumed reasonable was:

$$\Delta C_{\text{P air}} = 0.03 \text{ J/g K}$$

- **Case 2:** The same reference has given the nitrogen values and its variance with temperature,  $C_{\text{p N}_2} = 1.04 \pm 0.03 \text{ J/g K}$ .

$$\Delta C_{\text{P N}_2} = 0.03 \text{ J/g K}$$

- **Case 3:** This heat capacity value,  $C_{p\text{He}} = 5.193 \text{ J/g K}$ , remains constant with temperature up to 6000 K [73], so it was reasonable to assume zero variance.

$$\Delta C_{p\text{He}} = 0.00 \text{ J/g K}$$

- **Case 4:** Since the heat capacity for the inert gases in this case depends on both air content and the adsorbed water vapor content can  $\Delta C_{p\text{gas}}$  be expressed as:

$$C_{p\text{gas}} = \frac{C_{p\text{air}} \cdot m_{\text{air}} + C_{p\text{H}_2\text{O}(g)} \cdot m_{\text{H}_2\text{O}(g)}}{(m_{\text{air}} + m_{\text{H}_2\text{O}(g)})} \quad (5.12)$$

The expected uncertainty can be defined as:

$$\Delta C_{p\text{gas}} = \sqrt{\left(\frac{\partial C_p}{\partial C_{p\text{air}}} \Delta C_{p\text{air}}\right)^2 + \left(\frac{\partial C_p}{\partial C_{p\text{H}_2\text{O}(g)}} \Delta C_{p\text{H}_2\text{O}(g)}\right)^2 + \left(\frac{\partial C_p}{\partial m_{\text{air}}} \Delta m_{\text{air}}\right)^2 + \left(\frac{\partial C_p}{\partial m_{\text{H}_2\text{O}(g)}} \Delta m_{\text{H}_2\text{O}(g)}\right)^2} \quad (5.13)$$

Where the partial derivatives are respectively given by:

$$\frac{\partial C_p}{\partial C_{p\text{air}}} = \frac{m_{\text{air}}(m_{\text{air}} + m_{\text{H}_2\text{O}(g)})}{(m_{\text{air}} + m_{\text{H}_2\text{O}(g)})^2} \quad (5.14)$$

$$\frac{\partial C_p}{\partial C_{p\text{H}_2\text{O}(g)}} = \frac{m_{\text{H}_2\text{O}(g)}(m_{\text{air}} + m_{\text{H}_2\text{O}(g)})}{(m_{\text{air}} + m_{\text{H}_2\text{O}(g)})^2} \quad (5.15)$$

$$\frac{\partial C_p}{\partial m_{\text{air}}} = \frac{C_{p\text{air}}(m_{\text{air}} + m_{\text{H}_2\text{O}(g)}) - (C_{p\text{air}} \cdot m_{\text{air}} + C_{p\text{H}_2\text{O}(g)} \cdot m_{\text{H}_2\text{O}(g)})}{(m_{\text{air}} + m_{\text{H}_2\text{O}(g)})^2} \quad (5.16)$$

$$\frac{\partial C_p}{\partial m_{\text{H}_2\text{O}(g)}} = \frac{C_{p\text{H}_2\text{O}(g)}(m_{\text{air}} + m_{\text{H}_2\text{O}(g)}) - (C_{p\text{air}} \cdot m_{\text{air}} + C_{p\text{H}_2\text{O}(g)} \cdot m_{\text{H}_2\text{O}(g)})}{(m_{\text{air}} + m_{\text{H}_2\text{O}(g)})^2} \quad (5.17)$$

All the parameters are already known, except for the heat capacity for water vapor and how much this varies. The water vapor adsorbed in the material is assumed to be in the state of vapor during the whole experiment, this assumption is substantiated in chapter 0. This means that the water vapor adsorbed is in a very controversial state, and it is difficult to presume how the heat capacity will vary with any certainty. However, some heat capacity values at higher temperatures are accessible, and taking the basis in these values, is the guessed heat capacity value for water vapor;  $C_{p\text{H}_2\text{O}(g)} = 2.08 \pm 0.08 \text{ J/g K}$ .

$$\Delta C_{p\text{H}_2\text{O}(g)} = 0.08 \text{ J/g K}$$

These were the last parameters needed to calculate the variance of the gas in this last case.

$$\Delta C_{p\text{gas}} = 0.08 \text{ J/g K}$$

## 5.5 Total Uncertainty for the Measured Results

Since the heat capacity varies quite a lot with temperature, will the uncertainties differ depending on low heat capacities or higher ones. The total uncertainty is therefore depending on the case used, and the heat capacity being the lower or the higher value.

### 5.5.1 Case 1 - Air

- $\Delta C_p (0.16 \text{ J/g K}) = 0.00799 \text{ J/g K} \rightarrow 4.994\%$
- $\Delta C_p (1.27 \text{ J/g K}) = 0.0698 \text{ J/g K} \rightarrow 5.496\%$

### 5.5.2 Case 2 – N<sub>2</sub>

- $\Delta C_p (0.16 \text{ J/g K}) = 0.008 \text{ J/g K} \rightarrow 5.00\%$
- $\Delta C_p (1.27 \text{ J/g K}) = 0.0698 \text{ J/g K} \rightarrow 5.496\%$

### 5.5.3 Case 3 - He

- $\Delta C_p (0.16 \text{ J/g K}) = 0.00847 \text{ J/g K} \rightarrow 5.294\%$
- $\Delta C_p (1.27 \text{ J/g K}) = 0.07 \text{ J/g K} \rightarrow 5.512\%$

### 5.5.4 Case 4 – Air + H<sub>2</sub>O(g) Adsorbed

- $\Delta C_p (0.16 \text{ J/g K}) = 0.0114 \text{ J/g K} \rightarrow 7.125\%$
- $\Delta C_p (1.27 \text{ J/g K}) = 0.0689 \text{ J/g K} \rightarrow 5.425\%$

## 6 Conclusions

In this work, the specific heat capacity for one activated carbon, Norit R0.8 (1), and three microporous MOFs, Cu-btc (2), Fe-btc (3), and MIL-100(Fe) (4), have been measured, both for inactivated and activated material. The compounds were measured using an MDSC method on a Q2000 differential scanning calorimeter with an appurtenant liquefied nitrogen cooler system (LNCS), measuring heat capacity from  $-180^{\circ}\text{C}$  to  $150^{\circ}\text{C}$ .

The inactivated sample curves showed a general trend, where the heat capacities for inactivated material normally were higher than the heat capacities for the respective activated material. This tendency was assumed to be due to higher water content in the inactivated material.

A considerable number of measurements on each material were performed, without obtaining the expected results for the activated samples. The principal reason was that an unexplainable transition around  $-150^{\circ}\text{C}$  was present on almost half of the obtained data.

Several measurements were executed only to provide the cause behind the sudden heat capacity change, but the exact reason behind this anomaly was not found. However, the most likely error was the activation of the samples, based on analysis and investigation of the results. This presumption was stated mainly because the heat capacities for the inactivated samples increased in a smooth and continuous matter with increasing temperature, without this sudden heat capacity change around  $-150^{\circ}\text{C}$ . The conclusion is due to the time perspective of this work an assumption based on observations and personal experience. Further investigation on the matter is recommended, especially to find out if there was a problem in the actual activation procedure or a chemical change in the investigated materials.

The uncertainties for the different measurements were determined, and depending on the assumed water content, varied the uncertainty from 5% to 7%. The measurement accuracy depended very little on the inert gases present in the sample.

Figure 6-1 show the average heat capacities from the selected measurement curves for each material measured.



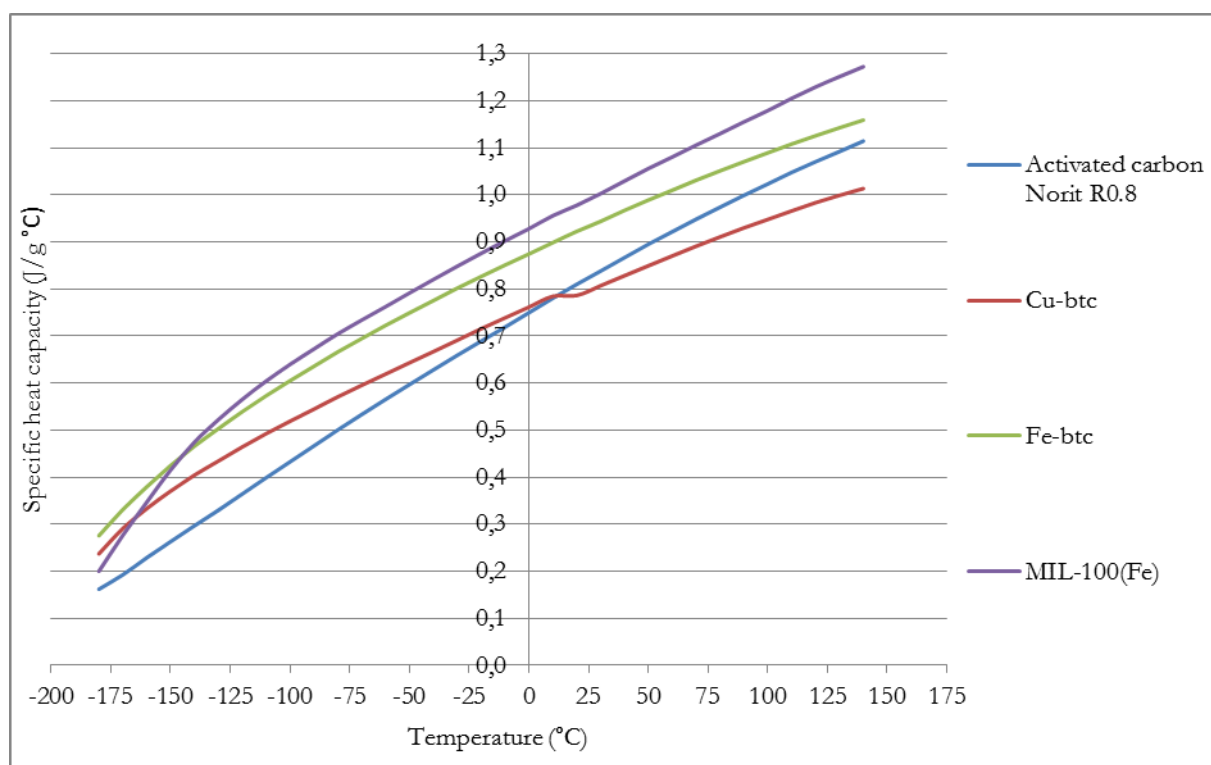


Figure 6-1: The average heat capacities from the selected measurement curves for each material measured.

## 7 Further work

This study has shown that it was more complicated to measure the heat capacity for the MOFs in question than anticipated. There has been performed a considerable number of measurements on each material, without obtaining the expected results. The principal reason being the unexplainable transition on almost half of the graphs around -150 °C in Figure 7-1.

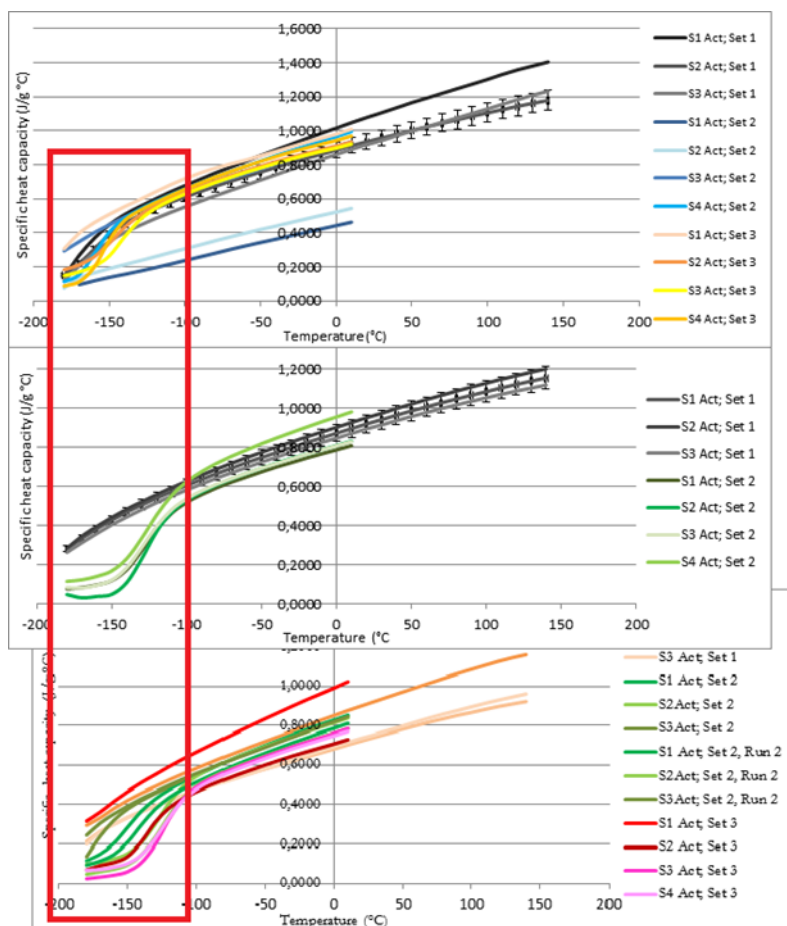


Figure 7-1: The activated sample values from MIL-100(Fe), Fe-btc and Cu-btc, respectively from above.

Several measurements were executed only to provide the cause behind the sudden heat capacity change, which evidently emerged on every material measured. Since the reason behind this anomaly was not found, mainly due to the time perspective of this work, further investigation on the matter should be carried out. The following suggestions for further investigations are made based on personal experience on the matter.

### Suggestions in conjunction with instrumental improvements:

- ✓ Perform a dry out on the instrument. If performed, it should be left longer than the standard two hours, maybe as much as 12 hours, or as long as the LNCS tank holds, to be sure that all water possibly present in the cell chamber is dried out.

- ✓ Run a calibration with sapphire repeatedly, checking the machines reproducibility and possible water content not visible on the first calibration run.
- ✓ Do a cell/cooler conditioning in order to dry the system.
- ✓ Perform a sensitivity analysis on the instrument, and look into how much an error of the pan and lid mass input constitute on the output heat capacity value.

**Suggestions in conjunction with the methodical procedures:**

- ✓ Improve the activation set-up.
- ✓ Improve the sample preparations precision and cleanliness.
- ✓ Repeat the experiments, with a temperature range up to 100 °C. This will show if there is any water content in the sample clearly influencing the measurement results.
- ✓ Work at a higher period than 40 sec, 60 sec e.g. to make sure the sample can follow the temperature modulation.
- ✓ Check for hysteresis in the material, do a warm up and a cool down on the sample.
- ✓ Investigate if there is a problem in the actual activation procedure or a variation in the material structure.

**Suggestions in conjunction with analysis and processing of the results:**

- ✓ Exaggerate the guessed errors causing the result deviation, to see if the variance increase or remain constant.
- ✓ Do further investigations on the adsorption rate of water on the material; this can have quite a large impact on the measured heat capacity.
- ✓ Investigate the water behavior of the water that is adsorbed by the material during an experimental run. Does it undergo any phase transitions?

## 8 References

1. Dargay, J. and D. Gately, *Income's effect on car and vehicle ownership, worldwide: 1960-2015*. Transportation Research Part A: Policy and Practice, 1999. **33**(2): p. 101-138.
2. Czaja, A.U., N. Trukhan, and U. Muller, *Industrial applications of metal-organic frameworks*. Chemical Society Reviews, 2009. **38**(5): p. 1284-1293.
3. Aleksic, P., *Experimental investigation of thermal effects in a hydrogen cryo-adsorption storage system*, in *Energy and process engineering* 2011, Norwegian University of Science and Technology: Trondheim. p. 186.
4. Murray, L.J., M. Dincă, and J.R. Long, *Hydrogen storage in metal-organic frameworks*. Chem. Soc. Rev., 2009. **38**(5): p. 1294-1314.
5. Saha, D. and S. Deng, *Hydrogen Adsorption on Metal-Organic Framework MOF-177*. Tsinghua Science & Technology, 2010. **15**(4): p. 363-376.
6. Thomas, K.M., *Hydrogen adsorption and storage on porous materials*. Catalysis today, 2007. **120**(3-4): p. 389-398.
7. Xiao, B. and Q. Yuan, *Nanoporous metal organic framework materials for hydrogen storage*. Particuology, 2009. **7**(2): p. 129-140.
8. Yang, Q. and C. Zhong, *Molecular simulation of adsorption and diffusion of hydrogen in metal-organic frameworks*. The Journal of Physical Chemistry B, 2005. **109**(24): p. 11862-11864.
9. Furukawa, H., et al., *Ultrahigh porosity in metal-organic frameworks*. Science, 2010. **329**(5990): p. 424.
10. Jiang, C.-H., et al., *Exceptional thermal stability and thermodynamic properties of lithium based metal-organic framework*. Journal of Thermal Analysis and Calorimetry, 2011. **103**(1): p. 373-380.
11. Jiang, C.-H., et al., *Determination of heat capacities and thermodynamic properties of two structurally unrelated but isotopic calcium and manganese(II) 2,6-naphthalene dicarboxylate-based MOFs*. Journal of Thermal Analysis and Calorimetry, 2011. **103**(3): p. 1095-1103.
12. Jiang, C.-H., et al., *Thermodynamic properties and heat capacities of Co(BTC)1/3 (DMF) (HCOO)*. Journal of Thermal Analysis and Calorimetry, 2010. **102**(3): p. 1087-1093.
13. Song, L.-F., et al., *Heat capacities and thermodynamic properties of MgBTC*. Journal of Thermal Analysis and Calorimetry, 2010. **101**(1): p. 365-370.
14. Song, L.-F., et al., *Heat capacities and thermodynamic properties of a novel mixed-ligands MOFs*. Journal of Thermal Analysis and Calorimetry, 2010. **100**(2): p. 679-684.
15. Zhou, Y.-X., et al., *Heat capacities and thermodynamic properties of M(HBTC)(4,4'-bipy)·3DMF (M = Ni and Co)*. Journal of Thermal Analysis and Calorimetry: p. 1-6.
16. Lv, X.C., et al., *Synthesis and thermodynamic properties of a metal-organic framework: [LaCu<sub>6</sub>(μ-OH)<sub>3</sub>(Gly)<sub>6</sub>(μ<sub>6</sub>-C<sub>10</sub>O<sub>4</sub>)<sub>6</sub>]*. Thermochimica acta, 2006. **450**(1-2): p. 102-104.
17. Thomas, L.C., *Making Accurate DSC and MDSC Specific Heat Capacity Measurements with the Q1000 Tzero DSC*.
18. Ginnings, D.C. and G.T. Furukawa, *Heat Capacity Standards for the Range 14 to 1200 K*. Journal of the American Chemical Society, 1953. **75**(3): p. 522-527.
19. Y. S. Touloukian, E.H.B., ed. *Specific heat nonmetallic solids*. Thermophysical properties of matter, ed. Y.S. Touloukian. Vol. 5. 1970, IFI/Plenum New York - Washington. 3a - 8a.
20. Gaskell, D.R., ed. *Introduction to the thermodynamics of materials*. Fifth Edition ed. 2008, Taylor & Francis.
21. Reif, F., ed. *Fundamentals of statistical and thermal physics*. 1965, McGraw-Hill. 253–254.
22. Kroemer, C.K.H., ed. *Thermal physics*. 2000. 78.
23. Petit, A.T. and P.L. Dulong, *Ann. Own Phys.*, 1819. **10**: p. 395.

24. Weber, H.F., XXI. *The specific heat of the elements carbon, boron, and silicon.—Part I. The relation between the specific heat of these elements in the free state and the temperature.* Philosophical Magazine Series 4, 1875. **49**(324): p. 161-183.
25. Einstein, A., *Planck's theory of radiation and the theory of specific heat.* Annalen der Physik, 1907. **22**: p. 180-190.
26. Kittel, C., ed. *Introduction to Solid State Physics.* Seven ed. 1996, John Wiley & Sons.
27. *Heat Capacity of Solids.* [cited 2012 12.04]; Available from: [http://chemwiki.ucdavis.edu/Physical\\_Chemistry/Quantum\\_Mechanics/Heat\\_Capacity\\_of\\_Solids](http://chemwiki.ucdavis.edu/Physical_Chemistry/Quantum_Mechanics/Heat_Capacity_of_Solids).
28. Debye, P., *Zur Theorie der spezifischen Wärmen.* Annalen der Physik, 1912. **344**(14): p. 789-839.
29. Tsuji, T., *Heat Capacity of Solids*, in *Thermodynamic Properties of Solids* 2010, Wiley-VCH Verlag GmbH & Co. KGaA. p. 159-196.
30. ; Available from: <http://vallance.chem.ox.ac.uk/pdfs/EinsteinDebye.pdf>.
31. Gopal, E.S.R., *Specific heats at low temperatures* 1966: Plenum Press.
32. Kittel, C., *Elementary solid state physics: a short course* 1962: Wiley.
33. Watson, E.S., *Differential microcalorimeter*, 1966, Google Patents.
34. Wunderlich, B., *Thermal Analysis* 1990, New York: Academic press.
35. Höhne, G., W. Hemminger, and H.J. Flammersheim, *Differential scanning calorimetry* 2003: Springer Verlag.
36. Danley, R.L., *Differential scanning calorimeter*, 2002, Google Patents.
37. Instruments, T. *DSC Q2000 brochure.* Available from: <http://www.tainstruments.com/pdf/brochure/DSC.pdf>.
38. Danley, R.L. and P.A. Caulfield. *DSC Baseline Improvements Obtained by a New Heat Flow Measurement.* 2001.
39. Danley, R.L., *Heat flux differential scanning calorimeter sensor*, 2002, Google Patents.
40. Blaine, R.L., *Isothermal Crystallization Using the Q Series™ DSC and Liquid Nitrogen Cooling System.*
41. Danley, R.L. and J.W. Schaefer, *Thermal analysis assembly with distributed resistance and integral flange for mounting various cooling devices*, 2003, Google Patents.
42. Bolland, O., *Power Generation: CO<sub>2</sub> Capture and Storage*, 2011, Norwegian University of Science and Technology: Trondheim. p. 392.
43. Li, J.-R., R.J. Kuppler, and H.-C. Zhou, *Selective gas adsorption and separation in metal-organic frameworks.* Chemical Society Reviews, 2009. **38**(5): p. 1477-1504.
44. Fischer, M., F. Hoffmann, and M. Froba, *Molecular simulation of hydrogen adsorption in metal-organic frameworks.* Colloids and Surfaces A: Physicochemical and Engineering Aspects, 2010. **357**(1-3): p. 35-42.
45. Panella, B., et al., *Hydrogen Adsorption in Metal–Organic Frameworks: Cu-MOFs and Zn-MOFs Compared.* Advanced Functional Materials, 2006. **16**(4): p. 520-524.
46. Liu, D., et al., *MOF-5 composites exhibiting improved thermal conductivity.* international journal of hydrogen energy, 2012.
47. Langmuir, I., *THE CONSTITUTION AND FUNDAMENTAL PROPERTIES OF SOLIDS AND LIQUIDS. PART I. SOLIDS.* Journal of the American Chemical Society, 1916. **38**(11): p. 2221-2295.
48. Langmuir, I., *The adsorption of gases on plane surfaces of glass, mica and platinum.* Journal of the American Chemical Society, 1918. **40**(9): p. 1361-1403.
49. Gomez-Serrano, V., C. González-García, and M. González-Martín, *Nitrogen adsorption isotherms on carbonaceous materials. Comparison of BET and Langmuir surface areas.* Powder technology, 2001. **116**(1): p. 103-108.
50. Brunauer, S., P.H. Emmett, and E. Teller, *Adsorption of gases in multimolecular layers.* Journal of the American Chemical Society, 1938. **60**(2): p. 309-319.

51. Walton, K.S. and R.Q. Snurr, *Applicability of the BET method for determining surface areas of microporous metal-organic frameworks*. Journal of the American Chemical Society, 2007. **129**(27): p. 8552-8556.
52. Adamson, A.W., Gast, A. P. , ed. *Physical Chemistry of Surfaces*. 6th ed. 1997, John Wiley & Sons: New York.
53. Jung, M.W., et al., *Adsorption characteristics of phenol and chlorophenols on granular activated carbons (GAC)*. Microchemical Journal, 2001. **70**(2): p. 123-131.
54. Rubio, A., et al., *A mechanism for cutting carbon nanotubes with a scanning tunneling microscope*. The European Physical Journal B - Condensed Matter and Complex Systems, 2000. **17**(2): p. 301-308.
55. Inc., N.A. *Datasheet; Norit R0 0.8*. Available from: <http://www.reskem.com/pdf/norit-ro08.pdf>.
56. Texier-Mandoki, N., et al., *Hydrogen storage in activated carbon materials: role of the nanoporous texture*. Carbon, 2004. **42**(12-13): p. 2735-2747.
57. Touloukian, Y.S. and E.H. Buyco, *Specific heat: nonmetallic solids*1970: IFI/Plenum.
58. Tomic, E.A., *Thermal stability of coordination polymers*. Journal of Applied Polymer Science, 1965. **9**(11): p. 3745-3752.
59. Li, H., et al., *Design and synthesis of an exceptionally stable and highly porous metal- organic framework*. Nature, 1999. **402**(6759): p. 276-279.
60. Chae, H.K., et al., *A route to high surface area, porosity and inclusion of large molecules in crystals*. Nature, 2004. **427**(6974): p. 523-527.
61. O. M. Yaghi, M.E., H. Li, J. Kim, N. Rosi, *ISORETICULAR METAL-ORGANIC FRAMEWORKS, PROCESS FOR FORMING THE SAME, AND SYSTEMATIC DESIGN OF PORE SIZE AND FUNCTIONALITY THEREIN, WITH APPLICATION FOR GAS STORAGE*, 2002.
62. Eddaoudi, M., et al., *Systematic design of pore size and functionality in isorecticular MOFs and their application in methane storage*. Science, 2002. **295**(5554): p. 469-472.
63. James, S.L., *Metal-organic frameworks*. Chemical Society Reviews, 2003. **32**(5): p. 276-288.
64. Seo, Y.-K., et al., *Energy-Efficient Dehumidification over Hierachically Porous Metal–Organic Frameworks as Advanced Water Adsorbents*. Advanced Materials, 2012. **24**(6): p. 806-810.
65. Streppel, B., *Hydrogen adsorption on metal-organic frameworks*. 2011.
66. Chui, S.S.-Y., et al., *A Chemically Functionalizable Nanoporous Material [Cu<sub>3</sub>(TMA)<sub>2</sub>(H<sub>2</sub>O)<sub>3</sub>]<sub>n</sub>*. Science, 1999. **283**(5405): p. 1148-1150.
67. Schlichtenmayer, M.U., *Wasserstoffspeicherkapazität poröser Materialien in Kryoadsorptionstanks*, in *Von der Fakultät Mathematik und Physik, Max-Planck-Institut für Intelligente Systeme*, 2012, Universität Stuttgart: Stuttgart. p. 219.
68. Damgaard Poulsen, R., et al., *Solvothermal synthesis, multi-temperature crystal structures and physical properties of isostructural coordination polymers, 2C<sub>4</sub>H<sub>12</sub>N<sup>+</sup> [M<sub>3</sub> (C<sub>8</sub>H<sub>4</sub>O<sub>4</sub>)<sub>4</sub> ]<sup>2-</sup>. 3C<sub>5</sub>H<sub>11</sub>NO, M= Co, Zn*. Acta Crystallographica Section B: Structural Science, 2006. **62**(2): p. 245-254.
69. Babu, K.F., et al., *Electrocatalytic activity of Basolite<sup><sup>TM</sup></sup> F300 metal-organic-framework structures*. Electrochemistry Communications, 2010. **12**(5): p. 632-635.
70. Lieb, A., et al., *MIL-100 (V)–A mesoporous vanadium metal organic framework with accessible metal sites*. Microporous and Mesoporous Materials, 2011.
71. *Gas encyclopaedia*. Available from: <http://encyclopedia.airliquide.com/encyclopedia.asp>.
72. Moran, M.J. and H.N. Shapiro, *Fundamentals of engineering thermodynamics*2004: Wiley.
73. Touloukian, Y.S. and T. Makita, *Specific heat: nonmetallic liquids and gases*1970: IFI/Plenum.
74. Tohei, T., et al., *Debye temperature and stiffness of carbon and boron nitride polymorphs from first principles calculations*. Physical Review B, 2006. **73**(6): p. 064304.
75. Ltd, R.S. and T.A.C. Specialists, *Sample handling and preparation*, in *DSC training course, section 4*.

76. Raznjevic, K., ed. *Handbook of Thermodynamic Tables and Charts*. 1976, Hemisphere publ. corp. /McGraw-Hill: London.
77. Incropera, F.P. and D.P. DeWitt, *Fundamentals of heat and mass transfer* 2007: John Wiley.

## Appendices

### Appendix I – Using the DSC

#### Using the DSC

A general outline for performing a DSC experiment in the same way as performed in this report:

1. Calibrating the instrument
2. Selecting the pan type and material
3. Preparing the sample
4. Creating or choosing the test procedure and entering sample and instrument information through the TA instrument control software
5. Setting the purge gas flow rate
6. Loading the sample and closing the cell lid
7. Starting the experiment.

#### Before starting an experiment

A general checklist, which involves checking that the DSC and the controller are installed properly:

- All necessary cable connections from the DSC to the computer must be made
- All gas lines must be connected
- The unit must be connected
- Any desired accessories must be connected
- The instrument must be connected with the controller
- The controller operations should be familiar
- If necessary, calibrate the DSC.

#### 1. Calibrating the instrument

##### - When to calibrate?

To obtain the most accurate measurement results, an accurate calibration of the instrument should be performed. This is normally done when installing the instrument, but should also be performed periodically. How to calibrate the DSC depends on what the DSC is going to measure, at what temperature range, with which gas the experiments are performed under, etc. Everything has to be considered before calibrating the DSC. This means that the DSC is calibrated to be very exact to the subsequent experiments. This also implies that when some parameters in the experiments change, some of the calibrations have to be redone.



The different calibration procedures are in chronological order:

- Cell/cooler conditioning
- Baseline conditioning
- Tzero™ (heat only)
- Enthalpy/temperature
- Heat capacity (MDSC)

The calibration should be performed within the required temperature range for the experiments. It is recommended to calibrate over the widest temperature range, because if your subsequent experiments cover a wider range, you may need to recalibrate.

Changing some of the parameters during measurements does not necessarily imply that all DSC calibrations need to be recalibrated.

**All** DSC calibrations need to be recalibrated for optimum results whenever **one** of the following parameters is changed:

- First use of a new cell
- Purge gas or base purge gas change
- Cooling device or accessory (FACS, LNCS, RCS, or Quench Cooler Can) change
- Temperature range change.

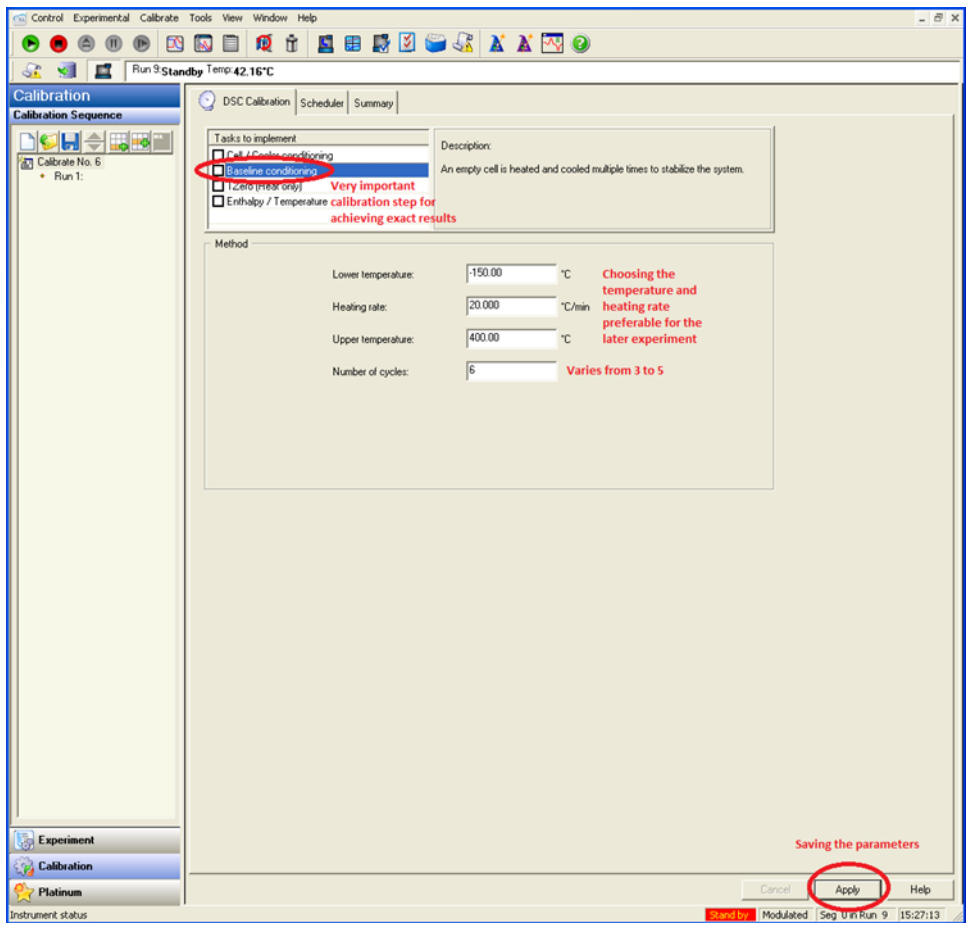
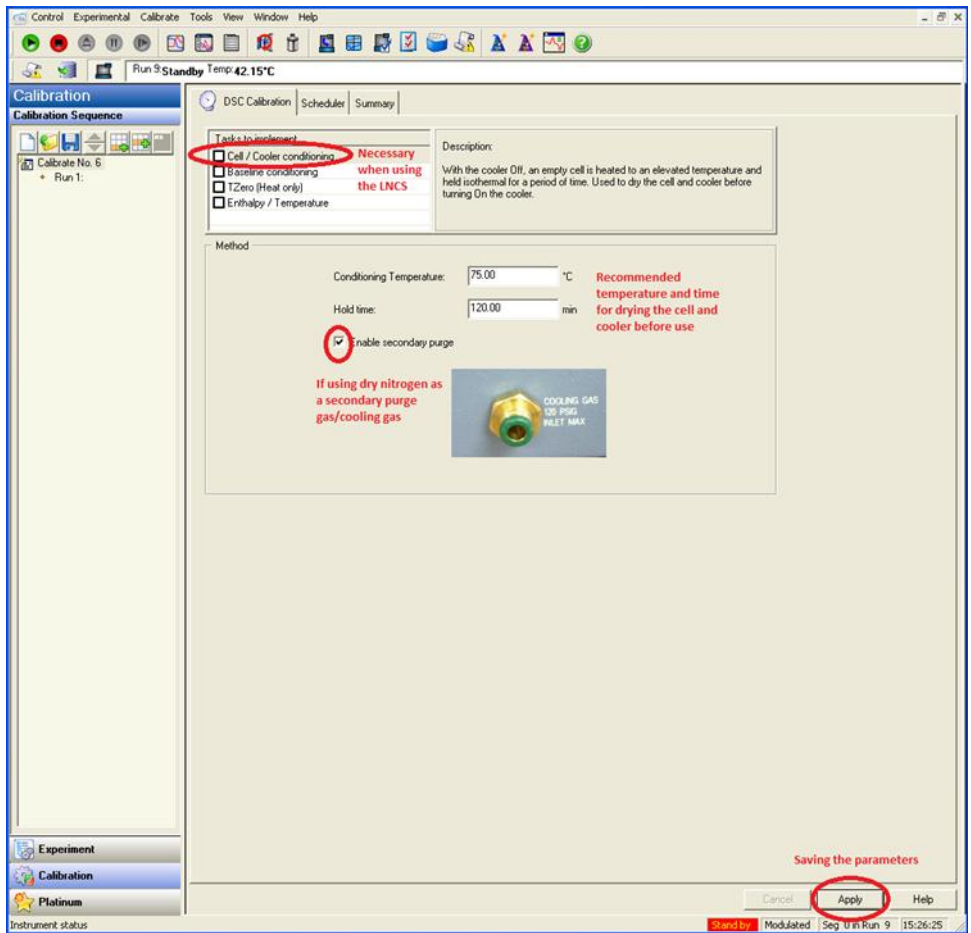
**All** DSC calibrations **except** Tzero™ and baseline calibration need to be recalibrated for optimum results whenever **one** of the following parameters is changed:

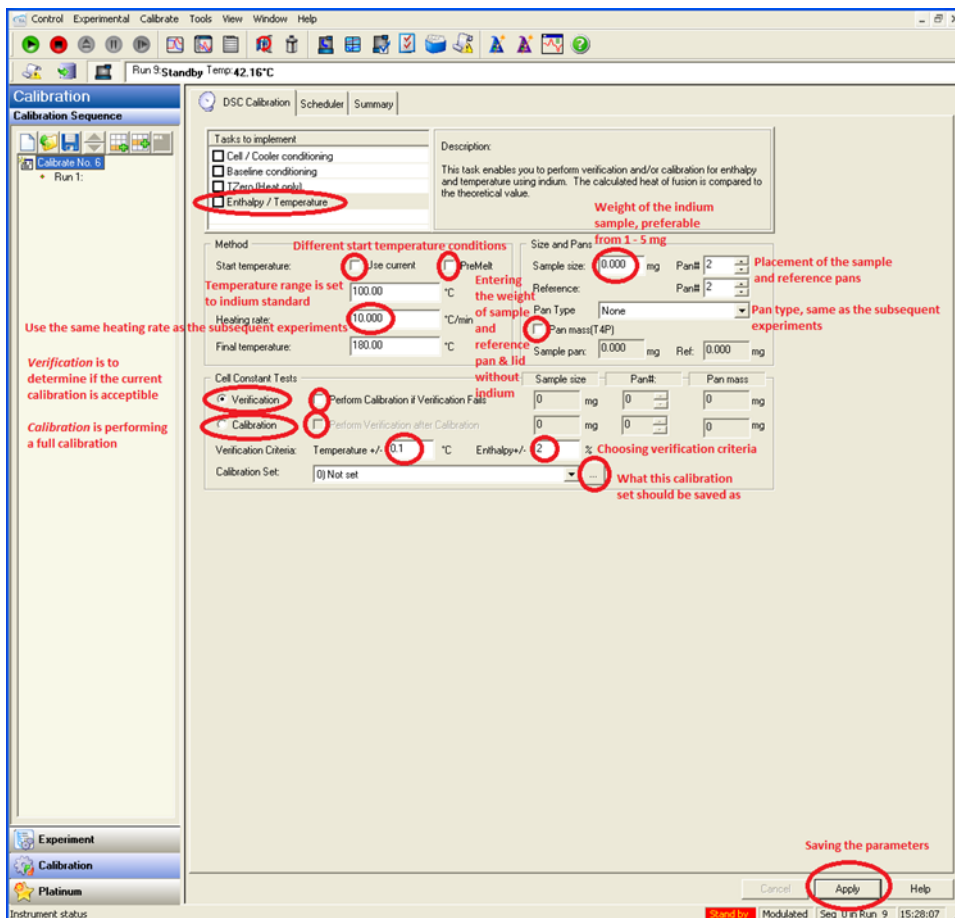
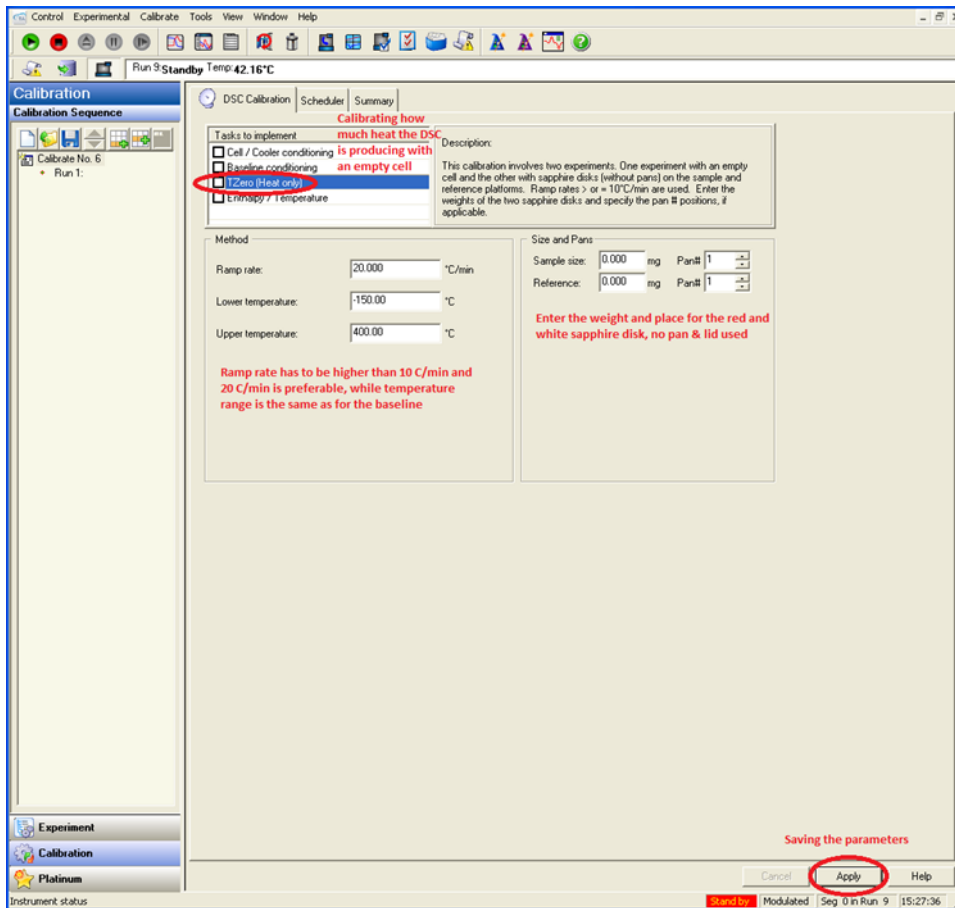
- Heat flow selection change (T4P, T4, etc.)
- Pressure (in PDSC experiments) change.
- Pan type change

#### - **How to calibrate**



The Platinum function will calibrate automatically, verify the results from the calibrations, and save the results in a calibration set. Several calibration sets can be saved when different experiments are executed with the need for different calibration setups. To create a new calibration run sequence one first select the *Platinum* button, then chooses *Auto Calibration* followed by *Create New Sequence*. Then the desired calibration procedures are chosen from the list of *Tasks to Implement*. The following steps on how to implement the right data for the calibration sequence are described further on in a chronological order.





- **Heat capacity (MDSC) calibration**

The calibration uses sapphire as a standard material with a known heat capacity at the specific temperature of interest. Before performing the calibration experiment, previously used calibration values need to be manually set to 1.0 for both *Heat Capacity* and *Reversing Heat Capacity*. Except for heating rate, the calibration experiment should be run under similar conditions (pan type, modulation amplitude, and period) as will be used for subsequent samples. The heating rate can be set to a nominal value of 2 to 3 °C/min or the calibration experiment can be performed isothermally, if only calibrating the Reversing Cp signal. This means that the heat capacity (MDSC) calibration is performed exactly the same as any experiment, just using sapphire (the small disc) instead of the testing material.

**2. Selecting the pan type and material**

Pan Type	Pan	Lid	Die Set	Software Pan Type	Application
<u>Tzero Aluminum</u>	<u>Tzero Pan</u>	<u>Tzero Lid</u>	Black	<u>Tzero Aluminum</u>	Basic DSC/MDSC applications
<u>Tzero Hermetic Aluminum</u>	<u>Tzero Pan</u>	<u>Tzero Hermetic Lid</u>	Blue	<u>Tzero Hermetic Aluminum</u>	DSC applications which require hermetic seals
<u>Tzero Hermetic Aluminum Alodined</u>	<u>Tzero Alodined Pan</u>	<u>Tzero Hermetic Alodined Lid</u>	Blue	<u>Tzero Hermetic Aluminum Alodined</u>	DSC applications which require hermetic seals and may evolve water
<u>Tzero Low-Mass Aluminum</u>	<u>Tzero Low-Mass Pan</u>	<u>Tzero Lid</u>	Black	<u>Tzero Aluminum</u>	High-sensitivity for low mass of sample

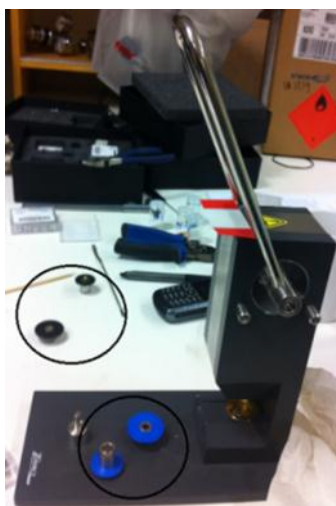
Type of Measurement	Sample Size (mg)	Heating Rate (°C/min)
<b>Glass transition</b>	10 to 20	10 to 20
<b>Melting point</b>	2 to 10	5 to 10
<b>Kinetics (Borchardt and Daniels)</b>	5 to 10	5 to 20
<b>Kinetics (ASTM)</b>	2 to 5*	0.5 to 20
<b>Heat capacity</b>	10 to 70	20**
<b>Purity</b>	1 to 3	0.5 to 1
<b>Crystallinity or oxidative stability</b>	5 to 10	5 to 10
<b>MDSC</b>	2 to 10	1 to 5

It is very important to match the weight of aluminum pan & lid on the sample side and on the reference side, because this will eliminate any contribution of aluminum on the results. The sample and reference pan & lid should therefore match their mass within 50  $\mu\text{g}$ .

### 3. Preparing the sample

The sample crimping is very important regarding the accuracy of the heat capacity measurements. The object is to get the sample pans tightly sealed with a hermetic lid, to prevent volatiles from the sample being released, and compressing the material, to obtain a very good thermal contact with the cup bottom. This means the better the thermal contact, the better the accuracy of the heat capacity measurements. The material has to be in good contact with the pan bottom, and to measure a material film or a powder densely packed in the Tzero™ pan is an advantage. The thermal contact is not only important between the sample material and the bottom of the cup, but also the contact surface area between the pan bottom and the sensor. This is why Tzero™ pans are used in heat capacity measurements, because of their flat pan bottom, but this also has to be kept very flat for best possible thermal contact. These considerations together with a very clean sensor surface give the most accurate result values.

The sample preparation for this assignment heat capacity measurements were executed using Tzero™ pans (PN 901683.901) and Tzero™ hermetic lids (PN 901684.901). The encapsulation of the sample cups was carried out using blue top and bottom parts for hermetic sealing, and black top and bottom parts for compressing the sample. The sample was then filled up with powder material, compressed with the black parts to an angle of 45° of the press' maximum, before sealed with the blue parts.



4. Creating or choosing the test procedure and entering sample and instrument information through the TA instrument control software

The screenshot shows the 'Experiment' window in the TA instrument control software. The 'Procedure Summary' tab is active, showing the following details:

- Mode:** Modulated (circled in red, with annotation: "Mode used for MDSC")
- Test:** Custom (circled in red, with annotation: "Custom the procedure")
- Sample Information:**
  - Sample Name: MDSC heat capacity (with annotation: "Personal name of sample")
  - Pan Type: Tzero Aluminum Hemetic (with annotation: "Pan type")
  - Sample: (with annotation: "Sample")
  - Sample Size: 11.946 mg (with annotation: "Only material")
  - Pan No: 22 (with annotation: "Ref")
  - Sample Mass: 52.242 mg (Sample) and 52.258 mg (Reference) (with annotation: "Only pan & lid")
  - Comments: AC Noit 8 (Flow 25 ml/min Helium) inactivated (with annotation: "Personal comments")
- Data File Name:** \Vep0382\2a\QSequences\DSC\Thea 2012\28.03 MD (with annotation: "Where to save the file")

On the right, the 'Signal' table lists various parameters and their values. Below it, the 'Running Segment Description' table lists experimental steps:

- Zero heat flow at -80.00 °C
- Sampling interval: 1.00 s/pt (with annotation: "Description of the experimental steps")
- Equilibrate at -180.00 °C
- Modulate ± 1.000 °C every 40 s
- Isothermal for 5.00 min

At the bottom, the 'Append' and 'Apply' buttons are circled in red, with annotations: "Makes a new run equal to the previous one" and "Saves changes to the run". The 'Run' number is 01 and the running time is 124.00 min.

The screenshot shows the 'Method' dialog box open over the 'Experiment' window. The 'Method Contents' dialog is the primary focus, showing a list of segments:

- Zero heat flow at -80.00 °C
- Sampling interval: 1.00 s/pt
- Equilibrate at -180.00 °C
- Modulate ± 1.000 °C every 40 s
- Isothermal for 5.00 min (circled in red, with annotation: "Choosing the order")
- Repeat ± 1.000 °C/min to 20.00 °C

The 'Segment list' on the right includes options like 'Jump', 'Equilibrate', 'Initial temperature', 'Ramp', 'Isothermal', 'Step', 'Increment temperature', 'Repeat', 'Repeat until', and 'Abort next segment on limit'. The 'Isothermal' option is circled in red, with annotation: "Choosing every step for the experiment procedure".

Back in the 'Experiment' window, the 'Test' dropdown is set to 'Custom' (with annotation: "Choosing to customize a procedure or choosing a ready-made procedure"). The 'Notes' field contains the text: "Editing the experimental procedure". The 'Editor...' button is circled in red.

At the bottom, the 'Apply' button is circled in red, with annotation: "Saving the procedure made".

## 5. Setting the purge gas flow rate

Control Experimental Calibrate Tools View Window Help

Run 9 Standby Temp 42.15°C

**Experiment**  
Standard Sequence

Sequence No. 5

- Run 1
- Run 2
- Run 3
- Run 4
- Run 5
- Run 6
- Run 7
- Run 8
- Run 9

Notes

Operator: **Tina Mow** *The name of the one executing the experiment*

Extended Text: MDSC heat capacity measurement of the AC Noir 8 inactivated.

Personal notes

**Cell chamber gas**

Mass Flow Control Settings

Sample: **#1 - Helium** Flow Rate: **25** mL/min

Auto Analysis

Autoanalyze

Analysis Macro

Calibration Set: [0] Not set

Signal

Signal	Value
Method Time	0.00 min
Segment Time	0.00 min
Remaining Run Time	0 min
Temperature	42.15 °C
Heat Flow	-0.595 mW
Rev Heat Flow	0.0000 mW
Nonrev Heat Flow	0.0000 mW
Heat Capacity	0.000 mJ/°C
Rev Cp	0.000 mJ/°C
Nonrev Cp	0.000 mJ/°C
Temp Amp (+/-)	0.000 °C
Heat Flow Amplitude	0.0000 mW
Modulated Temp	42.15 °C
Modulated Heat Flow	-0.5926 mW
Reference Sine Angle	0.000 rad
Set Point Temp	0.00 °C
Heater Power	0.000 W
Flange Temperature	42.86 °C
Heater Temperature	43.15 °C

Running Segment Description

- Zero heat flow at -80.00 °C
- Sampling interval: 1.00 s/pt
- Equilibrate at -180.00 °C
- Modulate ± 1.000 °C every 40 s
- Isothermal for 5.00 min

Heat Flow (mW)

Temperature (°C)

01 123.00 min

Append **Apply** Cancel Help

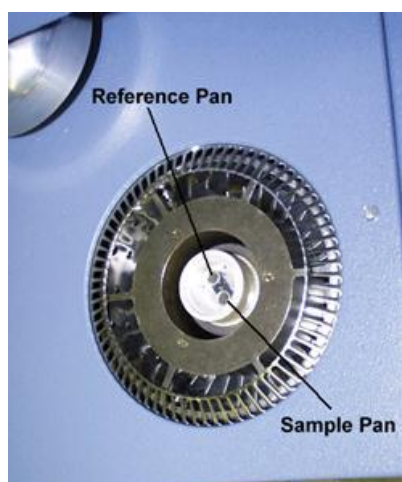
Instrument status: Standby | Modulated | Seg 0 in Run 9 | 15:25:16

*Flow rate into the cell chamber*

*Choosing the calibration set that was saved and executed with the same conditions as the experiment conditions*

*Saving changes, most important changing the flow rate*

## 6. Loading the sample and closing the cell lid



## 7. Starting the experiment

## Checklist

Make sure you have:

- ✓ Airtight pan & lid encapsulating
- ✓ Clean cell sensors
- ✓ Clean and even cup bottoms
- ✓ Clean equipment
- ✓ Tweezers and gloves as the only equipment used when handling with the samples
- ✓ Clean and correctly placed cell lid
- ✓ The autosampler correctly placing the samples on the sensors
- ✓ A straight baseline
- ✓ A correct temperature calibration
- ✓ Plotted Rev Cp and NOT total Cp signal





## Appendix II – Sample List

Type	Material	Pan & Lid before (mg)	Sample (mg)	Total before (mg)	Total after (mg)	Relative error	DSC	Pan & Lid after (mg)	Date	Comments	
Reference		54,551		54,551	54,555 mg		R3				
Calibration	Indium	54,534	4,749	59,283	59,287 mg		11	54,538	29.feb		
Reference		52,566		52,566	52,573 mg		R2				
Calibration 1	Sapphire	52,583	25,837	78,4207	78,425 mg		31	52,588			
Calibration 2	Sapphire	52,5286	25,837	78,364	78,37 mg		31	52,533			
Calibration 3	Sapphire	52,5286	25,837	78,364	78,37 mg		31	52,533			
Calibration 4	Sapphire	53,5286	26,837	79,364	79,37 mg		31	52,533	07.mar		
Test	Sapphire	54,5286	27,837	80,364	80,37 mg		31	52,533	04.mai		
		<b>Activation activated carbon Norit 8.0; 16 hours at 150 C and 0.045 torr (5,9995 Pa)</b>				<b>BET: 1384 - 1500 m2/g</b>					
Sample 1; Set 1	AC Norit 8.0	52,536	11,08	63,616	63,68 mg	0,10 %	32		08.mar		
Sample 2; Set 1	AC Norit 8.0	52,58	11,003	63,583	63,649 mg	0,10 %	33		08.mar		
Sample 3; Set 1	AC Norit 8.0	52,555	10,221	62,776	62,772 mg	-0,01 %	34		14.mar		
		<b>Activation activated carbon Norit 8.0; 3 days at 150 C and 0.06 torr (7,9993 Pa)</b>									
Sample 1; Set 2	AC Norit 8.0	52,575	16,949	69,524	69,631 mg	0,15 %	35		13.mar	No purge gas	
Sample 2; Set 2	AC Norit 8.0	52,532	12,892	65,424	65,505 mg	0,12 %	36		13.mar	No purge gas	
Sample 3; Set 2	AC Norit 8.0	52,588	17,115	69,703	69,626 mg	-0,11 %	37		13.mar	No purge gas	
		<b>Inactivated AC Norit 8.0</b>									
Sample 1; Set 1	AC Norit 8.0	52,574	9,798	62,372	62,06 mg	-0,50 %	38		14.mar	No purge gas	
Sample 2; Set 1	AC Norit 8.0	52,566	12,175	64,741	64,555 mg	-0,29 %	39		14.mar	No purge gas	
Sample 3; Set 1	AC Norit 8.0	52,581	10,193	62,774	62,567 mg	-0,33 %	40		14.mar	No purge gas	
		<b>Activation Fe-btc; 16 hours at 150 C and 0.045 torr (5,9995 Pa)</b>				<b>BET: 770 m2/g</b>					
Sample 1; Set 1	Fe-btc	52,535	21,195	73,73	75,959 mg	3,02 %	41		15.mar	Not sealed	
Sample 2; Set 1	Fe-btc	52,531	21,022	73,553	75,435 mg	2,56 %	42		15.mar	Not sealed	
Sample 3; Set 1	Fe-btc	52,605	23,425	76,03	76,132 mg	0,13 %	43		15.mar	Not sealed	
		<b>Inactivated Fe-btc</b>									
Sample 1; Set 1	Fe-btc	52,588	26,329	78,917	78,529 mg	-0,49 %	44		20.mar		
Sample 2; Set 1	Fe-btc	52,548	25,699	78,247	77,78 mg	-0,60 %	45		20.mar		
Sample 3; Set 1	Fe-btc	52,541	27,879	80,42	80,418 mg	0,00 %	46		20.mar		
		<b>Activation Cu-btc; 15 hours at 150 C and 0.063 torr (8.3993 Pa)</b>				<b>BET: 1500 - 2100 m2/g</b>					
Sample 1; Set 1	Cu-btc	52,546	10,496	63,042	63,351 mg	0,49 %	1		21.mar		
Sample 2; Set 1	Cu-btc	52,559	18,854	71,413	72,437 mg	1,43 %	2		21.mar	Not sealed	
Sample 3; Set 1	Cu-btc	52,58	19,119	71,699	71,699 mg	0,00 %	3		21.mar		
		<b>Inactivated Cu-btc</b>									
Sample 1; Set 1	Cu-btc	52,557	21,856	74,413	74,311 mg	-0,14 %	47		20.mar	No purge gas	
Sample 2; Set 1	Cu-btc	52,54	21,239	73,779	73,751 mg	-0,04 %	48		20.mar		
Sample 3; Set 1	Cu-btc	52,543	22,388	74,931	75,456 mg	0,70 %	49		20.mar		
		<b>Activation MIL-100; 15 hours at 150 C and 0.065 torr (8.66595 Pa)</b>				<b>BET: 2000 - 2400 m2/g</b>					
Sample 1; Set 1	MIL-100	52,567	14,638	67,205	67,21 mg	0,01 %	7		23.mar		
Sample 2; Set 1	MIL-100	52,534	10,972	63,506	63,508 mg	0,00 %	8		23.mar		
Sample 3; Set 1	MIL-100	52,547	15,911	68,458	68,459 mg	0,00 %	9		23.mar		
		<b>Inactivated MIL-100</b>									
Sample 1; Set 1	MIL-100	52,619	12,641	65,26	63,918 mg	-2,06 %	4		22.mar		
Sample 2; Set 1	MIL-100	52,533	15,533	68,066	65,68 mg	-3,51 %	5		22.mar		
Sample 3; Set 1	MIL-100	52,578	13,709	66,287	66,286 mg	0,00 %	6		22.mar		

Reference					52,258 mg		R1		26.mar
Inactivated <b>AC Norit 8.0</b> (24 - 24.4 C and RH = 23-26 %)									
Sample 1; Set 2	AC Norit 8.0	52,242	11,946	64,188	64,124 mg	-0,10 %	22		28.mar
Sample 2; Set 2	AC Norit 8.0	52,281	12,451	64,732	64,682 mg	-0,08 %	23		28.mar
Sample 3; Set 2	AC Norit 8.0	52,281	14,66	66,941	66,84 mg	-0,15 %	24		28.mar
Activation <b>Fe-btc</b> ; 16 hours at 150 C and 0.005 torr (0,6666 Pa)									
Sample 1; Set 2	Fe-btc	52,285	20,731	73,016	73,016 mg	0,00 %	18		04.mai
Sample 2; Set 2	Fe-btc	52,294	19,882	72,176	72,176 mg	0,00 %	19		04.mai
Sample 3; Set 2	Fe-btc	52,251	20,594	72,845	72,846 mg	0,00 %	20		04.mai A bit uneven cup bottom
Sample 4; Set 2	Fe-btc	52,227	20,565	72,792	72,793 mg	0,00 %	21		04.mai A bit uneven cup bottom
Inactivated <b>Fe-btc</b>									
Sample 1; Set 2	Fe-btc	52,23	30,858	83,088	83,088 mg	0,00 %	19		28.mar A bit uneven cup bottom
Sample 2; Set 2	Fe-btc	52,233	31,039	83,272	83,273 mg	0,00 %	20		28.mar
Sample 3; Set 2	Fe-btc	52,268	31,509	83,777	83,778 mg	0,00 %	21		28.mar
Inactivated <b>Cu-btc</b> (23.2 - 23.9 C and RH = 26 - 27 %)									
Sample 1; Set 2	Cu-btc	52,215	21,672	73,887	mg		12		27.mar
Sample 2; Set 2	Cu-btc	52,281	22,414	74,695	74,255 mg	-0,59 %	13		27.mar
Sample 3; Set 2	Cu-btc	52,267	22,556	74,823	74,316 mg	-0,68 %	14		27.mar
Activation <b>Cu-btc</b> ; 16 hours at 150 C and 0.063 torr (8.3993 Pa)									
Sample 1; Set 2	Cu-btc	52,226	18,657	70,883	70,882 mg	0,00 %	25		28.mar
Sample 2; Set 2	Cu-btc	52,272	16,322	68,594	68,591 mg	0,00 %	26		28.mar
Sample 3; Set 2	Cu-btc	52,291	13,359	65,65	65,673 mg	0,04 %	27		28.mar Not densely packed material
Activation <b>Cu-btc</b> ; 16 hours at 150 C and 0.005 torr (0.6666 Pa)									
Sample 1; Set 3	Cu-btc	52,252	15,308	67,56	68,888 mg	1,97 %	1		20.apr
Sample 2; Set 3	Cu-btc	52,232	20,648	72,88	72,882 mg	0,00 %	2		20.apr
Sample 3; Set 3	Cu-btc	52,234	15,471	67,705	67,707 mg	0,00 %	3		20.apr
Sample 4; Set 3	Cu-btc	52,243	16,182	68,425	68,429 mg	0,01 %	4		20.apr
Inactivated <b>Cu-btc (Test)</b>									
Sample 1; Set 3	Cu-btc	52,821	17,546	70,367	71,693 mg	1,88 %	11		02.mai
Sample 2; Set 3	Cu-btc	52,284	13,779	66,063	66,953 mg	1,35 %	16		03.mai
Sample 3; Set 3	Cu-btc	52,287	15,739	68,026	70,37 mg	3,45 %	15		03.mai Not sealed
Activation <b>MIL-100</b> ; 16 hours at 150 C and 0.064 torr (8.5326 Pa)									
Sample 1; Set 2	MIL-100	52,246	10,386	62,632	62,972 mg	0,54 %	15		27.mar
Sample 2; Set 2	MIL-100	52,242	13,148	65,39	66,062 mg	1,03 %	16		27.mar Not sealed
Sample 3; Set 2	MIL-100	52,284	12,069	64,353	65,963 mg	2,50 %	17		27.mar Almost sealed
Sample 4; Set 2	MIL-101	52,229	11,558	63,787	63,789 mg	0,00 %	18		27.mar
Inactivated <b>MIL-100</b> (23.2 - 23.9 C and RH = 26 - 27 %)									
Sample 1; Set 2	MIL-100	52,295	17,745	70,04	70,041 mg	0,00 %	28		27.mar
Sample 2; Set 2	MIL-100	52,275	15,443	67,718	64,836 mg	-4,26 %	29		27.mar
Sample 3; Set 2	MIL-100	52,272	17,272	69,544	69,545 mg	0,00 %	30		27.mar
Activation <b>MIL-100</b> ; 16 hours at 150 C and 0.005 torr (0.6666 Pa)									
Sample 1; Set 3	MIL-100	52,207	4,44	56,647	57,279 mg	1,12 %	12		03.apr Little material, poorly packed
Sample 2; Set 3	MIL-100	52,283	10,177	62,46	62,46 mg	0,00 %	13		03.apr Lighter color/activated
Sample 3; Set 3	MIL-100	52,262	10,377	62,639	62,64 mg	0,00 %	14		03.apr Good
Sample 4; Set 3	MIL-101	52,249	5,372	57,621	57,622 mg	0,00 %	17		03.apr Little material, poorly packed

## Appendix III – Selected Data Activated Carbon Norit R0.8

Temp. (°C)	$C_p(\text{exp})$ (J/g °C)						Standard deviation
	S2 Act; Set 2	S1 Act; Set 1	S1 (run 2) Act; Set 1	S2 Act; Set 1	S3 Act; Set 1	Average	
-180	0,1416	0,1905	0,1719	0,1665	0,1401	0,1621	0,021
-170	0,1779	0,2089	0,2006	0,1909	0,1857	0,1928	0,012
-160	0,2122	0,2452	0,2356	0,2266	0,2252	0,2289	0,012
-150	0,2447	0,2789	0,2680	0,2601	0,2639	0,2631	0,012
-140	0,2779	0,3126	0,3004	0,2931	0,3005	0,2969	0,013
-130	0,3104	0,3444	0,3319	0,3255	0,3375	0,3299	0,013
-120	0,3456	0,3793	0,3645	0,3602	0,3724	0,3644	0,013
-110	0,3817	0,4130	0,3976	0,3946	0,4080	0,3990	0,012
-100	0,4184	0,4461	0,4301	0,4279	0,4412	0,4327	0,011
-90	0,4548	0,4797	0,4623	0,4619	0,4744	0,4666	0,010
-80	0,4900	0,5133	0,4959	0,4958	0,5077	0,5005	0,010
-70	0,5227	0,5469	0,5280	0,5285	0,5405	0,5333	0,010
-60	0,5554	0,5787	0,5597	0,5606	0,5728	0,5654	0,010
-50	0,5874	0,6102	0,5909	0,5908	0,6052	0,5969	0,010
-40	0,6198	0,6419	0,6205	0,6208	0,6374	0,6281	0,011
-30	0,6508	0,6733	0,6510	0,6514	0,6685	0,6590	0,011
-20	0,6816	0,7031	0,6804	0,6814	0,6992	0,6891	0,011
-10	0,7111	0,7321	0,7095	0,7120	0,7298	0,7189	0,011
0	0,7431	0,7622	0,7386	0,7431	0,7610	0,7496	0,011
10	0,7743	0,7923	0,7687	0,7747	0,7918	0,7803	0,011
20	0,8033	0,8237	0,7969	0,8047	0,8202	0,8098	0,012
30	0,8316	0,8511	0,8253	0,8338	0,8476	0,8379	0,011
40	0,8606	0,8807	0,8540	0,8621	0,8753	0,8666	0,011
50	0,8861	0,9120	0,8825	0,8911	0,9039	0,8951	0,012
60	0,9116	0,9392	0,9101	0,9164	0,9306	0,9216	0,013
70	0,9362	0,9655	0,9385	0,9425	0,9583	0,9482	0,013
80	0,9610	0,9907	0,9667	0,9658	0,9840	0,9736	0,013
90	0,9848	1,0165	0,9944	0,9905	1,0078	0,9988	0,013
100	1,0093	1,0372	1,0209	1,0141	1,0334	1,0230	0,012
110	1,0329	1,0608	1,0474	1,0377	1,0599	1,0477	0,013
120	1,0584	1,0786	1,0709	1,0603	1,0834	1,0703	0,011
130	1,0804	1,0997	1,0929	1,0794	1,1074	1,0920	0,012
140	1,1025	1,1209	1,1151	1,1006	1,1315	1,1141	0,013

## Appendix IV – Selected Data Cu-btc

Temp. (°C)	CP(exp) (J/g °C)				Average	Standard deviation
	S1 Act; Set 1	S2 Act; Set 1	S3 Act; Set 1	S3Act; Set 2, Run 2		
-180	0,2945	0,2124	0,1982	0,2442	0,2373	0,043
-170	0,3327	0,2634	0,2614	0,3059	0,2909	0,035
-160	0,3804	0,3008	0,2993	0,3523	0,3332	0,040
-150	0,4213	0,3344	0,3338	0,3929	0,3706	0,044
-140	0,4581	0,3654	0,3641	0,4305	0,4045	0,047
-130	0,4904	0,3930	0,3908	0,4634	0,4344	0,050
-120	0,5229	0,4202	0,4177	0,4964	0,4643	0,053
-110	0,5541	0,4462	0,4429	0,5271	0,4926	0,057
-100	0,5828	0,4705	0,4665	0,5558	0,5189	0,059
-90	0,6109	0,4941	0,4895	0,5840	0,5446	0,062
-80	0,6400	0,5179	0,5136	0,6122	0,5709	0,065
-70	0,6674	0,5398	0,5351	0,6390	0,5953	0,068
-60	0,6946	0,5602	0,5578	0,6642	0,6192	0,071
-50	0,7207	0,5803	0,5809	0,6906	0,6431	0,073
-40	0,7463	0,6007	0,6034	0,7167	0,6668	0,076
-30	0,7729	0,6211	0,6266	0,7435	0,6910	0,079
-20	0,8005	0,6418	0,6498	0,7699	0,7155	0,082
-10	0,8253	0,6615	0,6722	0,7955	0,7386	0,084
0	0,8508	0,6818	0,6941	0,8192	0,7615	0,086
10	0,8757	0,7028	0,7152	0,8443	0,7845	0,088
20	0,8993	0,7231	0,7361		0,7861	0,098
30	0,9229	0,7427	0,7549		0,8068	0,101
40	0,9466	0,7616	0,7764		0,8282	0,103
50	0,9701	0,7809	0,7966		0,8492	0,105
60	0,9935	0,7992	0,8177		0,8702	0,107
70	1,0163	0,8176	0,8385		0,8908	0,109
80	1,0397	0,8341	0,8580		0,9106	0,112
90	1,0626	0,8510	0,8756		0,9298	0,116
100	1,0834	0,8653	0,8940		0,9476	0,119
110	1,1042	0,8816	0,9119		0,9659	0,121
120	1,1249	0,8962	0,9288		0,9833	0,124
130	1,1431	0,9089	0,9447		0,9989	0,126
140	1,1585	0,9213	0,9600		1,0133	0,127

## Appendix V – Selected Data Fe-btc

Temp. (°C)	CP(exp) (J/g °C)				Standard deviation
	S1 Act; Set 1	S2 Act; Set 1	S3 Act; Set 1	Average	
-180	0,2804	0,2837	0,2630	0,2757	0,011
-170	0,3352	0,3459	0,3125	0,3312	0,017
-160	0,3833	0,3957	0,3596	0,3796	0,018
-150	0,4284	0,4419	0,4043	0,4248	0,019
-140	0,4694	0,4845	0,4445	0,4661	0,020
-130	0,5055	0,5220	0,4818	0,5031	0,020
-120	0,5413	0,5588	0,5176	0,5393	0,021
-110	0,5743	0,5938	0,5511	0,5731	0,021
-100	0,6057	0,6264	0,5824	0,6048	0,022
-90	0,6356	0,6584	0,6129	0,6356	0,023
-80	0,6661	0,6895	0,6431	0,6662	0,023
-70	0,6941	0,7189	0,6708	0,6946	0,024
-60	0,7222	0,7476	0,6978	0,7225	0,025
-50	0,7482	0,7747	0,7245	0,7491	0,025
-40	0,7739	0,8018	0,7501	0,7753	0,026
-30	0,7999	0,8280	0,7770	0,8016	0,026
-20	0,8248	0,8538	0,8009	0,8265	0,026
-10	0,8488	0,8784	0,8251	0,8508	0,027
0	0,8725	0,9025	0,8477	0,8742	0,027
10	0,8963	0,9274	0,8714	0,8984	0,028
20	0,9200	0,9521	0,8945	0,9222	0,029
30	0,9417	0,9740	0,9149	0,9435	0,030
40	0,9644	0,9987	0,9373	0,9668	0,031
50	0,9863	1,0217	0,9586	0,9889	0,032
60	1,0070	1,0443	0,9782	1,0098	0,033
70	1,0279	1,0662	0,9991	1,0310	0,034
80	1,0474	1,0877	1,0176	1,0509	0,035
90	1,0664	1,1087	1,0357	1,0703	0,037
100	1,0853	1,1286	1,0536	1,0892	0,038
110	1,1042	1,1484	1,0714	1,1080	0,039
120	1,1220	1,1663	1,0883	1,1255	0,039
130	1,1392	1,1846	1,1036	1,1425	0,041
140	1,1556	1,2020	1,1189	1,1589	0,042

## Appendix VI – Selected Data MIL-100(Fe)

Temp. (°C)	CP(exp) (J/g °C)						Average	Standard deviation
	S1 Act; Set 1	S2 Act; Set 1	S3 Act; Set 1	S3 Act; Set 2	S1 Act; Set 3	S2 Act; Set 3		
-180	0,1408	0,1537	0,1213	0,2949	0,3068	0,1837	0,2002	0,081
-170	0,2687	0,2217	0,2072	0,3493	0,3987	0,2127	0,2764	0,080
-160	0,3688	0,3055	0,2836	0,4024	0,4606	0,2608	0,3470	0,077
-150	0,4493	0,3919	0,3509	0,4488	0,5101	0,3402	0,4152	0,066
-140	0,5081	0,4562	0,4027	0,4928	0,5550	0,4327	0,4746	0,055
-130	0,5554	0,5031	0,4447	0,5314	0,5959	0,5036	0,5224	0,052
-120	0,5986	0,5434	0,4834	0,5692	0,6395	0,5576	0,5653	0,053
-110	0,6402	0,5789	0,5195	0,6037	0,6816	0,6016	0,6043	0,055
-100	0,6783	0,6117	0,5536	0,6357	0,7195	0,6386	0,6396	0,057
-90	0,7154	0,6428	0,5860	0,6655	0,7521	0,6728	0,6724	0,058
-80	0,7524	0,6744	0,6187	0,6942	0,7815	0,7061	0,7046	0,058
-70	0,7867	0,7030	0,6497	0,7212	0,8052	0,7370	0,7338	0,057
-60	0,8207	0,7307	0,6805	0,7484	0,8283	0,7653	0,7623	0,056
-50	0,8555	0,7574	0,7114	0,7770	0,8536	0,7933	0,7914	0,056
-40	0,8883	0,7850	0,7423	0,8052	0,8790	0,8197	0,8199	0,056
-30	0,9206	0,8123	0,7731	0,8327	0,9054	0,8444	0,8481	0,056
-20	0,9536	0,8379	0,8035	0,8591	0,9319	0,8681	0,8757	0,057
-10	0,9857	0,8628	0,8334	0,8843	0,9562	0,8904	0,9021	0,058
0	1,0164	0,8873	0,8618	0,9091	0,9813	0,9117	0,9279	0,059
10	1,0483	0,9125	0,8911	0,9359	1,0102	0,9353	0,9556	0,061
20	1,0783	0,9356	0,9190				0,9776	0,088
30	1,1064	0,9578	0,9432				1,0025	0,090
40	1,1361	0,9797	0,9720				1,0293	0,093
50	1,1662	1,0026	0,9988				1,0559	0,096
60	1,1928	1,0242	1,0242				1,0804	0,097
70	1,2206	1,0451	1,0509				1,1055	0,100
80	1,2480	1,0656	1,0762				1,1299	0,102
90	1,2749	1,0866	1,1029				1,1548	0,104
100	1,3028	1,1055	1,1286				1,1790	0,108
110	1,3323	1,1253	1,1571				1,2049	0,111
120	1,3589	1,1451	1,1836				1,2292	0,114
130	1,3814	1,1624	1,2097				1,2511	0,115
140	1,4047	1,1788	1,2329				1,2721	0,118

## Appendix VII – Heat Capacity Measurement Values Activated Carbon Norit R8.0

Rev Cp (0,045 torr, 150 C 16 hours)										Rev Cp (0,06 torr, 150 C 3 days)					
Celsius	S1 Act; Set 1	S1 + KCp	S1 (run 2) Act; Set 1	S1, run 2 + KCp	S2 Act; Set 1	S2 + KCp	S3 Act; Set 1	S3 + KCp	KCp	S1 Act; Set 2	S1 + KCp	S2 Act; Set 2	S2 + KCp	S3 Act; Set 2	S3 + KCp
-180	0,304	0,191	0,275	0,172	0,266	0,167	0,224	0,140	0,626			0,226	0,142	0,355	0,222
-170	0,301	0,209	0,289	0,201	0,275	0,191	0,268	0,186	0,694	0,387	0,268	0,256	0,178	0,407	0,282
-160	0,336	0,245	0,323	0,236	0,310	0,227	0,309	0,225	0,730	0,428	0,312	0,291	0,212	0,449	0,327
-150	0,362	0,279	0,348	0,268	0,338	0,260	0,343	0,264	0,770	0,460	0,354	0,318	0,245	0,479	0,369
-140	0,389	0,313	0,374	0,300	0,365	0,293	0,374	0,301	0,803	0,492	0,395	0,346	0,278	0,510	0,410
-130	0,416	0,344	0,401	0,332	0,393	0,326	0,407	0,337	0,829	0,527	0,437	0,375	0,310	0,543	0,450
-120	0,446	0,379	0,428	0,365	0,423	0,360	0,438	0,372	0,851	0,566	0,481	0,406	0,346	0,580	0,493
-110	0,474	0,413	0,456	0,398	0,453	0,395	0,468	0,408	0,872	0,611	0,532	0,438	0,382	0,625	0,544
-100	0,503	0,446	0,485	0,430	0,483	0,428	0,498	0,441	0,886	0,668	0,592	0,472	0,418	0,683	0,605
-90	0,534	0,480	0,515	0,462	0,514	0,462	0,528	0,474	0,898	0,730	0,655	0,506	0,455	0,748	0,672
-80	0,563	0,513	0,544	0,496	0,544	0,496	0,557	0,508	0,912	0,783	0,714	0,538	0,490	0,810	0,738
-70	0,595	0,547	0,575	0,528	0,575	0,529	0,588	0,540	0,919	0,831	0,763	0,569	0,523	0,867	0,797
-60	0,625	0,579	0,605	0,560	0,606	0,561	0,619	0,573	0,925	0,871	0,806	0,600	0,555	0,915	0,847
-50	0,655	0,610	0,634	0,591	0,634	0,591	0,649	0,605	0,932	0,904	0,843	0,630	0,587	0,954	0,889
-40	0,684	0,642	0,661	0,621	0,661	0,621	0,679	0,637	0,939	0,932	0,875	0,660	0,620	0,989	0,928
-30	0,714	0,673	0,690	0,651	0,690	0,651	0,709	0,669	0,943	0,962	0,908	0,690	0,651	1,018	0,960
-20	0,743	0,703	0,719	0,680	0,720	0,681	0,739	0,699	0,946	0,988	0,935	0,721	0,682	1,048	0,991
-10	0,770	0,732	0,746	0,709	0,748	0,712	0,767	0,730	0,951	1,012	0,963	0,747	0,711	1,072	1,020
0	0,802	0,762	0,777	0,739	0,782	0,743	0,800	0,761	0,951	1,043	0,992	0,782	0,743	1,103	1,049
10	0,832	0,792	0,807	0,769	0,814	0,775	0,832	0,792	0,952	1,070	1,019	0,813	0,774	1,131	1,077
20	0,865	0,824	0,837	0,797	0,845	0,805	0,861	0,820	0,953	1,099	1,047	0,843	0,803	1,159	1,104
30	0,894	0,851	0,867	0,825	0,876	0,834	0,890	0,848	0,952	1,125	1,071	0,873	0,832	1,187	1,130
40	0,923	0,881	0,895	0,854	0,904	0,862	0,918	0,875	0,954	1,151	1,098	0,902	0,861	1,212	1,156
50	0,953	0,912	0,923	0,883	0,931	0,891	0,945	0,904	0,957	1,176	1,125	0,926	0,886	1,236	1,182
60	0,980	0,939	0,950	0,910	0,957	0,916	0,971	0,931	0,958	1,202	1,152	0,952	0,912	1,260	1,207
70	1,007	0,966	0,979	0,938	0,983	0,943	1,000	0,958	0,959	1,228	1,177	0,976	0,936	1,284	1,231
80	1,032	0,991	1,007	0,967	1,006	0,966	1,025	0,984	0,960	1,252	1,202	1,001	0,961	1,308	1,256
90	1,058	1,016	1,035	0,994	1,031	0,991	1,049	1,008	0,961	1,277	1,227	1,025	0,985	1,331	1,279
100	1,078	1,037	1,061	1,021	1,054	1,014	1,074	1,033	0,962	1,301	1,252	1,049	1,009	1,356	1,305
110	1,102	1,061	1,088	1,047	1,078	1,038	1,101	1,060	0,963	1,327	1,277	1,073	1,033	1,381	1,329
120	1,120	1,079	1,112	1,071	1,101	1,060	1,125	1,083	0,963	1,348	1,298	1,099	1,058	1,404	1,352
130	1,140	1,100	1,133	1,093	1,119	1,079	1,148	1,107	0,965	1,371	1,323	1,120	1,080	1,423	1,373
140	1,161	1,121	1,155	1,115	1,140	1,101	1,172	1,132	0,965	1,393	1,345	1,142	1,103	1,441	1,391



Celsius	Rev Cp (Inactivated)						Rev Cp (Inactivated)					
	S1 IA; Set 1	S1 + KCp	S2 IA; Set 1	S2 + KCp	S3 IA; Set 1	S3 + KCp	S1 IA; Set 2	S1 + KCp	S2 IA; Set 2	S2 + KCp	S3 IA; Set 2	S3 + KCp
-180							0,339	0,212	0,249	0,156	0,257	0,161
-170							0,324	0,225	0,270	0,187	0,291	0,202
-160							0,367	0,268	0,307	0,224	0,325	0,237
-150							0,400	0,308	0,335	0,258	0,352	0,271
-140							0,436	0,350	0,365	0,293	0,380	0,305
-130							0,472	0,391	0,395	0,328	0,409	0,339
-120	0,462	0,393	0,386	0,329	0,442	0,376	0,509	0,433	0,426	0,363	0,439	0,373
-110	0,492	0,429	0,420	0,366	0,464	0,405	0,548	0,477	0,456	0,397	0,467	0,407
-100	0,529	0,469	0,453	0,401	0,498	0,441	0,589	0,522	0,485	0,430	0,497	0,441
-90	0,566	0,508	0,485	0,435	0,532	0,478	0,630	0,566	0,512	0,460	0,528	0,475
-80	0,602	0,549	0,515	0,470	0,563	0,513	0,671	0,612	0,535	0,488	0,557	0,508
-70	0,639	0,587	0,545	0,501	0,594	0,546	0,714	0,656	0,557	0,512	0,589	0,541
-60	0,675	0,624	0,573	0,530	0,624	0,577	0,754	0,697	0,581	0,538	0,618	0,572
-50	0,707	0,659	0,600	0,559	0,652	0,608	0,788	0,734	0,606	0,565	0,646	0,602
-40	0,741	0,695	0,628	0,590	0,680	0,638	0,814	0,764	0,634	0,595	0,674	0,633
-30	0,772	0,728	0,658	0,621	0,710	0,670	0,841	0,793	0,663	0,626	0,702	0,663
-20	0,804	0,761	0,689	0,651	0,741	0,701	0,868	0,821	0,693	0,656	0,732	0,693
-10	0,834	0,794	0,716	0,681	0,771	0,734	0,893	0,849	0,722	0,687	0,760	0,723
0	0,871	0,828	0,750	0,713	0,807	0,767	0,927	0,881	0,754	0,717	0,792	0,753
10	0,906	0,863	0,781	0,743	0,840	0,800	0,963	0,917	0,786	0,748	0,824	0,785
20	0,942	0,897	0,811	0,773	0,872	0,831						
30	0,976	0,929	0,838	0,798	0,901	0,858						
40	1,009	0,962	0,861	0,822	0,926	0,884						
50	1,038	0,993	0,876	0,838	0,945	0,904						
60	1,065	1,020	0,886	0,849	0,957	0,917						
70	1,087	1,042	0,897	0,860	0,971	0,931						
80	1,093	1,049	0,910	0,873	0,986	0,947						
90	1,073	1,031	0,929	0,892	1,006	0,967						
100	1,034	0,995	0,948	0,912	1,027	0,988						
110	1,027	0,989	0,972	0,936	1,051	1,012						
120					1,076	1,036						
130					1,096	1,057						
140					1,118	1,079						

## Appendix VIII – Heat Capacity Measurement Values Cu-btc

Rev Cp (0,063 torr, 150 C 16 hours)								Rev Cp inactivated					
Celsius	S1 Act; Set 1	S1 + KCp	S2 Act; Set 1	S2 + KCp	S3 Act; Set 1	S3 + KCp	KCp	S1 IA; Set 1	S1 + KCp	S2 IA; Set 1	S2 + KCp	S3 IA; Set 1	S3 + KCp
-180	0,471	0,295	0,339	0,212	0,317	0,198	0,626						
-170	0,480	0,333	0,380	0,263	0,377	0,261	0,694						
-160	0,521	0,380	0,412	0,301	0,410	0,299	0,730						
-150	0,547	0,421	0,434	0,334	0,433	0,334	0,770						
-140	0,570	0,458	0,455	0,365	0,453	0,364	0,803						
-130	0,592	0,490	0,474	0,393	0,472	0,391	0,829						
-120	0,614	0,523	0,494	0,420	0,491	0,418	0,851	0,686	0,584	0,661	0,563	0,700	0,596
-110	0,636	0,554	0,512	0,446	0,508	0,443	0,872	0,681	0,594	0,658	0,574	0,683	0,596
-100	0,657	0,583	0,531	0,470	0,526	0,467	0,886	0,712	0,631	0,687	0,609	0,713	0,632
-90	0,680	0,611	0,550	0,494	0,545	0,490	0,898	0,743	0,667	0,718	0,645	0,745	0,669
-80	0,702	0,640	0,568	0,518	0,563	0,514	0,912	0,773	0,705	0,748	0,682	0,775	0,707
-70	0,726	0,667	0,587	0,540	0,582	0,535	0,919	0,807	0,741	0,780	0,717	0,809	0,743
-60	0,751	0,695	0,605	0,560	0,603	0,558	0,925	0,840	0,777	0,812	0,751	0,842	0,779
-50	0,773	0,721	0,623	0,580	0,623	0,581	0,932	0,872	0,813	0,845	0,788	0,874	0,814
-40	0,795	0,746	0,640	0,601	0,643	0,603	0,939	0,903	0,847	0,874	0,820	0,904	0,849
-30	0,819	0,773	0,658	0,621	0,664	0,627	0,943	0,935	0,882	0,905	0,853	0,936	0,883
-20	0,846	0,801	0,678	0,642	0,687	0,650	0,946	0,968	0,916	0,936	0,885	0,970	0,917
-10	0,868	0,825	0,695	0,662	0,707	0,672	0,951	0,999	0,950	0,963	0,916	0,999	0,951
0	0,895	0,851	0,717	0,682	0,730	0,694	0,951	1,034	0,983	0,996	0,947	1,034	0,983
10	0,920	0,876	0,738	0,703	0,751	0,715	0,952	1,067	1,016	1,027	0,978	1,067	1,016
20	0,944	0,899	0,759	0,723	0,773	0,736	0,953	1,101	1,049	1,057	1,007	1,099	1,047
30	0,969	0,923	0,780	0,743	0,793	0,755	0,952	1,131	1,077	1,088	1,036	1,129	1,075
40	0,992	0,947	0,798	0,762	0,814	0,776	0,954	1,162	1,108	1,118	1,066	1,156	1,103
50	1,014	0,970	0,816	0,781	0,833	0,797	0,957	1,190	1,138	1,147	1,097	1,179	1,128
60	1,037	0,994	0,834	0,799	0,854	0,818	0,958	1,214	1,163	1,178	1,129	1,196	1,146
70	1,060	1,016	0,853	0,818	0,875	0,838	0,959	1,236	1,185	1,209	1,159	1,204	1,154
80	1,083	1,040	0,869	0,834	0,894	0,858	0,960	1,251	1,201	1,239	1,189	1,201	1,153
90	1,106	1,063	0,886	0,851	0,911	0,876	0,961	1,257	1,208	1,268	1,218	1,185	1,138
100	1,126	1,083	0,899	0,865	0,929	0,894	0,962	1,247	1,200	1,293	1,244	1,154	1,110
110	1,147	1,104	0,916	0,882	0,947	0,912	0,963	1,227	1,181	1,319	1,270	1,121	1,079
120	1,168	1,125	0,931	0,896	0,964	0,929	0,963						
130	1,185	1,143	0,942	0,909	0,979	0,945	0,965						
140	1,200	1,159	0,954	0,921	0,994	0,960	0,965						

Rev Cp (0,063 torr, 150 C 16 hours)							Rev Cp inactivated						
Celsius	S1 Act; Set 2	S1 + KCp	S2Act; Set 2	S2 + KCp	S3Act; Set 2	S3 + KCp	S1 IA; Set 2	S1 + KCp	S2 IA; Set 2	S2 + KCp	S3 IA; Set 2	S3 + KCp	
-180	0,184	0,115	0,158	0,099	0,217	0,136	0,389	0,243	0,479	0,300	0,401	0,251	
-170	0,215	0,149	0,154	0,107	0,346	0,240	0,439	0,305	0,506	0,351	0,454	0,315	
-160	0,279	0,204	0,171	0,125	0,440	0,321	0,483	0,352	0,554	0,405	0,499	0,364	
-150	0,370	0,285	0,197	0,152	0,490	0,378	0,517	0,398	0,590	0,454	0,535	0,412	
-140	0,456	0,366	0,258	0,207	0,524	0,421	0,550	0,442	0,623	0,500	0,567	0,456	
-130	0,516	0,428	0,361	0,299	0,551	0,457	0,579	0,480	0,656	0,543	0,598	0,496	
-120	0,558	0,475	0,478	0,406	0,576	0,490	0,610	0,520	0,689	0,586	0,629	0,535	
-110	0,587	0,512	0,560	0,488	0,597	0,521	0,639	0,557	0,721	0,628	0,658	0,574	
-100	0,615	0,545	0,610	0,541			0,670	0,593	0,753	0,667	0,689	0,611	
-90	0,643	0,578	0,646	0,580			0,702	0,630	0,787	0,707	0,721	0,648	
-80	0,671	0,612	0,673	0,613			0,733	0,668	0,820	0,748	0,752	0,686	
-70	0,701	0,644	0,699	0,642			0,767	0,705	0,858	0,788	0,788	0,725	
-60	0,726	0,672	0,723	0,669			0,802	0,742	0,895	0,828	0,825	0,763	
-50	0,751	0,700	0,746	0,695			0,836	0,780	0,931	0,867	0,856	0,798	
-40	0,775	0,727	0,767	0,720			0,871	0,817	0,966	0,906	0,889	0,834	
-30	0,800	0,755	0,788	0,744			0,905	0,854	1,002	0,945	0,924	0,871	
-20	0,824	0,780	0,812	0,768			0,939	0,888	1,038	0,982	0,957	0,905	
-10	0,845	0,804	0,832	0,791			0,970	0,923	1,069	1,017	0,988	0,940	
0	0,870	0,827	0,856	0,814			1,005	0,956	1,107	1,053	1,024	0,974	
10	0,894	0,851	0,879	0,837			1,038	0,988	1,141	1,086	1,058	1,007	
20													
30													
40													
50													
60													
70													
80													
90													
100													
110													
120													
130													
140													

Rev Cp (0,063 torr, 150 C 16 hours) Set 2, 2 run						
Celsius	S1 Act; Set 2, Run 2	S1 + KCp	S2Act; Set 2, Run 2	S2 + KCp	S3Act; Set 2, Run 2	S3 + KCp
-180	0,148	0,093	0,073	0,046	0,390	0,244
-170	0,165	0,114	0,086	0,059	0,441	0,306
-160	0,201	0,147	0,099	0,072	0,483	0,352
-150	0,272	0,209	0,122	0,094	0,510	0,393
-140	0,370	0,297	0,181	0,145	0,536	0,430
-130	0,454	0,376	0,281	0,233	0,559	0,463
-120	0,510	0,434	0,401	0,341	0,583	0,496
-110	0,547	0,477	0,496	0,432	0,605	0,527
-100	0,577	0,512	0,554	0,491	0,627	0,556
-90	0,606	0,544	0,592	0,532	0,650	0,584
-80	0,632	0,577	0,620	0,566	0,672	0,612
-70	0,660	0,607	0,647	0,594	0,695	0,639
-60	0,686	0,635	0,671	0,621	0,718	0,664
-50	0,710	0,662	0,693	0,646	0,741	0,691
-40	0,733	0,688	0,715	0,671	0,764	0,717
-30	0,756	0,714	0,737	0,695	0,788	0,743
-20	0,781	0,738	0,760	0,719	0,814	0,770
-10	0,803	0,764	0,779	0,742	0,836	0,795
0	0,827	0,786	0,801	0,762	0,862	0,819
10	0,852	0,811	0,824	0,785	0,887	0,844
20						
30						
40						
50						
60						
70						
80						
90						
100						
110						
120						
130						
140						

Celsius	Rev Cp (0,005 torr, 150 C 16 hours)						Rev Cp inactivated							
	S1 Act; Set 3	S1 + KCp	S2 Act; Set 3	S2 + KCp	S3 Act; Set 3	S3 + KCp	S4 Act; Set 3	S4 + KCp	S1 IA; Test 1	S1 + KCp	S2 IA; Test 2	S2 + KCp	S3 IA; Test 3	S3 + KCp
-180	0,505	0,316	0,111	0,069	0,038	0,024	0,107	0,067	0,433	0,271	0,481	0,301	0,423	0,265
-170	0,522	0,362	0,130	0,090	0,046	0,032	0,101	0,070	0,478	0,331	0,490	0,340	0,468	0,325
-160	0,570	0,416	0,145	0,106	0,057	0,042	0,113	0,083	0,520	0,379	0,533	0,389	0,511	0,373
-150	0,604	0,466	0,177	0,136	0,077	0,059	0,132	0,102	0,554	0,427	0,566	0,436	0,543	0,419
-140	0,636	0,510	0,263	0,211	0,131	0,105	0,180	0,145	0,594	0,477	0,611	0,491	0,585	0,470
-130	0,664	0,550	0,374	0,310	0,235	0,195	0,273	0,226	0,634	0,525	0,653	0,541	0,626	0,519
-120	0,695	0,591	0,448	0,381	0,380	0,323	0,388	0,330	0,670	0,570	0,688	0,586	0,660	0,561
-110	0,722	0,629	0,492	0,429	0,488	0,426	0,480	0,418	0,698	0,608	0,718	0,626	0,688	0,600
-100	0,750	0,665	0,525	0,465	0,549	0,486	0,538	0,477	0,725	0,643	0,745	0,661	0,715	0,633
-90	0,779	0,700	0,553	0,497	0,587	0,527	0,577	0,518	0,754	0,677	0,773	0,694	0,742	0,667
-80	0,806	0,735	0,576	0,525	0,616	0,561	0,606	0,552	0,784	0,715	0,797	0,726	0,770	0,702
-70	0,837	0,769	0,600	0,552	0,642	0,590	0,632	0,581	0,814	0,748	0,822	0,756	0,799	0,734
-60	0,867	0,802	0,623	0,577	0,667	0,618	0,657	0,608	0,841	0,778	0,846	0,783	0,823	0,762
-50	0,896	0,835	0,645	0,601	0,691	0,644	0,680	0,634	0,867	0,808	0,870	0,810	0,846	0,789
-40	0,924	0,868	0,666	0,625	0,713	0,669	0,702	0,659	0,890	0,835	0,892	0,837	0,867	0,814
-30	0,954	0,900	0,686	0,647	0,736	0,694	0,724	0,683	0,912	0,860	0,913	0,862	0,888	0,837
-20	0,984	0,931	0,706	0,668	0,758	0,717	0,746	0,705	0,934	0,883	0,935	0,884	0,907	0,858
-10	1,010	0,961	0,723	0,688	0,777	0,739	0,764	0,727	0,950	0,904	0,951	0,904	0,924	0,879
0	1,042	0,991	0,745	0,708	0,800	0,761	0,787	0,748	0,972	0,924	0,971	0,924	0,944	0,898
10	1,074	1,023	0,766	0,729	0,824	0,784	0,809	0,770	0,991	0,944	0,993	0,945	0,965	0,919
20														
30														
40														
50														
60														
70														
80														
90														
100														
110														
120														
130														
140														

## Appendix IX – Heat Capacity Measurement Values Fe-btc

Celsius	Rev Cp (0,063 torr, 150 C 16 hours)						KcP	Rev Cp inactivated					
	S1 Act; Set 1	S1 + KcP	S2 Act; Set 1	S2 + KcP	S3 Act; Set 1	S3 + KcP		S1 IA; Set 1	S1 + KcP	S2 IA; Set 1	S2 + KcP	S3 IA; Set 1	S3 + KcP
-180	0,448	0,280	0,453	0,284	0,420	0,263	0,626						
-170	0,483	0,335	0,499	0,346	0,450	0,312	0,694						
-160	0,525	0,383	0,542	0,396	0,493	0,360	0,730						
-150	0,556	0,428	0,574	0,442	0,525	0,404	0,770						
-140	0,585	0,469	0,603	0,485	0,554	0,445	0,803						
-130	0,610	0,505	0,630	0,522	0,581	0,482	0,829						
-120	0,636	0,541	0,657	0,559	0,608	0,518	0,851	0,724	0,617	0,744	0,633	0,693	0,590
-110	0,659	0,574	0,681	0,594	0,632	0,551	0,872	0,742	0,647	0,750	0,654	0,723	0,630
-100	0,683	0,606	0,707	0,626	0,657	0,582	0,886	0,775	0,687	0,785	0,696	0,757	0,671
-90	0,708	0,636	0,733	0,658	0,682	0,613	0,898	0,808	0,726	0,821	0,738	0,791	0,711
-80	0,731	0,666	0,756	0,690	0,705	0,643	0,912	0,841	0,766	0,856	0,780	0,823	0,750
-70	0,755	0,694	0,782	0,719	0,730	0,671	0,919	0,876	0,805	0,893	0,820	0,859	0,789
-60	0,780	0,722	0,808	0,748	0,754	0,698	0,925	0,910	0,842	0,930	0,860	0,892	0,826
-50	0,803	0,748	0,831	0,775	0,777	0,724	0,932	0,945	0,881	0,966	0,900	0,927	0,864
-40	0,825	0,774	0,854	0,802	0,799	0,750	0,939	0,979	0,919	1,003	0,941	0,960	0,901
-30	0,848	0,800	0,878	0,828	0,824	0,777	0,943	1,014	0,957	1,040	0,981	0,995	0,939
-20	0,872	0,825	0,903	0,854	0,847	0,801	0,946	1,051	0,994	1,079	1,021	1,031	0,975
-10	0,892	0,849	0,923	0,878	0,867	0,825	0,951	1,083	1,030	1,113	1,059	1,066	1,014
0	0,918	0,872	0,949	0,903	0,892	0,848	0,951	1,123	1,068	1,155	1,098	1,105	1,051
10	0,941	0,896	0,974	0,927	0,915	0,871	0,952	1,160	1,104	1,193	1,136	1,143	1,088
20	0,966	0,920	1,000	0,952	0,939	0,895	0,953	1,200	1,143	1,231	1,173	1,181	1,125
30	0,989	0,942	1,023	0,974	0,961	0,915	0,952	1,236	1,177	1,266	1,205	1,216	1,158
40	1,011	0,964	1,047	0,999	0,983	0,937	0,954	1,270	1,211	1,298	1,238	1,249	1,191
50	1,031	0,986	1,068	1,022	1,002	0,959	0,957	1,300	1,244	1,324	1,267	1,281	1,226
60	1,051	1,007	1,090	1,044	1,021	0,978	0,958	1,329	1,273	1,346	1,290	1,313	1,258
70	1,072	1,028	1,112	1,066	1,042	0,999	0,959	1,358	1,302	1,361	1,305	1,345	1,290
80	1,091	1,047	1,133	1,088	1,060	1,018	0,960	1,381	1,326	1,362	1,308	1,375	1,320
90	1,110	1,066	1,154	1,109	1,078	1,036	0,961	1,404	1,349	1,350	1,297	1,404	1,349
100	1,128	1,085	1,173	1,129	1,095	1,054	0,962	1,417	1,363	1,320	1,270	1,426	1,372
110	1,147	1,104	1,193	1,148	1,113	1,071	0,963	1,420	1,367	1,282	1,234	1,447	1,393
120	1,165	1,122	1,211	1,166	1,130	1,088	0,963						
130	1,181	1,139	1,228	1,185	1,144	1,104	0,965						
140	1,197	1,156	1,245	1,202	1,159	1,119	0,965						

Rev Cp (0,063 torr, 150 C 16 hours)							Rev Cp inactivated							
Celsius	S1 Act; Set 2	S1 + KCp	S2 Act; Set 2	S2 + KCp	S3 Act; Set 2	S3 + KCp	S4 Act; Set 2	S4 + KCp	S1 IA; Set 2	S1 + KCp	S2 IA; Set 2	S2 + KCp	S3 IA; Set 2	S3 + KCp
-180	0,120	0,075	0,075	0,047	0,132	0,083	0,183	0,114	0,477	0,298	0,414	0,259	0,480	0,301
-170	0,119	0,083	0,044	0,030	0,116	0,080	0,176	0,122	0,549	0,381	0,509	0,353	0,532	0,369
-160	0,131	0,096	0,051	0,037	0,130	0,095	0,191	0,140	0,597	0,435	0,555	0,405	0,581	0,424
-150	0,154	0,118	0,062	0,048	0,157	0,121	0,218	0,168	0,635	0,489	0,591	0,455	0,619	0,477
-140	0,217	0,175	0,135	0,109	0,230	0,185	0,288	0,231	0,671	0,539	0,625	0,502	0,656	0,527
-130	0,328	0,272	0,278	0,230	0,348	0,289	0,405	0,336	0,707	0,586	0,658	0,546	0,691	0,573
-120	0,447	0,381	0,435	0,371	0,468	0,398	0,535	0,455	0,745	0,634	0,693	0,590	0,729	0,621
-110	0,532	0,464	0,538	0,469	0,553	0,482	0,636	0,554	0,786	0,685	0,731	0,637	0,769	0,670
-100	0,585	0,519	0,598	0,530	0,606	0,537	0,705	0,625	0,832	0,737	0,773	0,685	0,813	0,720
-90	0,622	0,559	0,637	0,573	0,643	0,578	0,753	0,676	0,878	0,789	0,817	0,734	0,858	0,771
-80	0,650	0,593	0,667	0,608	0,671	0,612	0,788	0,719	0,923	0,841	0,860	0,784	0,903	0,823
-70	0,677	0,623	0,695	0,639	0,698	0,641	0,821	0,755	0,972	0,893	0,905	0,832	0,950	0,873
-60	0,701	0,649	0,721	0,668	0,722	0,668	0,851	0,787	1,018	0,942	0,948	0,878	0,996	0,921
-50	0,724	0,675	0,745	0,694	0,745	0,694	0,879	0,819	1,062	0,990	0,991	0,923	1,040	0,969
-40	0,746	0,700	0,767	0,720	0,765	0,718	0,904	0,848	1,106	1,038	1,031	0,968	1,081	1,015
-30	0,766	0,722	0,789	0,744	0,787	0,742	0,929	0,876	1,146	1,081	1,071	1,010	1,121	1,058
-20	0,788	0,745	0,809	0,766	0,809	0,765	0,955	0,904	1,188	1,124	1,114	1,054	1,162	1,099
-10	0,806	0,767	0,828	0,788	0,828	0,787	0,978	0,931	1,224	1,165	1,149	1,093	1,199	1,141
0	0,828	0,787	0,852	0,810	0,850	0,808	1,005	0,956	1,265	1,203	1,188	1,130	1,240	1,179
10	0,850	0,809	0,874	0,832	0,871	0,830	1,031	0,982	1,305	1,243	1,227	1,168	1,279	1,218
20														
30														
40														
50														
60														
70														
80														
90														
100														
110														
120														
130														
140														

## Appendix X – Heat Capacity Measurement Values MIL-100(Fe)

Rev Cp (0,065 torr, 150 C 15 hours)								Rev Cp inactivated						
Celsius	S1 Act; Set 1	S1 + KCp	S2 Act; Set 1	S2 + KCp	S3 Act; Set 1	S3 + KCp	KCp	S1 IA; Set 1	S1 + KCp	S2 IA; Set 1	S2 + KCp	S3 IA; Set 1	S3 + KCp	
-180	0,225	0,141	0,246	0,154	0,194	0,121	0,626							
-170	0,387	0,269	0,320	0,222	0,299	0,207	0,694							
-160	0,505	0,369	0,419	0,306	0,389	0,284	0,730							
-150	0,583	0,449	0,509	0,392	0,456	0,351	0,770							
-140	0,633	0,508	0,568	0,456	0,501	0,403	0,803							
-130	0,670	0,555	0,607	0,503	0,537	0,445	0,829							
-120	0,703	0,599	0,638	0,543	0,568	0,483	0,851	0,870	0,741	0,896	0,763	0,877	0,747	
-110	0,735	0,640	0,664	0,579	0,596	0,519	0,872	0,934	0,814	0,963	0,839	0,961	0,837	
-100	0,765	0,678	0,690	0,612	0,625	0,554	0,886	1,038	0,920	1,064	0,943	1,061	0,941	
-90	0,796	0,715	0,716	0,643	0,652	0,586	0,898	1,138	1,022	1,166	1,048	1,160	1,042	
-80	0,825	0,752	0,740	0,674	0,679	0,619	0,912	1,230	1,121	1,258	1,147	1,248	1,138	
-70	0,856	0,787	0,765	0,703	0,707	0,650	0,919	1,329	1,221	1,355	1,245	1,343	1,234	
-60	0,887	0,821	0,790	0,731	0,735	0,681	0,925	1,435	1,328	1,460	1,351	1,444	1,336	
-50	0,918	0,856	0,813	0,757	0,763	0,711	0,932	1,538	1,433	1,565	1,459	1,543	1,438	
-40	0,946	0,888	0,836	0,785	0,791	0,742	0,939	1,631	1,531	1,657	1,555	1,631	1,531	
-30	0,976	0,921	0,861	0,812	0,819	0,773	0,943	1,703	1,607	1,733	1,635	1,704	1,608	
-20	1,008	0,954	0,886	0,838	0,849	0,803	0,946	1,763	1,668	1,792	1,695	1,764	1,669	
-10	1,036	0,986	0,907	0,863	0,876	0,833	0,951	1,802	1,714	1,833	1,744	1,805	1,717	
0	1,069	1,016	0,933	0,887	0,906	0,862	0,951	1,842	1,751	1,874	1,782	1,848	1,757	
10	1,101	1,048	0,958	0,913	0,936	0,891	0,952	1,871	1,781	1,905	1,814	1,880	1,790	
20	1,132	1,078	0,982	0,936	0,965	0,919	0,953	1,897	1,807	1,930	1,838	1,908	1,817	
30	1,162	1,106	1,006	0,958	0,991	0,943	0,952	1,920	1,828	1,951	1,858	1,929	1,837	
40	1,191	1,136	1,027	0,980	1,019	0,972	0,954	1,938	1,849	1,966	1,875	1,950	1,860	
50	1,219	1,166	1,048	1,003	1,044	0,999	0,957	1,951	1,866	1,976	1,890	1,969	1,884	
60	1,245	1,193	1,069	1,024	1,069	1,024	0,958	1,959	1,877	1,981	1,898	1,991	1,908	
70	1,273	1,221	1,090	1,045	1,096	1,051	0,959	1,963	1,882	1,976	1,895	2,010	1,927	
80	1,300	1,248	1,110	1,066	1,121	1,076	0,960	1,954	1,876	1,960	1,882	2,025	1,944	
90	1,327	1,275	1,131	1,087	1,148	1,103	0,961	1,936	1,860	1,949	1,873	2,045	1,965	
100	1,354	1,303	1,149	1,106	1,173	1,129	0,962	1,912	1,840	1,906	1,834	2,081	2,002	
110	1,384	1,332	1,169	1,125	1,202	1,157	0,963	1,870	1,800	1,812	1,744	2,143	2,063	
120	1,411	1,359	1,189	1,145	1,229	1,184	0,963							
130	1,432	1,381	1,205	1,162	1,254	1,210	0,965							
140	1,455	1,405	1,221	1,179	1,277	1,233	0,965							



Rev Cp (0,064 torr, 150 C 16 hours)									Rev Cp inactivated					
Celsius	S1 Act; Set 2	S1 + KCp	S2 Act; Set 2	S2 + KCp	S3 Act; Set 2	S3 + KCp	S4 Act; Set 2	S4 + KCp	S1 IA; Set 2	S1 + KCp	S2 IA; Set 2	S2 + KCp	S3 IA; Set 2	S3 + KCp
-180	0,005	0,003	0,121	0,076	0,471	0,295	0,182	0,114	0,410	0,257	0,164	0,102	0,118	0,074
-170	0,139	0,096	0,199	0,138	0,503	0,349	0,224	0,156	0,535	0,371	0,287	0,199	0,287	0,199
-160	0,163	0,119	0,227	0,166	0,551	0,402	0,381	0,278	0,630	0,460	0,322	0,235	0,369	0,269
-150	0,181	0,139	0,249	0,192	0,583	0,449	0,527	0,406	0,695	0,536	0,356	0,274	0,427	0,329
-140	0,196	0,157	0,267	0,214	0,614	0,493	0,605	0,486	0,756	0,607	0,391	0,314	0,477	0,383
-130	0,212	0,176	0,286	0,237	0,641	0,531	0,650	0,538	0,808	0,669	0,426	0,353	0,521	0,432
-120	0,230	0,196	0,306	0,260	0,669	0,569	0,685	0,583	0,862	0,733	0,464	0,394	0,568	0,483
-110	0,249	0,217	0,326	0,284	0,693	0,604	0,715	0,623	0,931	0,812	0,519	0,452	0,627	0,546
-100	0,269	0,238	0,347	0,307	0,717	0,636	0,743	0,659	1,031	0,914	0,600	0,532	0,710	0,629
-90	0,289	0,260	0,368	0,331	0,741	0,666	0,773	0,694	1,128	1,013	0,681	0,612	0,791	0,711
-80	0,309	0,281	0,389	0,354	0,761	0,694	0,799	0,728	1,217	1,110	0,757	0,690	0,865	0,789
-70	0,330	0,303	0,410	0,377	0,785	0,721	0,827	0,760	1,309	1,203	0,837	0,769	0,944	0,868
-60	0,351	0,324	0,432	0,399	0,809	0,748	0,856	0,792	1,407	1,302	0,922	0,853	1,027	0,950
-50	0,370	0,344	0,452	0,421	0,834	0,777	0,883	0,823	1,503	1,401	1,007	0,939	1,107	1,032
-40	0,387	0,363	0,470	0,441	0,858	0,805	0,910	0,854	1,589	1,491	1,081	1,015	1,176	1,104
-30	0,407	0,384	0,490	0,462	0,883	0,833	0,935	0,882	1,660	1,566	1,145	1,080	1,235	1,165
-20	0,427	0,404	0,510	0,483	0,908	0,859	0,964	0,912	1,718	1,625	1,195	1,131	1,284	1,215
-10	0,446	0,424	0,529	0,504	0,930	0,884	0,988	0,940	1,758	1,673	1,230	1,170	1,321	1,257
0	0,467	0,444	0,550	0,523	0,956	0,909	1,016	0,966	1,798	1,710	1,261	1,199	1,356	1,289
10	0,487	0,464	0,572	0,545	0,983	0,936	1,046	0,996	1,831	1,743	1,286	1,224	1,384	1,318
20														
30														
40														
50														
60														
70														
80														
90														
100														
110														
120														
130														
140														

	Rev Cp (0,005 torr, 150 C 20 hours)							
Celsius	S1 Act; Set 3	S1 + KCp	S2 Act; Set 3	S2 + KCp	S3 Act; Set 3	S3 + KCp	S4 Act; Set 3	S4 + KCp
-180	0,490	0,307	0,294	0,184	0,238	0,149	0,142	0,089
-170	0,575	0,399	0,307	0,213	0,247	0,171	0,164	0,114
-160	0,631	0,461	0,357	0,261	0,280	0,205	0,274	0,200
-150	0,662	0,510	0,442	0,340	0,345	0,266	0,466	0,359
-140	0,691	0,555	0,539	0,433	0,470	0,377	0,589	0,473
-130	0,719	0,596	0,608	0,504	0,575	0,476	0,642	0,532
-120	0,751	0,640	0,655	0,558	0,637	0,542	0,678	0,577
-110	0,782	0,682	0,690	0,602	0,677	0,590	0,710	0,619
-100	0,812	0,720	0,720	0,639	0,710	0,629	0,742	0,658
-90	0,837	0,752	0,749	0,673	0,738	0,663	0,771	0,693
-80	0,857	0,782	0,775	0,706	0,764	0,697	0,799	0,729
-70	0,876	0,805	0,802	0,737	0,790	0,726	0,828	0,761
-60	0,895	0,828	0,827	0,765	0,817	0,756	0,856	0,792
-50	0,916	0,854	0,851	0,793	0,839	0,782	0,881	0,821
-40	0,937	0,879	0,873	0,820	0,862	0,809	0,904	0,849
-30	0,960	0,905	0,895	0,844	0,884	0,834	0,928	0,876
-20	0,985	0,932	0,918	0,868	0,907	0,858	0,950	0,899
-10	1,005	0,956	0,936	0,890	0,924	0,879	0,969	0,922
0	1,032	0,981	0,959	0,912	0,945	0,899	0,992	0,943
10	1,061	1,010	0,982	0,935	0,969	0,923	1,018	0,969
20								
30								
40								
50								
60								
70								
80								
90								
100								
110								
120								
130								
140								



**Appendix XI – Risk Assessment Report**

# Risk Assessment Report

## Heat capacity measurements

<b>Prosjekttittel</b>	Heat capacity measurements
<b>Prosjektleder</b>	Erling Næss / Christian Schlemminger
<b>Enhet</b>	NTNU
<b>HMS-koordinator</b>	Erik Langørgen
<b>Linjeleder</b>	Olav Bolland
<b>Plassering</b>	VATlab - finlab
<b>Romnummer</b>	Room C165 c
<b>Riggansvarlig</b>	Christian Schlemminger / Reidar Tellebon
<b>Risikovurdering utført av</b>	Christian Schlemminger / Erik Langørgen

## TABLE OF CONTENTS

1	INTRODUCTION .....	1
2	ORGANISATION .....	1
3	RISK MANAGEMENT IN THE PROJECT .....	1
4	DRAWINGS, PHOTOS, DESCRIPTIONS OF TEST SETUP .....	2
5	EVACUATION FROM THE EXPERIMENT AREA .....	4
6	WARNING .....	5
6.1	Before experiments.....	5
6.2	Nonconformance.....	5
7	ASSESSMENT OF TECHNICAL SAFETY .....	6
7.1	HAZOP.....	6
7.2	Flammable, reactive and pressurized substances and gas .....	6
7.3	Pressurized equipment.....	6
7.4	Effects on the environment (emissions, noise, temperature, vibration, smell) .....	6
7.5	Radiation .....	6
7.6	Usage and handling of chemicals.....	6
7.7	EI safety (need to deviate from the current regulations and standards.) .....	6
8	ASSESSMENT OF OPERATIONAL SAFETY .....	7
8.1	Procedure HAZOP .....	7
8.2	Operation and emergency shutdown procedure .....	7
8.3	Training of operators.....	7
8.4	Technical modifications.....	7
8.5	Personal protective equipment .....	7
8.6	General Safety .....	8
8.7	Safety equipment .....	8
8.8	Special actions.....	8
9	QUANTIFYING OF RISK - RISK MATRIX.....	8
10	CONCLUSION .....	8
11	REGULATIONS AND GUIDELINES .....	9
12	DOCUMENTATION.....	10

## 1 INTRODUCTION

The thermal heat capacity of materials will be measured with a differential scanning calorimeter (DSC) type Q2000, which was delivered by TA-Instruments.

## 2 ORGANISATION

Rolle	NTNU	Sintef
Lab Ansvarlig:	Morten Grønli	Harald Mæhlum
Linjeleder:	Olav Bolland	Mona J. Mølsvik
HMS ansvarlig:	Olav Bolland	Mona J. Mølsvik
HMS koordinator	Erik Langørgen	Harald Mæhlum
HMS koordinator	Bård Brandåstrø	
Romansvarlig:	Harald Mæhlum	
Prosjekt leder:	Erling Næss / Christian Schlemminger	
Ansvarlig riggoperatører:	Christian Schlemminger	

## 3 RISK MANAGEMENT IN THE PROJECT

Hovedaktiviteter risikostyring	Nødvendige tiltak, dokumentasjon	DATE
Prosjekt initiering	Prosjekt initiering mal	n.a.
Veiledningsmøte Guidance Meeting	Skjema for Veiledningsmøte med pre-risikovurdering	n.a.
Innledende risikovurdering Initial Assessment	Fareidentifikasjon – HAZID Skjema grovanalyse	n.a.
Vurdering av teknisk sikkerhet Evaluation of technical security	Prosess-HAZOP Tekniske dokumentasjoner	n.a.
Vurdering av operasjonell sikkerhet Evaluation of operational safety	Prosedyre-HAZOP Opplæringsplan for operatører	n.a.
Sluttvurdering, kvalitetssikring Final assessment, quality assurance	Uavhengig kontroll Utstedelse av apparaturkort Utstedelse av forsøk pågår kort	n.a.

#### 4 DRAWINGS, PHOTOS, DESCRIPTIONS OF TEST SETUP

##### Test setup / location of important Equipment / and description

The thermal heat capacity of different non toxic materials shall be measured in the laboratory. The existing setup which is used is a Q2000 DSC from TA-Instruments.

The measurement device was bought from TA Instruments and installed by technicians of the deliverer. The setup is CE- certified and all gas supply lines are installed by authorized lab staff. The gas supply is realized by 50l gas cylinders and pressure regulators. The maximal pressure is set at the lower limit of the working pressure.



4-1 Q2000 DSC

All procedures are full fill the requirements of the in the manual presented once. The manual is located beside the DSC. Furthermore is the procedure for calibrations procedures in the same folder.

Due to the fact of the already certificated equipment, the documentation of the setup in the user manual and the installation of pressurized gas containing equipment from authorized lab personal the hazards are minimal. Therefore potentials hazards can only occur due to incorrect us (prevented due to operator training) or due to the sampling of the material.

##### Sample preparation

The sample crimping is very important regarding the accuracy of the heat capacity measurements. The object is to get the sample pans tightly sealed with a hermetic lid, to prevent volatiles from the sample being released, and the compressing the material, to obtain a very good thermal contact with the cup bottom. This means the better the thermal contact, the better the accuracy of the heat capacity measurements. The material has to be in good contact with the pan bottom, an advantage is to measure a material film or a powder densely packed in the Tzero®



pan. The thermal contact is not only important between the sample material and the bottom of the cup, but also the contact surface area between the pan bottom and the sensor. This is why Tzero® pans are used in heat capacity measurements, because of their flat pan bottom, but this also has to be kept very flat for best possible thermal contact. These considerations together with a very clean sensor surface give the most accurate result values.



4-2 The Tzero® sample press with its belonging blue and black press parts.

Every sample can be prepared in three different ways and crimped with a Tzero® sample press, see figure 4-2. The type of pans and lids used for our case, if not stated otherwise, was Tzero® pans (PN 901683.901) and Tzero® hermetic lids (PN 901684.901). The press had two sets of crimping parts for encapsulating the sample cups, blue top and bottom parts, used for hermetic sealing, and black top and bottom parts, used for compressing the sample.

The following steps shall be done before setting the sample in the DSC:

- Weigh pans and lids separately and choose the optimal pair for the existing reference pan (write it down)
- Use personal protection equipment (glasses, dusk mask, hand gloves)
- Fill sample material in the pan and weigh pan + sample (write it down)
- Use the chosen lid and put it on the pan
- Place the pan with lid and sample in the right bottom part (blue or black depending on sealed and unsealed samples)
- Insert the top part, which fits to the bottom part in the sample press (blue to blue or black to black)
- Mount the bottom part with sample
- Clouse the sample press down to the preferred height
- Open sample press
- Remove sample
- Control if lid is proper pressed on/in the pan and without cracks
- Control bottom surface of flatness
- Set the sample in the DSC
- Follow the DSC instructions to run proper experiments

The following presented figures show possible sampling failures.



4-3 sample too full top and side part is bended out



4-4 sample lid cracked



4-5 optimal sealed and compressed sample

## 5 EVACUATION FROM THE EXPERIMENT AREA

Evacuate at signal from the alarm system or local gas alarms with its own local alert with sound and light outside the room in question, see 6.2

Evacuation from the rigging area takes place through the marked emergency exits to the meeting point, (corner of Old Chemistry Kjelhuset or parking 1a-b.)

## 6 WARNING

### 6.1 Before experiments

E-mail with information about the test run duration, (hour) and the involved to HMS koordinator NTNU/SINTEF

[Erik.langorgen@ntnu.no](mailto:Erik.langorgen@ntnu.no)

[Baard.brandaastro@ntnu.no](mailto:Baard.brandaastro@ntnu.no)

Project Managers on neighboring units alerted for clarification around the use of the exhaust system without fear or interference of any kind, see rig matrix.

All experiments should be planned and put into the activity calendar for the lab. Experiment leader must get confirmation that the experiments are coordinated with other activity before start up.

### 6.2 Nonconformance

#### FIRE

Fire you are not able to put out with locally available fire extinguishers, activate, the nearest fire alarm and evacuate area. Be then available for fire brigade and building caretaker to detect fire place.

If possible, notify:

NTNU	SINTEF
Labsjef Morten Grønli, tlf: 918 97 515	Labsjef Harald Mæhlum tlf 930 149 86
HMS: Erik Langørgen, tlf: 91897160	Forskningssjef Mona J MølInvik tlf 930 08 868
Instituttleder: Olav Bolland, tlf: 91897209	
Prosjektleder: Christian Schlemminger, tlf: 41063418	

#### GASALARM

At a gas alarm, close gas bottles immediately and increase ventilation rate in the area. If the level of gas concentration not decrease within a reasonable time, activate the fire alarm and evacuate the lab. Designated personnel or fire department checks the leak to determine whether it is possible to seal the leak and ventilate the area in a responsible manner.

Alert Order in the above paragraph.

#### PERSONAL INJURY

- First aid kit in the fire / first aid stations
- Shout for help
- Start life-saving first aid

**CALL 113** if there is any doubt whether there is a serious injury

#### Other Nonconformance (AVVIK)

**NTNU:**

Reporting form for nonconformance at:

[http://www.ntnu.no/hms/2007\\_Nettsider/HMSRV0401\\_avvik.doc](http://www.ntnu.no/hms/2007_Nettsider/HMSRV0401_avvik.doc)

**SINTEF:**

Synergi

## 7 ASSESSMENT OF TECHNICAL SAFETY

### 7.1 HAZOP

*See Chapter 14 "Guide to the report template".*

The experiment set up is divided into the following nodes:

Node 1	-
--------	---

**Attachments:, skjema: Hazop\_mal**

**Conclusion:** Risks are minimal with the passive and active safety improvements

### 7.2 Flammable, reactive and pressurized substances and gas

Contains the experiments Flammable, reactive and pressurized substances and gas

NEI	YES
-----	-----

**Attachments: -**

**Conclusion : -**

### 7.3 Pressurized equipment

**Contain the set up pressurized equipment?**

NEI	YES
-----	-----

**Attachments:-**

**Conclusion: -**

### 7.4 Effects on the environment (emissions, noise, temperature, vibration, smell)

NEI	YES
-----	-----

**Conclusion: -**

### 7.5 Radiation

*See Chapter 14 "Guide to the report template".*

NEI	JA, Radiation source need to have an own risk assessment
-----	----------------------------------------------------------

**Attachments: -**

**Conclusion: -**

### 7.6 Usage and handling of chemicals.

*See Chapter 14 "Guide to the report template".*

NEI	JA, Do a risk assessment of the use
-----	-------------------------------------

**Attachments: MSDS's of: Fe-btc-MOF; Cu-btc-MOF; Liquid Nitrogen**

**Conclusion:**

- 1) Use gloves during handling
- 2) Use dusk mask during handling

### 7.7 El safety (need to deviate from the current regulations and standards.)

NEI	JA, El safety have to be evaluated
-----	------------------------------------

Her forstås montasje og bruk i forhold til normer og forskrifter med tanke på berøringsfare

**Attachments:**

**Conclusion:**

## 8 ASSESSMENT OF OPERATIONAL SAFETY

Ensures that established procedures cover all identified risk factors that must be taken care of through procedures. Ensures that the operators and technical performance have sufficient expertise.

### 8.1 Procedure HAZOP

*See Chapter 14 "Guide to the report template".*

The method is a procedure to identify causes and sources of danger to operational problems.

**Attachments:** see user manual DSC Q2000

**Conclusion:** CE-certificated instrument

### 8.2 Operation and emergency shutdown procedure

*See Chapter 14 "Guide to the report template".*

The operating procedure is a checklist that must be filled out for each experiment.

Emergency procedure should attempt to set the experiment set up in a harmless state by unforeseen events.

**Attachments:** see user manual DSC Q2000

### 8.3 Training of operators

A Document showing training plan for operators

*What are the requirements for the training of operators?*

- *What it takes to be an independent operator*
- *Job Description for operators*

**Attachments:** see user manual DSC Q2000

### 8.4 Technical modifications

- Technical modifications made by the Operator
  - Inlet pressures up to allowed maximal pressures written in the user manual for the Q2000
- Technical modifications that must be made by Technical staff:
  - n.a.
- What technical modifications give a need for a new risk assessment:
  - n.a.

**Conclusion:** All safety relevant changes needs to be double checked by an 2ed person, which is familiar with the used standards and procedures.

### 8.5 Personal protective equipment

- It is mandatory use of eye protection by sampling.
- Use gloves during handling with MOF's
- Use dusk mask during handling MOF's

**Conclusion:** The personal protection minimizes the risks to an extreme low level.

## 8.6 General Safety

- Electrical wires and flexible tubes shall not be installed in the area of the direct exit

### Safety concept

#### *CE – certified setup*

#### Attachments:

User manual Q2000 DSC

#### Conclusion:

Is Operator allowed to leave during the experiment?

Yes, as long as the setup is running normally.

## 8.7 Safety equipment

- Warning signs

## 8.8 Special actions.

- NON

## 9 QUANTIFYING OF RISK - RISK MATRIX

*See Chapter 14 "Guide to the report template".*

The risk matrix will provide visualization and an overview of activity risks so that management and users get the most complete picture of risk factors.

n.a.

## 10 CONCLUSJON

The rig is built in good laboratory practice (GLP).

The setup can only be used in the operating conditions written in the manual and after allowed changes with TA-Instruments

Experiment unit card get a period of **24 months**

Experiment in progress card get a period of **24 months**

## 11 REGULATIONS AND GUIDELINES

Se <http://www.arbeidstilsynet.no/regelverk/index.html>

- Lov om tilsyn med elektriske anlegg og elektrisk utstyr (1929)
- Arbeidsmiljøloven
- Forskrift om systematisk helse-, miljø- og sikkerhetsarbeid (HMS Internkontrollforskrift)
- Forskrift om sikkerhet ved arbeid og drift av elektriske anlegg (FSE 2006)
- Forskrift om elektriske forsyningsanlegg (FEF 2006)
- Forskrift om utstyr og sikkerhetssystem til bruk i eksplosjonsfarlig område NEK 420
- Forskrift om håndtering av brannfarlig, reaksjonsfarlig og trykksatt stoff samt utstyr og anlegg som benyttes ved håndteringen
- Forskrift om Håndtering av eksplosjonsfarlig stoff
- Forskrift om bruk av arbeidsutstyr.
- Forskrift om Arbeidsplasser og arbeidslokaler
- Forskrift om Bruk av personlig verneutstyr på arbeidsplassen
- Forskrift om Helse og sikkerhet i eksplosjonsfarlige atmosfærer
- Forskrift om Høytrykksspyling
- Forskrift om Maskiner
- Forskrift om Sikkerhetsskilting og signalgivning på arbeidsplassen
- Forskrift om Stillaser, stiger og arbeid på tak m.m.
- Forskrift om Sveising, termisk skjæring, termisk sprøyting, kullbuemeisling, lodding og sliping (varmt arbeid)
- Forskrift om Tekniske innretninger
- Forskrift om Tungt og ensformig arbeid
- Forskrift om Vern mot eksponering for kjemikalier på arbeidsplassen (Kjemikalieforskriften)
- Forskrift om Vern mot kunstig optisk stråling på arbeidsplassen
- Forskrift om Vern mot mekaniske vibrasjoner
- Forskrift om Vern mot støy på arbeidsplassen

Veiledninger fra arbeidstilsynet

se: <http://www.arbeidstilsynet.no/regelverk/veiledninger.html>

## 12 DOCUMENTATION

- MSDS of used materials
  - FE-btc
  - Cu-btc
  - Indium
  - Sapphire



## SAFETY DATA SHEET

according to Regulation (EC) No. 1907/2006

Version 3.1 Revision Date 07.06.2011

Print Date 21.09.2011

GENERIC EU MSDS - NO COUNTRY SPECIFIC DATA - NO OEL DATA

**1. IDENTIFICATION OF THE SUBSTANCE/MIXTURE AND OF THE COMPANY/UNDERTAKING****1.1 Product identifiers**

Product name : Basolite™ C 300

Product Number : 688614

Brand : Aldrich

**1.2 Relevant identified uses of the substance or mixture and uses advised against**

Identified uses : Laboratory chemicals, Manufacture of substances

**1.3 Details of the supplier of the safety data sheet**Company : Sigma-Aldrich Norway AS  
Tevlingvn. 23  
N-1081 OSLO

Telephone : +47 23 176000

Fax : +47 23 176010

E-mail address : eurtechserv@sial.com

**1.4 Emergency telephone number**

Emergency Phone # : Giftinformasjonssentralen 22 59 13 00

**2. HAZARDS IDENTIFICATION****2.1 Classification of the substance or mixture****Classification according to Regulation (EC) No 1272/2008 [EU-GHS/CLP]**

Acute toxicity, Oral (Category 3)

Skin irritation (Category 2)

Eye irritation (Category 2)

Acute aquatic toxicity (Category 1)

Chronic aquatic toxicity (Category 1)

**Classification according to EU Directives 67/548/EEC or 1999/45/EC**

Harmful if swallowed. Irritating to eyes and skin. Very toxic to aquatic organisms, may cause long-term adverse effects in the aquatic environment.

**2.2 Label elements****Labelling according Regulation (EC) No 1272/2008 [CLP]**

Pictogram



Signal word

Danger

Hazard statement(s)

H301

Toxic if swallowed.

H315

Causes skin irritation.

H319

Causes serious eye irritation.

H410

Very toxic to aquatic life with long lasting effects.

Precautionary statement(s)

P273

Avoid release to the environment.

P301 + P310

IF SWALLOWED: Immediately call a POISON CENTER or doctor/physician.

P305 + P351 + P338 IF IN EYES: Rinse cautiously with water for several minutes. Remove contact lenses, if present and easy to do. Continue rinsing.  
 P501 Dispose of contents/ container to an approved waste disposal plant.  
 Supplemental Hazard Statements none

**According to European Directive 67/548/EEC as amended.**

Hazard symbol(s)



R-phrase(s)

R22 Harmful if swallowed.  
 R36/38 Irritating to eyes and skin.  
 R50/53 Very toxic to aquatic organisms, may cause long-term adverse effects in the aquatic environment.

S-phrase(s)

S26 In case of contact with eyes, rinse immediately with plenty of water and seek medical advice.  
 S61 Avoid release to the environment. Refer to special instructions/ Safety data sheets.

**2.3 Other hazards - none**

**3. COMPOSITION/INFORMATION ON INGREDIENTS**

**3.2 Mixtures**

Synonyms : Copper benzene-1,3,5-tricarboxylate  
 Cu-BTC MOF

Formula : C<sub>18</sub>H<sub>6</sub>Cu<sub>3</sub>O<sub>12</sub>

Component	Classification	Concentration
<b>Copper benzene-1,3,5-tricarboxylate</b>		
CAS-No. 51937-85-0	Acute Tox. 3; Skin Irrit. 2; Eye Irrit. 2; Aquatic Acute 1; H301, H315, H319, H400 Xn, R22 - R36/38 - R50	>= 88 %
<b>Copper sulphate</b>		
CAS-No. 7758-98-7 EC-No. 231-847-6 Index-No. 029-004-00-0	Acute Tox. 4; Eye Irrit. 2; Skin Irrit. 2; Aquatic Acute 1; Aquatic Chronic 1; H302, H315, H319, H410 Xn, N, R22 - R36/38 - R50/53	<= 5 %
<b>Ethylene glycol</b>		
CAS-No. 107-21-1 EC-No. 203-473-3 Index-No. 603-027-00-1	Acute Tox. 4; H302 Xn, R22	<= 2 %
<b>Methanol</b>		
CAS-No. 67-56-1 EC-No. 200-659-6 Index-No. 603-001-00-X	Flam. Liq. 2; Acute Tox. 3; STOT SE 1; H225, H301, H311, H331, H370 F, T, R11 - R23/24/25 - R39/23/24/25	<= 2 %
<b>Benzene-1,3,5-tricarboxylic acid</b>		
CAS-No. 554-95-0	Skin Irrit. 2; Eye Irrit. 2; STOT	<= 3 %

EC-No.	209-077-7	SE 3; H315, H319, H335 Xi, R36/37/38	
--------	-----------	-----------------------------------------	--

For the full text of the H-Statements and R-Phrases mentioned in this Section, see Section 16

---

#### 4. FIRST AID MEASURES

##### 4.1 Description of first aid measures

###### General advice

Consult a physician. Show this safety data sheet to the doctor in attendance.

###### If inhaled

If breathed in, move person into fresh air. If not breathing, give artificial respiration. Consult a physician.

###### In case of skin contact

Wash off with soap and plenty of water. Take victim immediately to hospital. Consult a physician.

###### In case of eye contact

Rinse thoroughly with plenty of water for at least 15 minutes and consult a physician.

###### If swallowed

Never give anything by mouth to an unconscious person. Rinse mouth with water. Consult a physician.

##### 4.2 Most important symptoms and effects, both acute and delayed

Symptoms of systemic copper poisoning may include: capillary damage, headache, cold sweat, weak pulse, and kidney and liver damage, central nervous system excitation followed by depression, jaundice, convulsions, paralysis, and coma. Death may occur from shock or renal failure. Chronic copper poisoning is typified by hepatic cirrhosis, brain damage and demyelination, kidney defects, and copper deposition in the cornea as exemplified by humans with Wilson's disease. It has also been reported that copper poisoning has lead to hemolytic anemia and accelerates arteriosclerosis., To the best of our knowledge, the chemical, physical, and toxicological properties have not been thoroughly investigated.

##### 4.3 Indication of any immediate medical attention and special treatment needed

no data available

---

#### 5. FIRE-FIGHTING MEASURES

##### 5.1 Extinguishing media

###### Suitable extinguishing media

Use water spray, alcohol-resistant foam, dry chemical or carbon dioxide.

##### 5.2 Special hazards arising from the substance or mixture

Carbon oxides, Sulphur oxides, Borane/boron oxides, Copper oxides

##### 5.3 Advice for firefighters

Wear self contained breathing apparatus for fire fighting if necessary.

##### 5.4 Further information

no data available

---

#### 6. ACCIDENTAL RELEASE MEASURES

##### 6.1 Personal precautions, protective equipment and emergency procedures

Wear respiratory protection. Avoid dust formation. Avoid breathing vapors, mist or gas. Ensure adequate ventilation. Evacuate personnel to safe areas. Avoid breathing dust.

##### 6.2 Environmental precautions

Prevent further leakage or spillage if safe to do so. Do not let product enter drains. Discharge into the environment must be avoided.

##### 6.3 Methods and materials for containment and cleaning up

Pick up and arrange disposal without creating dust. Sweep up and shovel. Keep in suitable, closed containers for disposal.

##### 6.4 Reference to other sections

For disposal see section 13.

---

## 7. HANDLING AND STORAGE

### 7.1 Precautions for safe handling

Avoid contact with skin and eyes. Avoid formation of dust and aerosols. Provide appropriate exhaust ventilation at places where dust is formed.

### 7.2 Conditions for safe storage, including any incompatibilities

Store in cool place. Keep container tightly closed in a dry and well-ventilated place.

### 7.3 Specific end uses

no data available

---

## 8. EXPOSURE CONTROLS/PERSONAL PROTECTION

### 8.1 Control parameters

#### Components with workplace control parameters

### 8.2 Exposure controls

#### Appropriate engineering controls

Avoid contact with skin, eyes and clothing. Wash hands before breaks and immediately after handling the product.

#### Personal protective equipment

##### Eye/face protection

Face shield and safety glasses Use equipment for eye protection tested and approved under appropriate government standards such as NIOSH (US) or EN 166(EU).

##### Skin protection

Handle with gloves. Gloves must be inspected prior to use. Use proper glove removal technique (without touching glove's outer surface) to avoid skin contact with this product. Dispose of contaminated gloves after use in accordance with applicable laws and good laboratory practices. Wash and dry hands.

The selected protective gloves have to satisfy the specifications of EU Directive 89/686/EEC and the standard EN 374 derived from it.

##### Body Protection

Complete suit protecting against chemicals, The type of protective equipment must be selected according to the concentration and amount of the dangerous substance at the specific workplace.

##### Respiratory protection

Where risk assessment shows air-purifying respirators are appropriate use a full-face particle respirator type N99 (US) or type P2 (EN 143) respirator cartridges as a backup to engineering controls. If the respirator is the sole means of protection, use a full-face supplied air respirator. Use respirators and components tested and approved under appropriate government standards such as NIOSH (US) or CEN (EU).

---

## 9. PHYSICAL AND CHEMICAL PROPERTIES

### 9.1 Information on basic physical and chemical properties

- |                                            |                             |
|--------------------------------------------|-----------------------------|
| a) Appearance                              | Form: solid<br>Colour: blue |
| b) Odour                                   | no data available           |
| c) Odour Threshold                         | no data available           |
| d) pH                                      | no data available           |
| e) Melting point/freezing point            | no data available           |
| f) Initial boiling point and boiling range | no data available           |

- |                                                 |                   |
|-------------------------------------------------|-------------------|
| g) Flash point                                  | no data available |
| h) Evaporation rate                             | no data available |
| i) Flammability (solid, gas)                    | no data available |
| j) Upper/lower flammability or explosive limits | no data available |
| k) Vapour pressure                              | no data available |
| l) Vapour density                               | no data available |
| m) Relative density                             | no data available |
| n) Water solubility                             | insoluble         |
| o) Partition coefficient: n-octanol/water       | no data available |
| p) Autoignition temperature                     | no data available |
| q) Decomposition temperature                    | no data available |
| r) Viscosity                                    | no data available |
| s) Explosive properties                         | no data available |
| t) Oxidizing properties                         | no data available |

## 9.2 Other safety information

no data available

---

## 10. STABILITY AND REACTIVITY

### 10.1 Reactivity

no data available

### 10.2 Chemical stability

no data available

### 10.3 Possibility of hazardous reactions

no data available

### 10.4 Conditions to avoid

no data available

### 10.5 Incompatible materials

Strong bases, Acids, Oxidizing agents, Alkali metals, Powdered metals, Strong oxidizing agents, Strong acids, Acid chlorides, Acid anhydrides, Reducing agents, Aldehydes, hydroxylamine, Aluminum, Strong reducing agents, Magnesium

### 10.6 Hazardous decomposition products

Other decomposition products - no data available

---

## 11. TOXICOLOGICAL INFORMATION

### 11.1 Information on toxicological effects

#### Acute toxicity

no data available

#### Skin corrosion/irritation

no data available

#### Serious eye damage/eye irritation

no data available

**Respiratory or skin sensitization**

no data available

**Germ cell mutagenicity**

no data available

**Carcinogenicity**

IARC: No component of this product present at levels greater than or equal to 0.1% is identified as probable, possible or confirmed human carcinogen by IARC.

**Reproductive toxicity**

no data available

**Specific target organ toxicity - single exposure**

no data available

**Specific target organ toxicity - repeated exposure**

no data available

**Aspiration hazard**

no data available

**Potential health effects**

<b>Inhalation</b>	Toxic if inhaled. Causes respiratory tract irritation.
<b>Ingestion</b>	Toxic if swallowed.
<b>Skin</b>	Toxic if absorbed through skin. Causes skin irritation.
<b>Eyes</b>	Causes serious eye irritation.

**Signs and Symptoms of Exposure**

Symptoms of systemic copper poisoning may include: capillary damage, headache, cold sweat, weak pulse, and kidney and liver damage, central nervous system excitation followed by depression, jaundice, convulsions, paralysis, and coma. Death may occur from shock or renal failure. Chronic copper poisoning is typified by hepatic cirrhosis, brain damage and demyelination, kidney defects, and copper deposition in the cornea as exemplified by humans with Wilson's disease. It has also been reported that copper poisoning has lead to hemolytic anemia and accelerates arteriosclerosis., To the best of our knowledge, the chemical, physical, and toxicological properties have not been thoroughly investigated.

**Additional Information**

RTECS: Not available

---

**12. ECOLOGICAL INFORMATION****12.1 Toxicity**

no data available

**12.2 Persistence and degradability**

no data available

**12.3 Bioaccumulative potential**

no data available

**12.4 Mobility in soil**

no data available

**12.5 Results of PBT and vPvB assessment**

no data available

**12.6 Other adverse effects**

Very toxic to aquatic life.

---

**13. DISPOSAL CONSIDERATIONS****13.1 Waste treatment methods****Product**

Offer surplus and non-recyclable solutions to a licensed disposal company. Dissolve or mix the material with a combustible solvent and burn in a chemical incinerator equipped with an afterburner and scrubber.



R11	Highly flammable.
R22	Harmful if swallowed.
R23/24/25	Toxic by inhalation, in contact with skin and if swallowed.
R36/37/38	Irritating to eyes, respiratory system and skin.
R36/38	Irritating to eyes and skin.
N	Dangerous for the environment
T	Toxic
R39/23/24/25	Toxic: danger of very serious irreversible effects through inhalation, in contact with skin and if swallowed.
R50	Very toxic to aquatic organisms.
R50/53	Very toxic to aquatic organisms, may cause long-term adverse effects in the aquatic environment.
Xi	Irritant
Xn	Harmful

**Further information**

Copyright 2011 Sigma-Aldrich Co. License granted to make unlimited paper copies for internal use only. The above information is believed to be correct but does not purport to be all inclusive and shall be used only as a guide. The information in this document is based on the present state of our knowledge and is applicable to the product with regard to appropriate safety precautions. It does not represent any guarantee of the properties of the product. Sigma-Aldrich Co., shall not be held liable for any damage resulting from handling or from contact with the above product. See reverse side of invoice or packing slip for additional terms and conditions of sale.

---



## SAFETY DATA SHEET

according to Regulation (EC) No. 1907/2006

Version 4.1 Revision Date 01.03.2011

Print Date 21.09.2011

GENERIC EU MSDS - NO COUNTRY SPECIFIC DATA - NO OEL DATA

**1. IDENTIFICATION OF THE SUBSTANCE/MIXTURE AND OF THE COMPANY/UNDERTAKING****1.1 Product identifiers**

Product name : Basolite™ F300

Product Number : 690872

Brand : Aldrich

CAS-No. : 1195763-37-1

**1.2 Relevant identified uses of the substance or mixture and uses advised against**

Identified uses : Laboratory chemicals, Manufacture of substances

**1.3 Details of the supplier of the safety data sheet**Company : Sigma-Aldrich Norway AS  
Tevlingvn. 23  
N-1081 OSLO

Telephone : +47 23 176000

Fax : +47 23 176010

E-mail address : eurtechserv@sial.com

**1.4 Emergency telephone number**

Emergency Phone # : Giftinformasjonssentralen 22 59 13 00

**2. HAZARDS IDENTIFICATION****2.1 Classification of the substance or mixture****Classification according to Regulation (EC) No 1272/2008 [EU-GHS/CLP]**

Acute toxicity, Oral (Category 4)

Skin irritation (Category 2)

Eye irritation (Category 2)

Specific target organ toxicity - single exposure (Category 2)

**Classification according to EU Directives 67/548/EEC or 1999/45/EC**

Harmful by inhalation, in contact with skin and if swallowed. Harmful: possible risk of irreversible effects through inhalation, in contact with skin and if swallowed. Irritating to eyes and skin.

**2.2 Label elements****Labelling according Regulation (EC) No 1272/2008 [CLP]**

Pictogram



Signal word

Warning

Hazard statement(s)

H302

Harmful if swallowed.

H315

Causes skin irritation.

H319

Causes serious eye irritation.

H371

May cause damage to organs.

Precautionary statement(s)

P260


Do not breathe dust/ fume/ gas/ mist/ vapours/ spray.

P305 + P351 + P338

IF IN EYES: Rinse cautiously with water for several minutes. Remove contact lenses, if present and easy to do. Continue rinsing.

Supplemental Hazard Statements none

**According to European Directive 67/548/EEC as amended.**

Hazard symbol(s) 

R-phrase(s)  
R20/21/22 Harmful by inhalation, in contact with skin and if swallowed.  
R36/38 Irritating to eyes and skin.  
R68/20/21/22 Harmful: possible risk of irreversible effects through inhalation, in contact with skin and if swallowed.

S-phrase(s)  
S26 In case of contact with eyes, rinse immediately with plenty of water and seek medical advice.  
S36/37 Wear suitable protective clothing and gloves.

Caution - this mixture contains a substance not yet fully tested.

**2.3 Other hazards - none**

---

**3. COMPOSITION/INFORMATION ON INGREDIENTS**

**3.2 Mixtures**

Synonyms : Iron 1,3,5-benzenetricarboxylate  
Fe-BTC

Formula :  $C_9H_3FeO_6$

Component	Classification	Concentration
<b>Iron-1,3,5-benzenetricarboxylate</b>		
	Acute Tox. 4; Skin Irrit. 2; Eye Irrit. 2; H302, H315, H319 Xn, R22 - R36/38	>= 89 %
<b>Methanol</b>		
CAS-No. 67-56-1 EC-No. 200-659-6 Index-No. 603-001-00-X	Flam. Liq. 2; Acute Tox. 3; STOT SE 1; H225, H301, H311, H331, H370 F, T, R11 - R23/24/25 - R39/23/24/25	<= 3 %
<b>Diiron trioxide</b>		
CAS-No. 1309-37-1 EC-No. 215-168-2	Skin Irrit. 2; Eye Irrit. 2; STOT SE 3; H315, H319, H335 Xi, R36/37/38	<= 1,2 %

For the full text of the H-Statements and R-Phrases mentioned in this Section, see Section 16

---

**4. FIRST AID MEASURES**

**4.1 Description of first aid measures**

**General advice**

Consult a physician. Show this safety data sheet to the doctor in attendance.

**If inhaled**

If breathed in, move person into fresh air. If not breathing, give artificial respiration. Consult a physician.

**In case of skin contact**

Wash off with soap and plenty of water. Take victim immediately to hospital. Consult a physician.

**In case of eye contact**

Rinse thoroughly with plenty of water for at least 15 minutes and consult a physician.

**If swallowed**

Never give anything by mouth to an unconscious person. Rinse mouth with water. Consult a physician.

**4.2 Most important symptoms and effects, both acute and delayed**

To the best of our knowledge, the chemical, physical, and toxicological properties have not been thoroughly investigated.

**4.3 Indication of any immediate medical attention and special treatment needed**

no data available

---

**5. FIRE-FIGHTING MEASURES****5.1 Extinguishing media****Suitable extinguishing media**

Use water spray, alcohol-resistant foam, dry chemical or carbon dioxide.

**5.2 Special hazards arising from the substance or mixture**

Carbon oxides, Iron oxides

**5.3 Advice for firefighters**

Wear self contained breathing apparatus for fire fighting if necessary.

**5.4 Further information**

no data available

---

**6. ACCIDENTAL RELEASE MEASURES****6.1 Personal precautions, protective equipment and emergency procedures**

Use personal protective equipment. Avoid dust formation. Avoid breathing vapors, mist or gas. Ensure adequate ventilation. Evacuate personnel to safe areas. Avoid breathing dust.

**6.2 Environmental precautions**

Prevent further leakage or spillage if safe to do so. Do not let product enter drains.

**6.3 Methods and materials for containment and cleaning up**

Pick up and arrange disposal without creating dust. Sweep up and shovel. Keep in suitable, closed containers for disposal.

**6.4 Reference to other sections**

For disposal see section 13.

---

**7. HANDLING AND STORAGE****7.1 Precautions for safe handling**

Avoid contact with skin and eyes. Avoid formation of dust and aerosols. Provide appropriate exhaust ventilation at places where dust is formed.

**7.2 Conditions for safe storage, including any incompatibilities**

Store in cool place. Keep container tightly closed in a dry and well-ventilated place.

**7.3 Specific end uses**

no data available

---

**8. EXPOSURE CONTROLS/PERSONAL PROTECTION****8.1 Control parameters****Components with workplace control parameters****8.2 Exposure controls****Appropriate engineering controls**

Handle in accordance with good industrial hygiene and safety practice. Wash hands before breaks and at the end of workday.

## Personal protective equipment

### Eye/face protection

Face shield and safety glasses Use equipment for eye protection tested and approved under appropriate government standards such as NIOSH (US) or EN 166(EU).

### Skin protection

Handle with gloves. Gloves must be inspected prior to use. Use proper glove removal technique (without touching glove's outer surface) to avoid skin contact with this product. Dispose of contaminated gloves after use in accordance with applicable laws and good laboratory practices. Wash and dry hands.

The selected protective gloves have to satisfy the specifications of EU Directive 89/686/EEC and the standard EN 374 derived from it.

### Body Protection

Complete suit protecting against chemicals, The type of protective equipment must be selected according to the concentration and amount of the dangerous substance at the specific workplace.

### Respiratory protection

Where risk assessment shows air-purifying respirators are appropriate use a full-face particle respirator type N99 (US) or type P2 (EN 143) respirator cartridges as a backup to engineering controls. If the respirator is the sole means of protection, use a full-face supplied air respirator. Use respirators and components tested and approved under appropriate government standards such as NIOSH (US) or CEN (EU).

---

## 9. PHYSICAL AND CHEMICAL PROPERTIES

### 9.1 Information on basic physical and chemical properties

- |                                                 |                              |
|-------------------------------------------------|------------------------------|
| a) Appearance                                   | Form: solid<br>Colour: brown |
| b) Odour                                        | odourless                    |
| c) Odour Threshold                              | no data available            |
| d) pH                                           | no data available            |
| e) Melting point/freezing point                 | no data available            |
| f) Initial boiling point and boiling range      | no data available            |
| g) Flash point                                  | no data available            |
| h) Evaporation rate                             | no data available            |
| i) Flammability (solid, gas)                    | no data available            |
| j) Upper/lower flammability or explosive limits | no data available            |
| k) Vapour pressure                              | no data available            |
| l) Vapour density                               | no data available            |
| m) Relative density                             | no data available            |
| n) Water solubility                             | no data available            |
| o) Partition coefficient: n-octanol/water       | no data available            |
| p) Autoignition temperature                     | no data available            |
| q) Decomposition temperature                    | no data available            |

- r) Viscosity no data available
- s) Explosive properties no data available
- t) Oxidizing properties no data available

## 9.2 Other safety information

Bulk density 160 - 350 kg/m<sup>3</sup>

---

## 10. STABILITY AND REACTIVITY

### 10.1 Reactivity

no data available

### 10.2 Chemical stability

no data available

### 10.3 Possibility of hazardous reactions

no data available

### 10.4 Conditions to avoid

no data available

### 10.5 Incompatible materials

Strong oxidizing agents

### 10.6 Hazardous decomposition products

Other decomposition products - no data available

---

## 11. TOXICOLOGICAL INFORMATION

### 11.1 Information on toxicological effects

#### Acute toxicity

#### Skin corrosion/irritation

no data available

#### Serious eye damage/eye irritation

no data available

#### Respiratory or skin sensitization

no data available

#### Germ cell mutagenicity

no data available

#### Carcinogenicity

IARC: 3 - Group 3: Not classifiable as to its carcinogenicity to humans (Diiron trioxide)

#### Reproductive toxicity

no data available

#### Specific target organ toxicity - single exposure

no data available

#### Specific target organ toxicity - repeated exposure

no data available

#### Aspiration hazard

no data available

#### Potential health effects

##### Inhalation

Toxic if inhaled. Causes respiratory tract irritation.

##### Ingestion

Toxic if swallowed.

##### Skin

Toxic if absorbed through skin. Causes skin irritation.

##### Eyes

Causes serious eye irritation.



## 15.2 Chemical Safety Assessment

no data available

---

## 16. OTHER INFORMATION

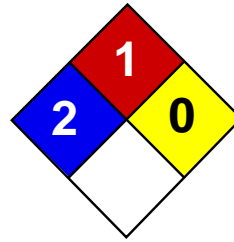
### Text of H-code(s) and R-phrases mentioned in Section 3

Acute Tox.	Acute toxicity
Eye Irrit.	Eye irritation
Flam. Liq.	Flammable liquids
H225	Highly flammable liquid and vapour.
H301	Toxic if swallowed.
H302	Harmful if swallowed.
H311	Toxic in contact with skin.
H315	Causes skin irritation.
H319	Causes serious eye irritation.
H331	Toxic if inhaled.
H335	May cause respiratory irritation.
H370	Causes damage to organs.
Skin Irrit.	Skin irritation
STOT SE	Specific target organ toxicity - single exposure
F	Highly flammable
R11	Highly flammable.
R22	Harmful if swallowed.
R23/24/25	Toxic by inhalation, in contact with skin and if swallowed.
R36/37/38	Irritating to eyes, respiratory system and skin.
T	Toxic
Xi	Irritant
R36/38	Irritating to eyes and skin.
R39/23/24/25	Toxic: danger of very serious irreversible effects through inhalation, in contact with skin and if swallowed.
Xn	Harmful

### Further information

Copyright 2011 Sigma-Aldrich Co. License granted to make unlimited paper copies for internal use only. The above information is believed to be correct but does not purport to be all inclusive and shall be used only as a guide. The information in this document is based on the present state of our knowledge and is applicable to the product with regard to appropriate safety precautions. It does not represent any guarantee of the properties of the product. Sigma-Aldrich Co., shall not be held liable for any damage resulting from handling or from contact with the above product. See reverse side of invoice or packing slip for additional terms and conditions of sale.

---



Health	2
Fire	2
Reactivity	0
Personal Protection	E

# Material Safety Data Sheet

## Indium MSDS

### Section 1: Chemical Product and Company Identification

**Product Name:** Indium

**Catalog Codes:** SLI1033

**CAS#:** 7440-74-6

**RTECS:** NL1050000

**TSCA:** TSCA 8(b) inventory: Indium

**CI#:** Not applicable.

**Synonym:**

**Chemical Name:** Indium

**Chemical Formula:** In

**Contact Information:**

**Sciencelab.com, Inc.**

14025 Smith Rd.

Houston, Texas 77396

US Sales: **1-800-901-7247**

International Sales: **1-281-441-4400**

Order Online: [ScienceLab.com](http://ScienceLab.com)

**CHEMTREC (24HR Emergency Telephone), call:**

1-800-424-9300

**International CHEMTREC, call:** 1-703-527-3887

**For non-emergency assistance, call:** 1-281-441-4400

### Section 2: Composition and Information on Ingredients

**Composition:**

Name	CAS #	% by Weight
Indium	7440-74-6	100

**Toxicological Data on Ingredients:** Indium LD50: Not available. LC50: Not available.

### Section 3: Hazards Identification

**Potential Acute Health Effects:**

Hazardous in case of ingestion, of inhalation (lung irritant). Slightly hazardous in case of skin contact (irritant), of eye contact (irritant), .

**Potential Chronic Health Effects:**

Hazardous in case of ingestion. Slightly hazardous in case of skin contact (irritant), of eye contact (irritant), of inhalation. CARCINOGENIC EFFECTS: Not available. MUTAGENIC EFFECTS: Not available. TERATOGENIC EFFECTS: Not available. DEVELOPMENTAL TOXICITY: PROVEN The substance is toxic to blood, kidneys, the reproductive system, liver, heart, upper respiratory tract, skin, eyes. Repeated or prolonged exposure to the substance can produce target organs damage.

### Section 4: First Aid Measures

**Eye Contact:** No known effect on eye contact, rinse with water for a few minutes.



**Skin Contact:**

After contact with skin, wash immediately with plenty of water. Gently and thoroughly wash the contaminated skin with running water and non-abrasive soap. Be particularly careful to clean folds, crevices, creases and groin. Cover the irritated skin with an emollient. If irritation persists, seek medical attention. Wash contaminated clothing before reusing.

**Serious Skin Contact:** Not available.

**Inhalation:** Allow the victim to rest in a well ventilated area. Seek immediate medical attention.

**Serious Inhalation:**

Evacuate the victim to a safe area as soon as possible. Loosen tight clothing such as a collar, tie, belt or waistband. If breathing is difficult, administer oxygen. If the victim is not breathing, perform mouth-to-mouth resuscitation. Seek medical attention.

**Ingestion:**

Do not induce vomiting. Loosen tight clothing such as a collar, tie, belt or waistband. If the victim is not breathing, perform mouth-to-mouth resuscitation. Seek immediate medical attention.

**Serious Ingestion:** Not available.

### Section 5: Fire and Explosion Data

**Flammability of the Product:** Flammable.

**Auto-Ignition Temperature:** Not available.

**Flash Points:** Not available.

**Flammable Limits:** Not available.

**Products of Combustion:** Not available.

**Fire Hazards in Presence of Various Substances:** Not available.

**Explosion Hazards in Presence of Various Substances:**

Risks of explosion of the product in presence of mechanical impact: Not available. Risks of explosion of the product in presence of static discharge: Not available.

**Fire Fighting Media and Instructions:**

Flammable solid. SMALL FIRE: Use DRY chemical powder. LARGE FIRE: Use water spray or fog. Cool containing vessels with water jet in order to prevent pressure build-up, autoignition or explosion.

**Special Remarks on Fire Hazards:** Not available.

**Special Remarks on Explosion Hazards:** Not available.

### Section 6: Accidental Release Measures

**Small Spill:** Use appropriate tools to put the spilled solid in a convenient waste disposal container.

**Large Spill:**

Flammable solid. Stop leak if without risk. Do not touch spilled material. Use water spray curtain to divert vapor drift. Prevent entry into sewers, basements or confined areas; dike if needed. Eliminate all ignition sources. Call for assistance on disposal. Be careful that the product is not present at a concentration level above TLV. Check TLV on the MSDS and with local authorities.

### Section 7: Handling and Storage

**Precautions:**

Keep away from heat. Keep away from sources of ignition. Ground all equipment containing material. Do not breathe dust.

**Storage:**

Flammable materials should be stored in a separate safety storage cabinet or room. Keep away from heat. Keep away from sources of ignition. Keep container tightly closed. Keep in a cool, well-ventilated place. Ground all equipment containing material. Keep container dry. Keep in a cool place.

**Section 8: Exposure Controls/Personal Protection****Engineering Controls:**

Use process enclosures, local exhaust ventilation, or other engineering controls to keep airborne levels below recommended exposure limits. If user operations generate dust, fume or mist, use ventilation to keep exposure to airborne contaminants below the exposure limit.

**Personal Protection:** Safety glasses. Lab coat. Dust respirator. Be sure to use an approved/certified respirator or equivalent. Gloves.

**Personal Protection in Case of a Large Spill:**

Splash goggles. Full suit. Dust respirator. Boots. Gloves. A self contained breathing apparatus should be used to avoid inhalation of the product. Suggested protective clothing might not be sufficient; consult a specialist BEFORE handling this product.

**Exposure Limits:**

TWA: 0.1 (mg/m<sup>3</sup>) from OSHA (PEL) TWA: 0.1 (mg/m<sup>3</sup>) from ACGIH Consult local authorities for acceptable exposure limits.

**Section 9: Physical and Chemical Properties**

**Physical state and appearance:** Solid.

**Odor:** Odorless.

**Taste:** Not available.

**Molecular Weight:** 114.82 g/mole

**Color:** Not available.

**pH (1% soln/water):** Not applicable.

**Boiling Point:** 2000°C (3632°F)

**Melting Point:** 156.17°C (313.1°F)

**Critical Temperature:** Not available.

**Specific Gravity:** 7.31 (Water = 1)

**Vapor Pressure:** Not applicable.

**Vapor Density:** Not available.

**Volatility:** Not available.

**Odor Threshold:** Not available.

**Water/Oil Dist. Coeff.:** Not available.

**Ionicity (in Water):** Not available.

**Dispersion Properties:** Is not dispersed in cold water, hot water.

**Solubility:** Insoluble in cold water, hot water.

**Section 10: Stability and Reactivity Data**

**Stability:** The product is stable.

**Instability Temperature:** Not available.

**Conditions of Instability:** Not available.

**Incompatibility with various substances:** Not available.

**Corrosivity:** Non-corrosive in presence of glass.

**Special Remarks on Reactivity:** Not available.

**Special Remarks on Corrosivity:** Not available.

**Polymerization:** No.

## Section 11: Toxicological Information

**Routes of Entry:** Absorbed through skin. Eye contact. Inhalation. Ingestion.

**Toxicity to Animals:**

LD50: Not available. LC50: Not available.

**Chronic Effects on Humans:**

DEVELOPMENTAL TOXICITY: PROVEN The substance is toxic to blood, kidneys, the reproductive system, liver, heart, upper respiratory tract, skin, eyes.

**Other Toxic Effects on Humans:**

Hazardous in case of ingestion, of inhalation (lung irritant). Slightly hazardous in case of skin contact (irritant), .

**Special Remarks on Toxicity to Animals:** Not available.

**Special Remarks on Chronic Effects on Humans:** Not available.

**Special Remarks on other Toxic Effects on Humans:** Not available.

## Section 12: Ecological Information

**Ecotoxicity:** Not available.

**BOD5 and COD:** Not available.

**Products of Biodegradation:**

Possibly hazardous short term degradation products are not likely. However, long term degradation products may arise.

**Toxicity of the Products of Biodegradation:** The products of degradation are more toxic.

**Special Remarks on the Products of Biodegradation:** Not available.

## Section 13: Disposal Considerations

**Waste Disposal:**

## Section 14: Transport Information

**DOT Classification:** CLASS 4.1: Flammable solid.

**Identification:** : Metal Powder, Flammable, n.o.s.(Indium Powder) : UN3089 PG: III

**Special Provisions for Transport:** Not available.

## Section 15: Other Regulatory Information

### Federal and State Regulations:

Rhode Island RTK hazardous substances: Indium Pennsylvania RTK: Indium Florida: Indium Minnesota: Indium Massachusetts RTK: Indium New Jersey: Indium TSCA 8(b) inventory: Indium

### Other Regulations:

OSHA: Hazardous by definition of Hazard Communication Standard (29 CFR 1910.1200). EINECS: This product is on the European Inventory of Existing Commercial Chemical Substances.

### Other Classifications:

#### WHMIS (Canada):

CLASS B-4: Flammable solid. CLASS D-2A: Material causing other toxic effects (VERY TOXIC).

**DSCL (EEC):** R37- Irritating to respiratory system.

#### HMIS (U.S.A.):

**Health Hazard:** 2

**Fire Hazard:** 2

**Reactivity:** 0

**Personal Protection:** E

#### National Fire Protection Association (U.S.A.):

**Health:** 2

**Flammability:** 1

**Reactivity:** 0

**Specific hazard:**

#### Protective Equipment:

Gloves. Lab coat. Dust respirator. Be sure to use an approved/certified respirator or equivalent. Wear appropriate respirator when ventilation is inadequate. Safety glasses.

## Section 16: Other Information

**References:** Not available.

**Other Special Considerations:** Not available.

**Created:** 10/09/2005 05:49 PM

**Last Updated:** 11/01/2010 12:00 PM

*The information above is believed to be accurate and represents the best information currently available to us. However, we make no warranty of merchantability or any other warranty, express or implied, with respect to such information, and we assume no liability resulting from its use. Users should make their own investigations to determine the suitability of the information for their particular purposes. In no event shall ScienceLab.com be liable for any claims, losses, or damages of any third party or for lost profits or any special, indirect, incidental, consequential or exemplary damages, howsoever arising, even if ScienceLab.com has been advised of the possibility of such damages.*



## V. HEALTH HAZARD INFORMATION:

Threshold Limit Value: 10 mg/m<sup>3</sup> (15 mg/m<sup>3</sup>)

### Effects of Over Exposure:

**Swallowing:** No evidence of adverse effects from available information.

**Skin Absorption:** No evidence of adverse effects from available information.

**Inhalation:** Dust may cause irritation of the nose throat, accompanied by cough and discomfort. Dust may cause upper respiratory tract irritation with discomfort of nose and throat. Aluminum oxide does not cause pneumoconiosis in man.

**Skin contact:** Dust may cause drying of the skin.

**Eye contact:** Dust may cause irritation.

**Medical conditions aggravated by overexposure:** A knowledge of available toxicology information and of the physical and chemical properties of the material suggest that overexposure is unlikely to aggravate existing medical conditions.

### EMERGENCY AND FIRST AID PROCEDURES:

**EYES:** Flush with copious amounts of water for 15 minutes.

**SKIN:** Wash with soap and water and a large volume of water. Seek medical assistance as necessary, especially if irritation develops or persists.

**INHALATION:** Remove from exposure, seek immediate medical attention.

**INGESTION:** If ingested in large quantities, drink 2 glasses of water and induce vomiting if patient is conscious.

**NOTES TO PHYSICIAN:** Treatment of overexposure should be directed at the control of symptoms and the clinical conditions.

---

## VI. REACTIVITY DATA:

**Stability:** Stable

**Incompatibility (Material to avoid):** Ethylene Oxide, Chlorine Trifluoride

**Hazardous Decomposition Products:** None known

**Hazardous Polymerization:** Will not occur

---

## VII. SPILL OR LEAK PROCEDURES:

**Steps to be taken in case material is released or spilled:** Vacuum collection is preferable.

**Waste Disposal Method:** In accordance with Local, State and Federal Waste Disposal Regulations.

---

## VIII. SPECIAL PROTECTION INFORMATION:

**Respiratory Protection (Specify Type):** If excessive dusting, wear NIOSH or MSHA approved respirator.

**Ventilation:** Local dust pick up recommended when machining.

**Protective Gloves:** Not required but recommended. Prolonged contact with dust or powder may cause drying of skin.

**Eye Protection:** Safety Glasses.

**Other Protective Equipment:** Normal Lab wears.

---

## **IX. SPECIAL PRECAUTIONS:**

**Precautions to be taken in Handling and Storing:** No special considerations for the product. When machining product, avoid dusting and use with adequate ventilation. Do not take internally.

**Other Handling and Storing Conditions:** Wash thoroughly after handling. Do not breathe dust, vapor, mist, or gas.

**CAUTION:** Use of this Crystal in laser operations should be supervised by qualified, knowledgeable personnel, in accordance with ANSL Z 136.1, American National Standard for the safe use of lasers.

## **X. CONTACT INFORMATION**

ISP Optics Corporation, 1 Bridge Street, Irvington, NY 10533

Tel: 914-591-3070

Fax:914-591-3715

Revised on 01/15/2008-Rev.2, Joseph Menaker